The Control of Structural Morphology of Polyethylene by Shear-induced Crystallization

By Masayuki Okura

Department of Chemistry

The University of Sheffield

Submitted to the University of Sheffield

In fulfilment of the requirements for the award of

Doctor of Philosophy

October 2010

Abstracts:

The focus of this study is the mechanism of flow induced crystallization in polymers. The boundary flow conditions required for the formation of an oriented morphology was investigated by polarized light imaging (PLI) and small angle X-ray scattering (SAXS) on various model polyethylenes in order to clarify the relationship between molecular weight distribution and the conditions, and to predict the boundary flow conditions in polydisperse polymers. Also, the structural analysis of the oriented morphology in a sheared model polyethylene was carried out using optical microscopy, SAXS and wide-angle X-ray diffraction.

Torsional flow was applied to hydrogenated polybutadiene (h-PBD) bimodal and trimodal blends comprising of long chains in a short chain matrix and the results were compared to those of polydisperse materials. While a single boundary associated with the onset of the oriented morphology is observed in bimodal blends, two boundaries corresponding to the orientation of the longest chains and next longest chains are detected in the trimodal blend. It is suggested, by comparison, that the boundary flow conditions of polydisperse polymers are dictated by the longest chains and that shorter chains can form flow-induced precursors which contribute to the formation of nuclei at higher flow rates.

The critical work, which represents the boundary flow conditions, was measured against a series of the h-PBD bimodal blends. A series of short chain matrices were used to which long chains were added. The work is proportional to the matrix molecular weight in power law when the matrix molecular weight is relatively high. The matrix inhibits the formation of shish nuclei, the nuclei being instrumental in the formation of the oriented morphology. The work is independent of the matrix molecular weight when the matrix molecular weight is relatively low. It corresponds to the critical work of the long chains without any contribution by the matrix.

Publications and Conferences List:

Publications list

European Polymer Journal, accepted (Part of Chapter 1 and 3)

Macromolecules, submitted (Chapter 5)

Physical Review Letters, will be submitted (Chapter 6)

Conference list

21/7/2009

Macro Group YRM 2009 (Sheffield, UK) / Poster

8/9/2009 - 9/9/2009

UK Polymer Showcase (Sheffield, UK) / Poster

21/10/2009 -23/10/2009

FAPS international (Nagoya, Japan) / Oral

14/12/2009 - 15/12/2009

BSR Rheology (Edinburgh, UK) / Poster

29/4/2010 - 30/4/2010

Macro Group YRM 2010 (Nottingham, UK) / Poster

27/5/2010 - 28/5/2010

Workshop on Polymer Crystallization during Processing (Genoa, Italy) / Oral

Acknowledgements:

My research and thesis were never finalized without Sasha. You always showed me the right way to carry forward my research. I studied many things from you such as physics, rheology, scattering, data analysis and how to write a high quality paper (and how to swim in Mediterranean Sea!). I managed to study quite comfortably owing to your delightful atmosphere and positive mood.

I was very happy that I could study under the supervision of Tony and Patrick. The luckiest thing for me was that Tony introduced me this research subject. The subject was not only meaningful from the viewpoint of academic research but also quite useful for my job in our company. I never stood in tough situation in my study because of your thoughtful supervision. (Long and cold Xmas walking organized by Patrick was a bit tough, though)

Also I would like to say thank you to Pierre and Christine. Your synthesis work was necessary piece of the study. Thursday friendly football game organized by Pierre was one of the best memories in the lab. Angel Christine gave me many useful advices as a specialist of synthesis and also you supported my chemical experiments and English writing.

I want to say thank you to the rest of members in Tony Ryan group for discussions about research and good memories. The team cinema & World Cup, Anne-Cecile, Susi, Mar and Obed, I will miss the cinema and pub nights with you. Matt and Yu Hao, I really enjoyed football in Chinese Society, badminton and extremely long mah-jong. Our pool team, Gary & Masa, was excellent and I wanted play in tournament once more. Chris and Lewis, thank you very much for entertaining me by your funny talk and drawing every time. Sarah, please contact me anytime if you miss Kaeru-manju.

I appreciate technicians, Pete and Nick for liquid nitrogen issue for many many many times, Harry for wide angle x-ray diffraction, Chris for microtome and Rob for differential scanning calorimetry. Also, I could not finish my PhD without thoughtful cooperation with Elaine Fisher, thank you very much!

Special thanks to my parents, grandmother and brothers. I could concentrate my study owing to that all of you have been healthy for these two years and 4 month.

Lastly, I would like to appreciate to our company, Kureha Corporation for giving me the opportunity to study in the University of Sheffield.

Curriculum vitae:

My basic science and engineering skills were developed at the Gunma National College of Technology (NCT) in Japan where I entered the Chemistry and Materials Science Department in 1993; in addition to courses in science, mathematics and physics I also studied English and in my final year, I completed a graduate research project investigating the decomposition mechanism of a fluorine compound by mass spectrometer.

In 1998, I entered Tokyo Institute of Technology (TIT), where after passing a transfer examination; I was admitted into the third-year class during my first year. From that point onwards, my primary focus was polymer science, especially polymer structure, property, and processing. During this period, I also had the opportunity to study under Professor Takashi Inoue and associate professor Toshiaki Ougizawa for a year, researching the unique crystallization behaviour of linear polyethylene using techniques including light and X-ray scattering and thermal analysis.

I went on to the master's degree course at TIT in 2000, devoting myself to polymer research under associate professor Toshiaki Ougizawa for two years and writing my master's thesis on the state of the amorphous phase in crystalline polymers by Pressure-Volume-Temperature behaviour measurement and free volume measurement using Positron Annihilation Lifetime Spectroscopy. In addition, I strengthened my familiarity with other important techniques in polymer processing such as polymer blending.

After completing my master's in 2002, my ambition to develop polymer products with a broad range of uses that might ultimately benefit society led to my decision to join the Kureha Corporation, a manufacturing company, which specializes in the research and development of new polymer products.

Initially, my work focused on the development of food-packaging materials. In my research and development, I conducted oxygen transmission rate measurement, free volume measurement by Positron Annihilation Lifetime Spectroscopy, and EXAFS for analyzing the food-packaging materials. Soon I was entrusted with an especially

challenging project; to search for new research theme. Thus I investigated countless technical papers and the patents of other companies, and specifically, I looked into low-cost processes for producing high-oxygen barrier films and an electrolyte membrane for fuel cells. These developments were not successful; however, I acquired 6 patents and learned to perform GPC, XPS, as well as some electrical measurements. Then, I was involved with research focused on a bi-oriented film, a promising product given its high resistance to heat. Within this team, I was in charge of improving the orientation process and analyzing the structure of stretched films by using X-ray analysis and birefringence measurements.

In 2008, I started to study about flow induced crystallization of polymers as a PhD student under the supervision of Professor Anthony J Ryan and Dr J Patrick A Fairclough at the University of Sheffield in the United Kingdom.

Common Abbreviations:

h-PBD	:	hydrogenated polybutadiene
M_w	:	weight average molecular weight
M_n	:	number average molecular weight
SAXS	:	small angle X-ray scattering
WAXD	:	wide angle X-ray scattering
PLI	:	polarized light imaging
DSC	:	differential scanning calorimetry
τ_R	:	Rouse time
τ_d	:	Reptation time
τ_e	:	equilibration time
M_e	:	entanglement molecular weight
$\dot{\gamma}$	:	shear rate
$\dot{\gamma}_{min}$	:	minimum shear rate
$\dot{\gamma}_b$	:	boundary shear rate
γ	:	stress
γ_b	:	boundary stress
t_s	:	shear duration
η	:	viscosity
$\lvert\eta^*\rvert$	:	complex viscosity
G'	:	storage modulus
G''	:	loss modulus
ω	:	angular frequency
Ω	:	angular velocity
TTS	:	time-temperature superposition
G_e	:	plateu modulus
w_b	:	boundary specific work
w_c	:	critical specific work

Contents:

Chapter 1: Background

Chapter 2: Methodology

Chapter 3: Characterization of low-polydispersity hydrogenated polybutadiene

Chapter 4: Structural Analysis of Sheared Hydrogenated Polybutadiene Blends

Chapter 5: Using Multi-modal Blends to Elucidate the Mechanism of Flow-induced Crystallisation in Polymers

Chapter 6: Understanding of Essential Mechanical Work for Flow-induced Crystallisation in Polymers

Chapter 7: Conclusions and Future Work

Chapter 1

Background

1.1. Introduction

In 2007, 260 million tonnes of polymer were produced in the world and the production of polymer has increased approximately 9% every year from 1.5 million tonnes in 1950.[1] In European countries, 65 million tonnes (25% of world-wide production) were produced in 2007. On the other hand, the demand of converters in Europe has been reported 52.5 million tonnes. The percentage of polyethylene and polypropylene in 52.5 million tonnes are 29 % and 18 % respectively. The major applications of them are packaging, construction and automotive materials.

The improvement of polymer properties has been pursued for a long time. The properties of polymers depend on various factors (**Figure 1.1**). Firstly, basic properties are decided by the native of the materials such as a chemical structure, molecular weight and its distribution. Secondly, the properties can be changed by the formation of oriented morphology through processing. This relationship between materials, morphologies and properties is complicated and is not fully understood. This thesis aims to develop that understanding.

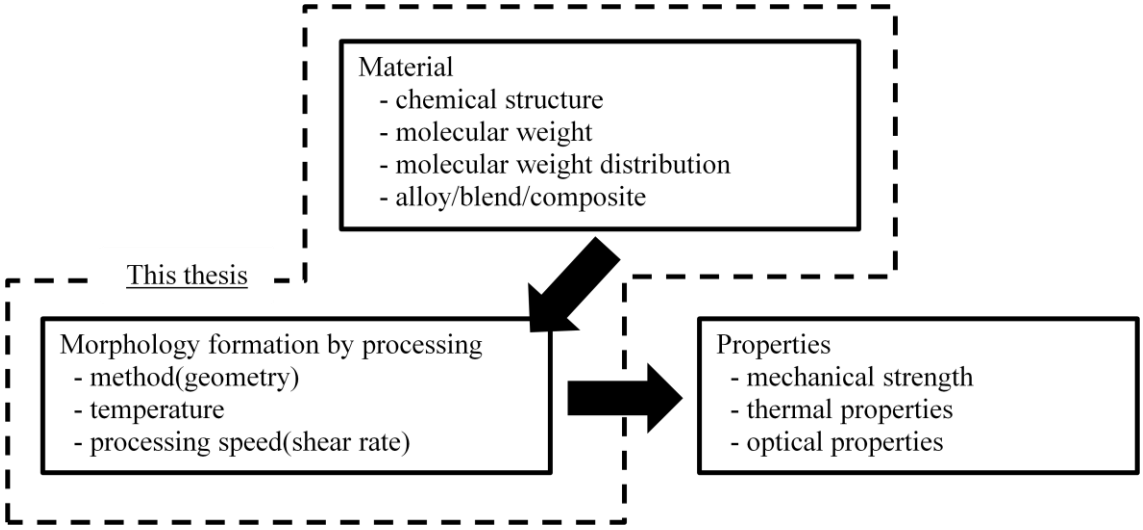

Figure 1.1. Relationship between the material, morphology and properties. The dotted line indicates the area of the research in this thesis.

The main difficulty in understanding the relationships could be the high molecular weight of polymers. The most of all, polymers have a broad molecular weight distribution. The effects on the morphology formation by high and low molecular weight content are difficult to separate. In addition, entanglements of polymer chains caused by their high molecular weight dramatically affect the properties. The number of entanglements depends on not only the molecular weight but also the chemical structure. In summary, it is significant problem to clarify the relationship between structure, process conditions and properties of polymers having broad polydispersity.

The current condition of the development of processed polymer products in industry is dependent on practical methods. Although industrial companies are producing highly-functional products, the understanding of the process-structure-properties relationship has not caught up the level of empirical commercial practice. In order to close the gap, further researches about the relationship are required.

1.2. Polyolefin

1.2.1. History of polyolefin

Polyolefins are the most widely used polymer nowadays. Polyolefins comprise of carbon and hydrogen atoms and their simple structure make them light and harmless materials. The price of polyolefins is relatively cheap; therefore it has been used for many applications such as films, fibres, bottles and injection-moulded products. The usage of polyolefin is over 150 million metric tons per year.[2] Although polyolefin has been a popular material from a long time, the industrial importance of it has not changed until recently and the research to improve its properties and to reduce cost is continuing actively.[3-6]

Polyethylene is the simplest polyolefin and made by the polymerization of ethylene monomer. In 1930s, first polyethylene was discovered by bulk polymerization in high pressure conditions. The polyethylene produced by this method is called low density polyethylene (LDPE). It has a lot of branches in a polymer chain as shown in **Figure 1.2**. The low density and low crystallinity of LDPE are the result of its highly branched structure.

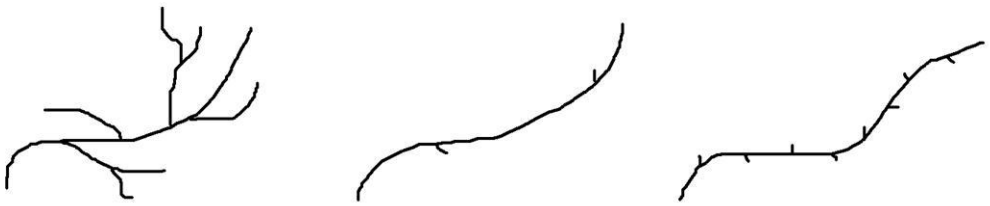

LDPE HDPE (m-)LLDPE

Figure 1.2. The difference of the blanch structures of polyethylenes.

The discovery of Ziegler-Natta catalyst in 1950s was a major technological innovation for polyethylene. The catalyst was found by Ziegler[7] and then it was improved by Natta.[8, 9] High density polyethylene (HDPE) and linear low density polyethylene (LLDPE) started to be produced by this catalyst. HDPE has high melting point due to its high crystallinity and has been used for the applications which require thermal stability. On the other hand, LLDPE has higher impact strength at low melting temperature than LDPE and this property is suitable for the applications which can be used at low temperature such as food packaging materials.

A more recent innovation was the development of a metallocene catalyst. The catalyst was found by Kaminsky in 1980s[10] and it is also called Kaminsky catalyst. This innovation made possible further structural control of polyolefin. LLDPE made by the metallocene catalyst (m-LLDPE) has uniformly-sized lamellae crystals and this uniformity is giving some advantages to m-LLDPE such as high transparency and narrow melting point distribution.

Polypropylene (PP) is second-simplest polyolefin and is produced by the polymerization of propylene. The first polypropylene was made by using Ziegler-Natta catalyst by Natta in 1950s.[11] The crystallinity and properties of polypropylene depend on its tacticity. For example, although atactic PP is a rubbery material, isotactic PP has high melting point (188 ºC).

Polyolefin is playing an important role as a suitable material for not only its commercial use, but also academic research. The advantages of polyolefin for academic research are its simple, symmetric and non-polar molecular structure. These advantages make

possible the investigations with a minimum number of assumptions. In addition, many different primary structures of polyolefin can be designed to answer research purposes by using various synthesis methods such as catalysts and co-monomers.

The control of molecular weight distribution of polyolefins has been attempted for a long time. Since its inception in the 1950s [12] "living" anionic polymerization has become one of the foremost methods for producing polymers with a low polydispersity i.e. $\bar{M}_w/\bar{M}_n < 1.1$. The procedures required for successful polymerizations are rigorous and exacting[13] but the excellent molecular mass control and the ability to produce specific architectures, particularly through the use of chlorosilane chemistry, compensate for this.

The route to producing well-defined polyethylene analogues is via the anionic polymerization, and subsequent hydrogenation, of polybutadiene. Typically, the polymerization is initiated using a butyllithium initiator (BuLi). The propagation is via a Michael addition (**Figure 1.3**) and this can either proceed via 1,4-addition or a 1,2-addition (Detail about the proportion of 1,4 and 1,2 will be mentioned in the next chapter). Then the hydrogenation of polybutadiene to form poly(ethylene-*co*-butene) is accomplished using several different methods in order to form LLDPE analogue with low polydispersity and well-controlled branching (**Figure 1.4**). Heterogeneous catalysts such as Wilkinson's catalyst[14] or homogeneous catalysis such as Pd on $CaCO_3$[15] have proved effective.

The quantity and distribution of the ethyl branches determines the crystallisation behaviour of the polymers, the melting and crystallization temperatures becoming increasingly low as the ethyl branch content rises. Ethyl branches are believed to be excluded from crystalline lamellae and as a result the lamellae are generally thinner with a greater proportion of amorphous material being present[16].

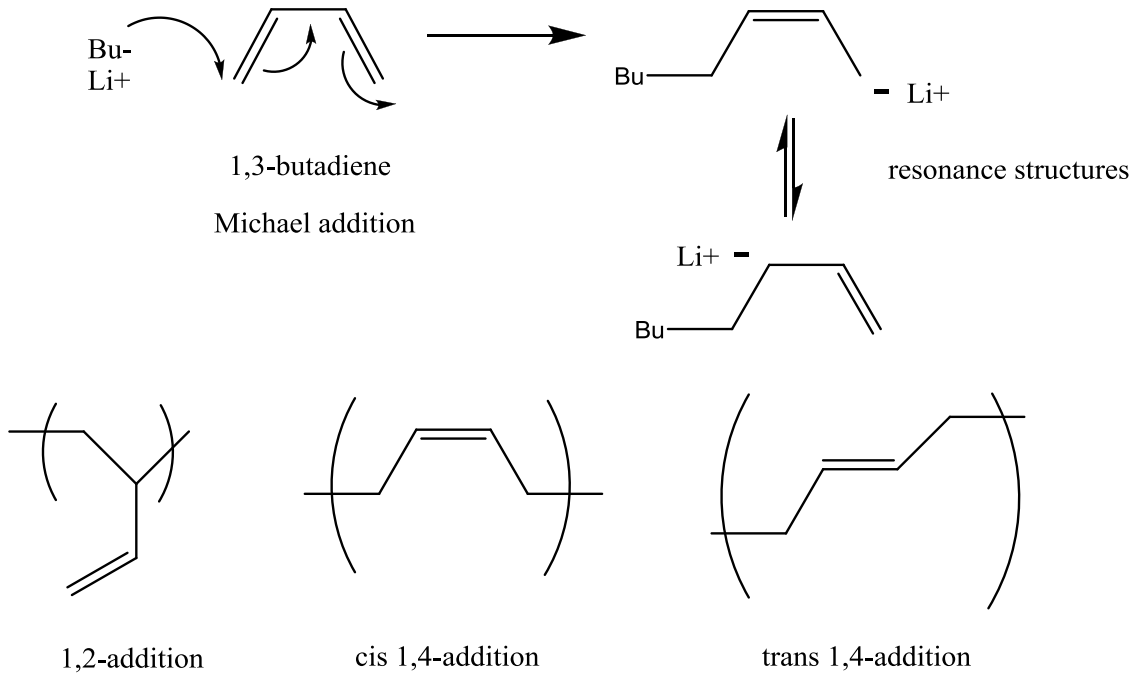

Figure 1.3. Polymerization of butadiene via an anionic polymerisation.

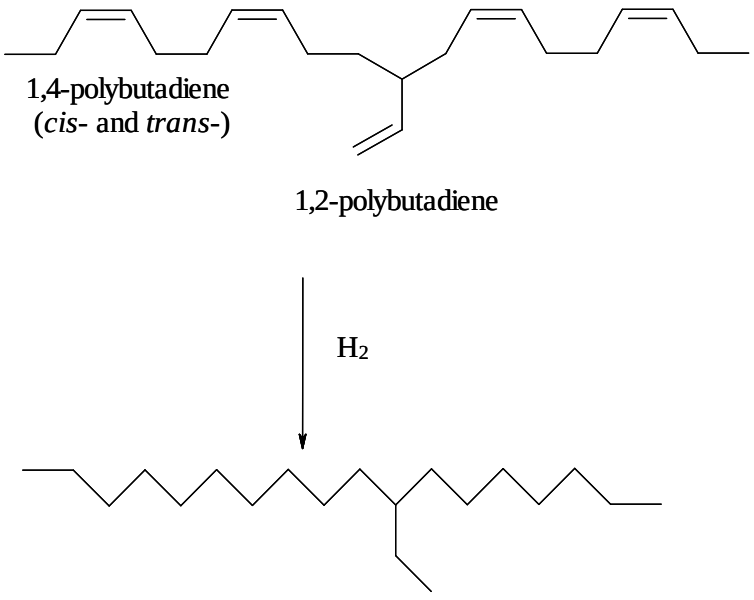

Figure 1.4. Hydrogenation of polybutadiene to form an LLDPE analogue.

1.2.2. The processing of polyolefin

Various methods can be applied to process the raw materials of polyolefin and to change them to useful forms. Extrusion by screw is the most general way of polymer processing for semi-crystalline polymer such as polyolefin.[17] **Figure 1.5** shows the simplified schematic depiction of the extrusion system.

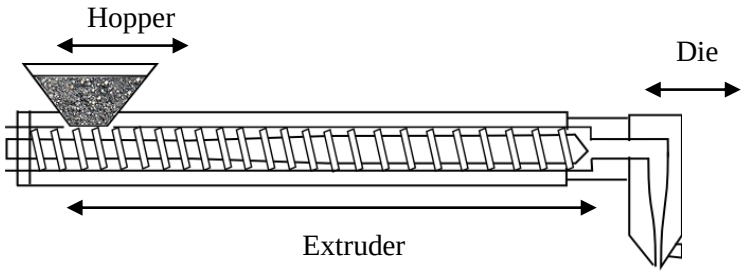

Figure 1.5. Extrusion system. This figure shows the extruder and the die for sheeting.

Pellets of polyolefin which have fallen down from the hopper are heated up above the melting point and are kneaded by the rotating screw. In this process, the polymer melt has a high shear applied between the screw and the barrel to effect homogeneous mixing. Then mixed polymer is sent to the die to form the shape. In the die, flowing melt polymer is also under shear stress again which is caused by the velocity profile in the capillary.[18] The shear stress in extruders and dies can cause the orientation of molecular chains and can influence the properties of the polyolefin. However, the specific effect of shear for structure and properties of polymer is still a controversial problem. In the next few sections, the research relating to the shear effect on polyolefin structure and properties is reviewed.

1.3. The oriented crystals of polyolefin

1.3.1. The origin of shish-kebab structure

Shish-kebab structure grows in polyolefin under a certain magnitude of shear flow. This phenomenon has been known for a long time. The main target of the research of shish-

kebab structure has been focused on the formation of the structure in polyethylene[19-30] and polypropylene[31-45].

In 1963, Blakadder et al reported the growth of shish-kebab structure in dilute polyethylene solution as "crystals of an unfamiliar type".[19] In the research, a dilute polyethylene solution was formed in hot p-xylene and then it was maintained under an ultrasonic field. Then shish-kebab structure was observed by an electron microscope in a gold-palladium shadowed sample which was taken from the solution. As shown in the image (**Figure 1.6**), the shish-kebab structure consists of a central backbone (shish) and a string of plates (kebab).

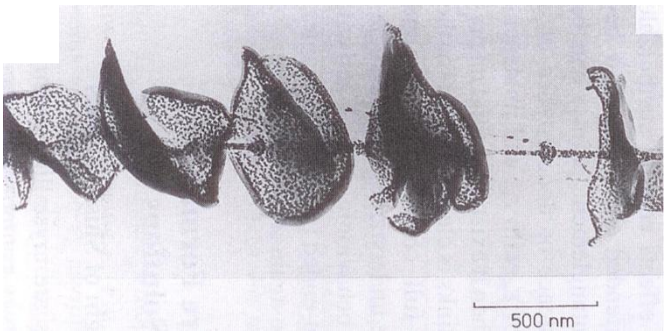

Figure 1.6. The shish-kebab structure found from an agitated polyethylene solution by Hill et al.[46] (reproduced with permission)

Pennings et al reported a pioneering result on the structural information of shish-kebab structure in 1965.[20] The shish-kebab structure was obtained from mechanically agitated dilute polyolefin solution and then the bundle of the shish-kebab was collected from the solution. A stress-strain measurement was carried out on the collected bundles. The result showed that the bundles had high tensile strength and small elongation of only 10%. From the result, it was suggested that the shish part was composed of oriented molecular chains. This notion was also supported by the electron diffraction pattern from the same samples.

Keller had an important role in the observation of shish-kebab structure in the bulk polymer. In 1967, Keller and Machin reported that the shish-kebab structure was also observed in a bulk cross-linked polyethylene which was crystallized under stress.[21]

Keller et al also performed some research on the mechanism of shish-kebab structure formation. A proposal concerning the mechanism of shish-kebab formation were particularly summarised in the book written in 1997 by Keller.[22] When the stress is applied to melt polyolefin, longer molecular chains are stretched and form shish nuclei at first (**Figure 1.7 a**). And then the shorter chains crystallize in the direction perpendicular to the shish nuclei and form the kebab crystals (**Figure 1.7 b**). This mechanism has been supported by some results which report the effect of high molecular weight polymer chains on crystallization.[28, 47]

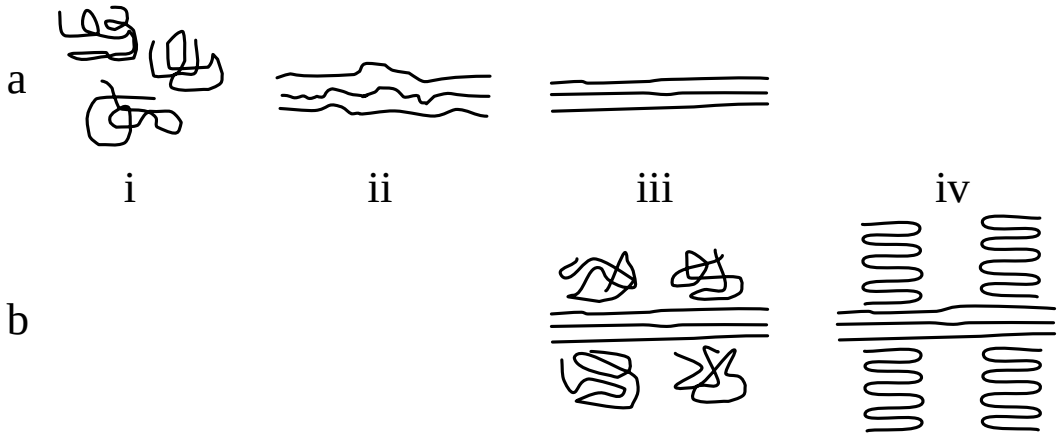

Figure 1.7. (a); i-random coils, ii-oriented chains, iii-shish-nuclei, (b); iii-the relaxed chains are left in amorphous region, iv-formation of kebab crystals.

This mechanism, that the shish nuclei first grow by high molecular weight polymer chains and then the kebab crystals grow on the shish nuclei, can be interpreted by using a chain relaxation time. The longer chains can be stretched at lower shear rate because of their longer relaxation time. This relationship between shish-kebab structure and the relaxation time is explained in the later section with the explanation of important rheology models.

The relationship between the oriented morphology and the properties of polyolefin should be considered before moving to the next section. The shish-kebab structure affects the properties (such as mechanical and thermal) significantly. Although it is obvious that the oriented morphology in polyethylene has higher thermal stability than

the lamellae crystals in spherulites[48], it is difficult to be observed directly because the amount of shish nuclei existing in polymer is typically less than one part in a thousand of the crystallisation material. However, an indirect method by using the memory effect of shish nuclei implied that the melting temperature of the shish nuclei is much higher that lamellae crystals in spherulites.[24] It was reported that the shish nuclei had a high thermal stability, and elongated molecular chains of shish structure remain after the thermal treatment even at equilibrium temperature because of a long relaxation time of the stretched chains of the shish nuclei.

Keller et al also investigated the melting process of shish-kebab structure in polyethylene by transmission electron microscopy (TEM). It was found that the shish nuclei had higher melting point than kebab crystals.[46, 49, 50] This fact is quite convenient for the researchers of flow-induced crystallization because the polymers can be sheared above the melting point of the kebab crystals but below the melting point of shish nuclei to investigate the formation of the shish-nuclei whilst avoiding the effect from any other crystallization.

The representative example of the improvement of the properties is known as 'Hard Elastic' fibre.[22] Polyolefin fibres which include the enough amounts of the shish-kebab structure indicate a high elasticity, longer elongation and high thermal stability compared to normal polyolefin fibres. Moreover, these 'Hard Elastic' fibres show great recovery against elongation. This phenomenon can be explained that the mechanism of the morphology change by stretching is the entropy effect such as the re-arrangement of the oriented morphology.

1.3.2. The morphology examination of shish-kebab structure

The morphology of the shish-kebab structure has been analysed by various methods. It is possible to observe the morphology directly by TEM and atomic force microscopy (AFM). In addition, X-ray scattering, neutron scattering and birefringence measurement can provide the average information of the morphology at wider area in sheared samples than the direct observation. Also, the formation of the oriented morphology can be supposed by some property measurements such as thermal and mechanical properties.

Hobbs reported the melting behaviour of a shish-kebab structure which can be observed by AFM.[29, 51] A low-polydispersity polyethylene was melted and was applied a shear stress by using a razor blade method. And then the sheared polyethylene was set onto a hot stage and its surface was investigated by the AFM at the temperature above the melting point of un-oriented crystals. The shish-kebab structure and its melt process were observed with increasing temperature.

Small angle X-ray scattering (SAXS) is one of the most effective way to evaluate the orientation of the lamellae crystals and it was used several times.[23] The existence of the oriented morphology can be checked by specific scattering patterns of an oriented lamellae structure. In addition, the degree of orientation calculated from the scattering patterns can be used as the criterion of the orientation of the morphology. In the previous report, P2 orientation function[52] was used to evaluate the degree of orientation of the oriented morphology. Moreover, in-situ SAXS and WAXD measurement under flow is also possible.[53, 54]

The structural information about shish-kebab structure also can be checked by a small angle neutron scattering (SANS). Although deutrated samples need to be used to have enough scattering contrast and scattering pattern, the SANS is a powerful method to measure the structural information of polymer chains. Some attempts have been made to apply SANS to evaluate the oriented morphology of sheared polyolefins. Also, in-situ measurement is available to investigate the morphology change in polymers under shear flow. For instance, Bent et al reported the in-situ SANS data which was applied to deutrated polystyrene extensional flow.[55]

Polarized light imaging (PLI)[23] is also a powerful technique to confirm the formation of the oriented morphology in sheared polymers. The principle of the PLI technique is as follows. When the shish-kebab structure has formed in a polymer, polymer chains constructing the kebab crystals have arranged parallel to a flow direction. In that case, the refractive index parallel to the flow direction is greater than perpendicular direction. Therefore, the polymer involving shish-kebab structure has a birefringence. This birefringence can be detected between two polarizers crossed at 90 °.

1.4. The oriented crystals and rheology

In this section, two rheology models which are necessary to describe the relaxation behaviour of polymer chains are mentioned. Then, the relationship between the formation of the oriented morphology and rheology is explained.

1.4.1. The Rouse model

In order to consider the behaviour of one polymer chain, Rouse introduced a simple spring and bead model, called the Rouse model[56] (**Figure 1.8**).

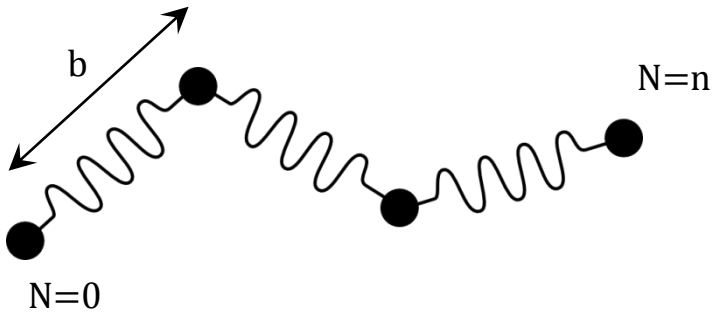

Figure 1.8. Rouse model.

There are three assumptions for the Rouse model, which are (1) both the springs and beads do not have a volume, (2) all springs have same a spring constant and (3) no interaction exists between the springs. If some stress was added to this model polymer chain from an external source, this stress is relaxed after a certain time. This certain time which is required to relax the chain is called as the Rouse relaxation time, τ_R, and is defined as follows.[57]

$$\tau_R = \frac{\xi N^2 b^2}{3\pi^2 k_B T} \qquad \textbf{Eq. 1.1}$$

ξ : friction coefficient b : segment length

N : number of segment k_B : Boltzmann constant

T : temperature

This model describes the relaxation behaviour of the local part of the chain (such as the inside of the diameter of the tube in the next section) which is not affected by the surrounding entanglements of chains.

1.4.2. Tube model

The relaxation behaviour of a concentrated polymer solution is affected by surrounding entanglements. De Gennes explained this effect of the prevention of movement of the chains by surrounding entanglements by assuming a tube model (**Figure 1.9**).

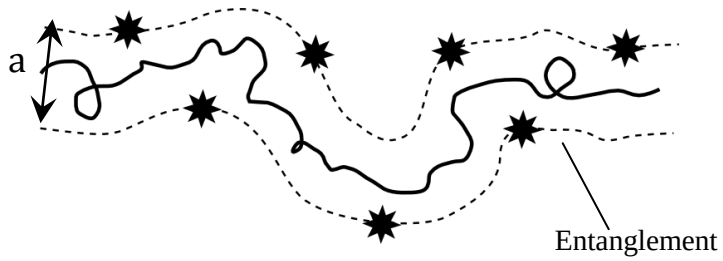

Figure 1.9. Tube model.

The polymer chains can move only parallel to the tube direction in this tube. The relaxation time defined in this model is equal to the time necessary for the chain to slip through the tube. This relaxation time is called the reptation time, τ_d, and is represented as follows.[58]

$$\tau_d = \frac{\xi N^3 b^4}{\pi^2 k_B T a^2} \qquad \textbf{Eq. 1.2}$$

a : tube diameter

On the other hand, on length scale < a, molecular segments are not affected by the surrounding entanglements. Therefore, the relaxation behaviour in this scale can be described by the simple Rouse relaxation. The relaxation time at this local scale is called the equilibration time τ_e. The relationship between τ_d and τ_e is represented as follows using the tube segment number, Z, corresponding to the number of entanglements per molecule.

$$\tau_d = 3Z^3\tau_e \qquad \textbf{Eq. 1.3}$$

$$Z = \frac{5}{4}\frac{M}{M_e^F} \qquad \textbf{Eq. 1.4}$$

M : polymer molecular weight M_e^F : entanglement molecular weight

Also, the relationship between τ_d and τ_R can be indicated as follows.

$$\tau_d = \frac{3Nb^2}{a^2}\tau_R \qquad \textbf{Eq. 1.5}$$

The relaxation times can be obtained by a linear and non-linear rheology measurement of low polydispersity samples (in the next chapter).

1.5. Recent research scene

In this section, the latest research relating to oriented nuclei generation under shear flow is introduced. There are three novelties in the present research which are (1) the research approach by using multimodal blend as the model of polydisperse polymer, (2) the hypothesis of the multi-step formation mechanism of the oriented morphology under flow and (3) using mechanical work which is required to form the oriented morphology as the criterion. My research subject is based on the recent research background.

1.5.1. Multimodal blend approach

A number of approaches have been explored to overcome the limitations of poorly defined polydisperse materials (**Figure 1.10 a**): a fractionation of polydisperse polymers followed by a preparation of binary blends with a systematic variation of concentration of long chains in the blends [38]; making blends of polydisperse polymers with an ultrahigh molecular weight polymer[48]; a single stage catalyst-controlled synthesis of a bimodal polymer with a high- and low-molecular-weight fractions [59] or using advantages of anionic polymerization - synthesising polymers of variable molecular weight (from 1 kDa to 10000 kDa) with low polydispersity (**Figure 1.10 b**) and blending them in the required proportions[60, 61]. The latter approach is the most versatile as it offers a wide range of flexibility in formulating a desirable molecular weight distribution in a polymer ensemble with known relaxation times. This enables polymer blends of controlled polydispersity with a wide dynamic range of relaxation times to be produced starting from the most simple variant of mixing long linear chains in a matrix of short chains (bimodal blends) of variable concentration and molecular weight simulating the effect of long-chain molecules (**Figure 1.10 c**)[61].

More elaborate blends such as trimodal blends (**Figure 1.11 d**) and multimodal blends can also be made to directly compare with industrial materials in terms of molecular weight distribution. The fact that variable molecular architectures can be synthesised via anionic polymerization route expands its application towards an opportunity to establish the effect of molecular architectures and not only molecular weights on the structural morphology[60], e.g. branched polymers.

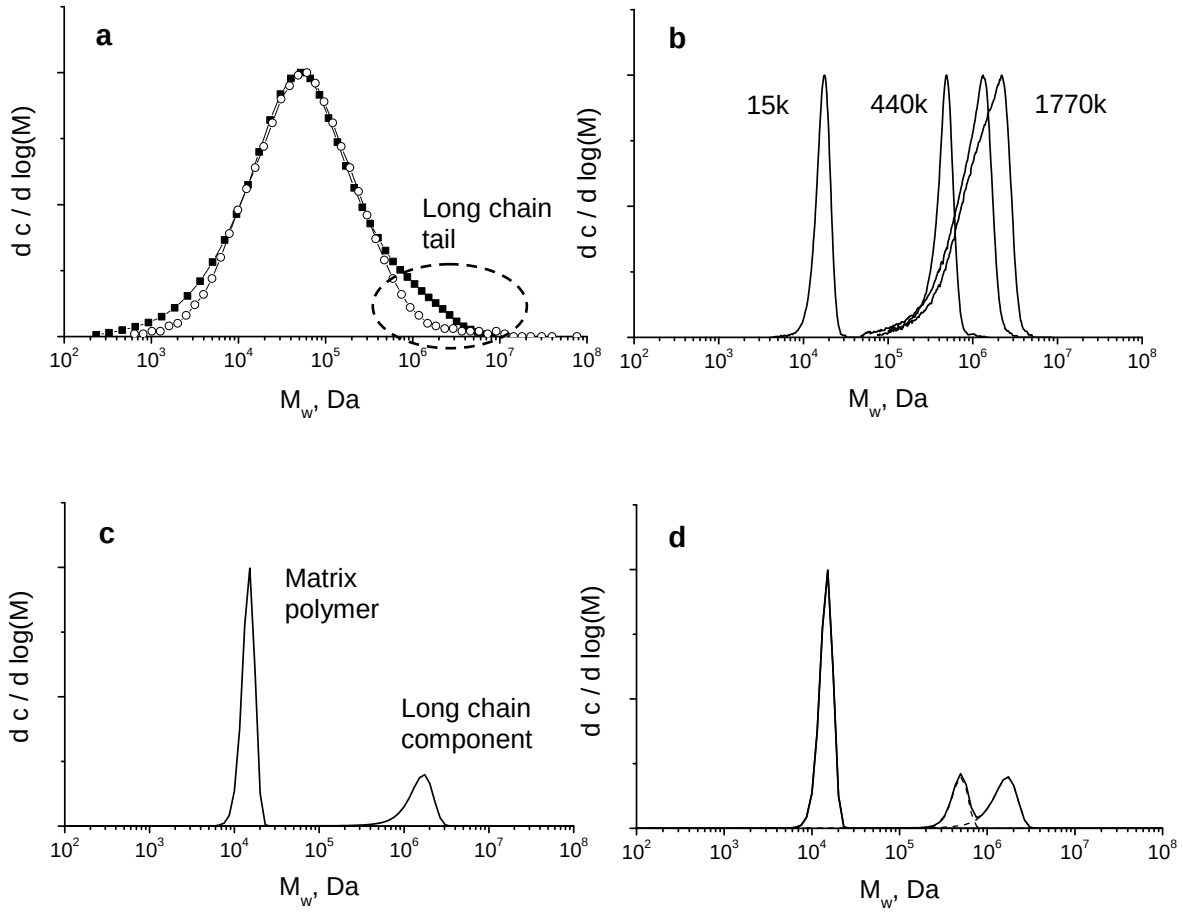

Figure 1.10. Molecular weight distribution in different polymer systems: a) polyethylene of industrial grades (squares - high-density polyethylene, M_w = 220 kDa, M_w / M_n = 14, circles - low-density polyethylene, M_w = 240 kDa, M_w / M_n = 14), b) hydrogenated polybutadiene of low polydispersity synthesised by anionic polymerization (M_w = 15 kDa, M_w / M_n = 1.1; M_w = 440 kDa, M_w / M_n = 1.2; M_w = 1330 kDa, M_w / M_n = 1.4 and M_w = 1770 kDa, M_w / M_n = 1.5) and a schematic of polymer blends of controlled polydispersity (bimodal blend, c and trimodal blend, d). All the curves are normalized to the peak maximum.

1.5.2. Formation mechanism of oriented morphology

The mechanism of formation of shish-kebab morphology continues to be a matter for discussion ever since it was first reported and the initial attempts to understand the underlying processes of polymer crystallization from an oriented state were made [62-65]. Subsequent studies based on the results of nucleation kinetics under flow conditions

have led to a number of models based on scattering, birefringence and microscopy results[38, 66-69]. Recent quantitative measurements of flow-induced crystallization using bimodal linear-linear blends enabled the four stages in shish-kebab formation under flow conditions to be distinguished : stretching (stage 1), nucleation (stage 2), alignment (stage 3) and fibrillation (stage 4) (**Figure 1.11 a**)[70]. Note, there is no fundamental difference between the influence of mechanical work put into the sample either by shear flow or by extensional flow[71].

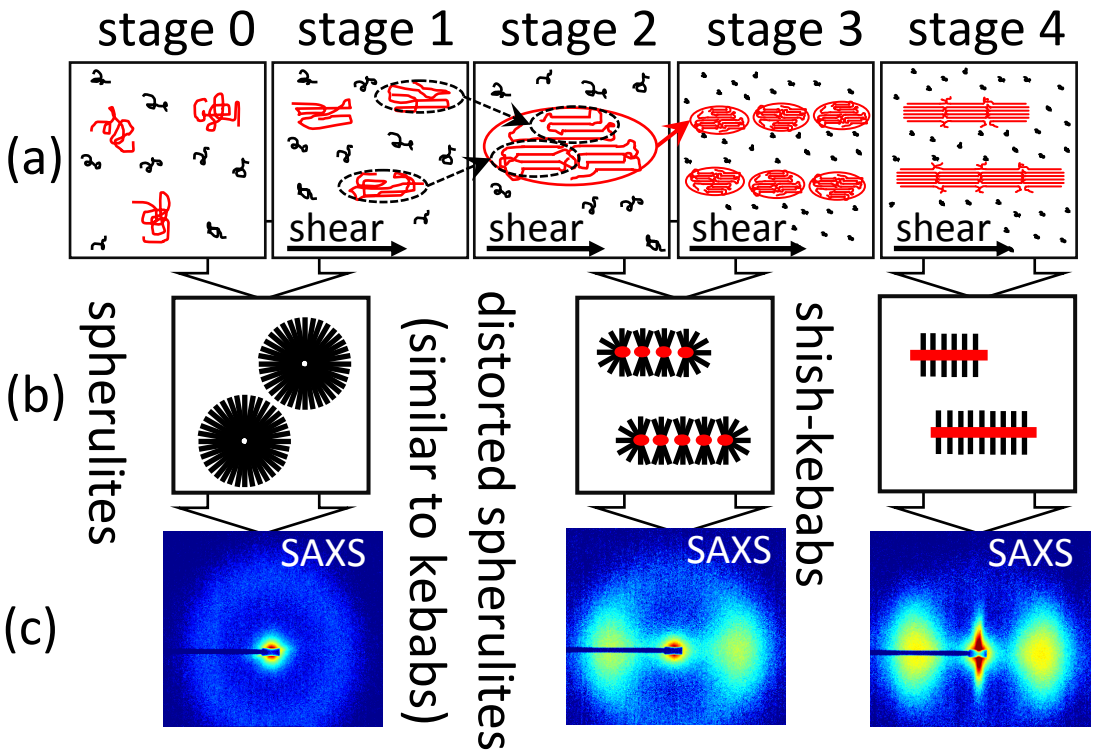

Figure 1.11. A schematic diagram of the formation of shear-induced structural morphologies in polymers: a four-stage model of shish formation in the polymer melt under shear conditions combined of stretching of long chain molecules (Stage 1), nucleation (Stage 2), alignment of shish nuclei (Stage 3) and fibrillation (Stage 4) (a); structural morphologies formed in the polymer after crystallization at different stages of the shish formation (b) and their small-angle X-ray scattering patterns (SAXS) (c). Stage 0 represents the polymer melt at quiescent conditions. The entanglements of the molecules have not been shown for clarity.

(1) Stretching

Flow has two main effects on structural behaviour of the polymer molecules: 1) orientation of the primitive path of the molecules along the flow direction and 2) stretching of the molecular segments along the flow at higher shear rates. While the orientation is controlled by moderate shear rates, $\dot{\gamma}$, described by disengagement time of the molecules, τ_d where $\dot{\gamma} > 1/\tau_d$, stretching is caused at higher shear rates corresponding to Rouse relaxation time of the molecules, τ_R (where $\dot{\gamma} > 1/\tau_R > 1/\tau_d$). The first observations of the shish-kebab structure led to the hypothesis that stretching of the molecules under flow conditions plays an important role in the formation of this morphology[67]. A few decades later a systematic review of the data on flow-induced crystallization of polymers accumulated during this period has supported the idea of stretching[72]. Finally this hypothesis has been confirmed by direct experimental measurements using linear-linear hydrogenated polybutadiene blends of controlled polydispersity, where a direct correlation between the Rouse time of long-chain molecules, the parameter describing stretching, and threshold conditions for the formation of oriented shish-kebab morphology has been demonstrated[61]. These results suggest that it is not enough just to orient the molecules along the flow to create a shish morphology, stretching has also to be induced in the molecules to form the shish. Thus, stretching should be considered as the first step in the formation of shish morphology (stage 1). If, however, the molecules were to be stretched by a very short shear pulse of duration comparable with the Rouse relaxation time of the molecules, then the molecules would relax into their original state, similar to quiescent conditions, with no signs of irreversible structural transformations. If the polymer were to be crystallized after this event, a spherulitic morphology would be formed (**Figure 1.11 b**) producing a characteristic ring in a SAXS pattern (**Figure 1.11 c**) corresponding to a periodical lamellar structure with a random orientation. Thus, stretching is a necessary condition, but not a sufficient condition, for the formation of shish-kebab morphology.

(2) Nucleation

Since the shish is a crystalline phase[48, 73], its formation should be initiated by the formation of crystal nuclei. It has been demonstrated in a set of previous studies on shear-induced crystallization that flow can induce nucleation in polymer melts[66, 74]. In accordance with classical nucleation theory[75] a stable nucleus is formed when its volume free energy exceeds its surface free energy by the value of volumetric free energy difference between liquid and crystalline phase (ΔG). The latter is considered as an energy barrier required for the nuclei of a critical size must jump over to become stable at a certain thermodynamic conditions. Under quiescent conditions $\Delta G = \Delta G_q$ is a temperature-dependent parameter, however, the polymer melt under flow conditions is supplied with additional energy which should be counted in the energy balance of the system. The effect of flow on the polymer melt can be described via an extra term (ΔG_f): $\Delta G = \Delta G_q + \Delta G_f$ [76]. This term reduces the energy barrier required for the nuclei to be stable and, therefore, increases the nucleation rate under certain thermodynamic conditions. Phenomenologically, the process of nucleation under flow conditions can be described as the following: the flow stretches polymer segments introducing conformational order into the polymer chains and also delivers one stretched segment to another until they collide and form an aggregate of stretched segments which is larger than the critical size of a stable nucleus (stage 2). These nuclei can be considered as point nuclei; however, some anisotropy should be present as they have been formed under directional conditions created by flow[77]. It would be useful to call these species shish nuclei to make them distinguishable from the general term of point nuclei used in scientific literature.

The number of stretched segments required for the formation of shish nuclei is controlled by both the critical size of the stable nucleus, which can be defined by a classical theory of nucleation[66, 75], and the length of stretched segments. The latter parameter should depend on both the molecular weight distribution of polymer, and in particular, on the molecular weight of long chains in multimodal blends, and on the flow rate applied to the polymer. The number of collisions of the stretched segments during the flow controls the formation of stable shish nuclei. This is a probabilistic

process, dependent on both the time of shearing (strain) and the concentration of stretched segments in the polymer ensemble. The stretched segments have to come into proximity in order to collide and, therefore, the relative distance between them should be changing (fluctuating). For a specific case where there are1770 kg / mol long-chain molecules in a bimodal linear hydrogenated polybutadiene blend (1 wt %), it can be estimated that at an overlap concentration of fluctuations of at least a radius of gyration of the molecules would be required to cause collisions of two neighbouring molecules (and, therefore, collisions of the stretched segments). However, this estimation does not exclude from consideration the possibility that the two stretched segments belong to one molecule.

The moment when the size of aggregates of stretched segments reaches the critical size of a stable nucleus should be considered as the nucleation stage (stage 2). At this stage the flow has had an irreversible effect on the polymer and after the cessation of the flow the polymer melt does not totally relax back to its original quiescent conditions as some molecules remain as crystal nuclei (unless the temperature of the melt is increased).

(3) Alignment

It has to be pointed out that the effect of the flow cannot be excluded from further consideration after the shish nuclei have been formed. There is a phase boundary between the melt and the nuclei making the nuclei act as a particle surrounded by viscoelastic liquid and there have been a number of studies on the behaviour of particles in viscoelastic liquids under flow conditions, which illuminate our discussion here. Adding particles to a nonlinear viscoelastic fluid, such as a polymer, can considerably increase the rheological complexity of the system[78] as exemplified by particle aggregation and flow-induced alignment[79]. It was suggested in earlier studies that the alignment of the particles occurred at high shear rates such that the Weissenberg number, that is the ratio of the first normal stress difference over the shear stress, exceeded a critical value[79]. However, later studies based on quantitative measurements by small-angle light scattering suggested that the Weissenberg number is not a sufficient condition and to a first approximation the particle alignment can be strain-

controlled[80]. Although, particle alignment is not fully understood, these observations indicate that a similar effect could occur with shear-induced nuclei, after their formation in the polymer melt (stage 3).

That alignment does indeed occur is supported by recent rheology measurements on shear-induced crystallization[81], which suggests that point nuclei form first and then, after reaching a saturation point, transform into another morphology corresponding to one dimensional (fibrillar) structure. Thus, following their initial formation, point nuclei require some time (strain) to align and aggregate further into fibrillar morphology. The existence of, and differentiation between, these separate stages can also be identified in the cross-section of solidified samples after shear-induced crystallization using a slot flow[68]. Since this geometry produces a range of shear rates across sheared samples (from wall to wall of the duct), the polymer melt experiences different flow conditions. Three distinctive layers separated by clear boundaries can be observed in such samples: a spherulitic core in the centre of the sample corresponding to small shear rates followed by a transitional fine grained layer (shish nuclei) at moderate shear rates and, finally, a highly oriented layer (fibrillar morphology) at high shear rates. Thus, there is a transitional stage before the formation of fibrils (shishes) during flow.

A further substantive argument towards the stage of alignment prior to the formation of the fibrillar (shish) morphology comes from SAXS observations. Three types of scattering patterns could be registered for polymers after shear-induced crystallization (**Figure 1.11 c**): a diffraction ring indicating spherulitic morphology, two strong reflections indicating oriented lamellar stacks with the layer normal parallel to the flow and a pattern corresponding to shish-kebab morphology with a streak parallel to the flow direction and two oriented reflections corresponding to kebabs with layer normal parallel to the flow direction. The second type of SAXS patterns, demonstrating oriented structure, is observed in polymers after flow-induced crystallization at moderate flow conditions prior to the conditions when the shish-kebab morphology is formed[60, 82, 83]. This observation suggests that some kind of structural orientation occurs in the sheared polymers before the formation of shish morphology. The phenomena of nuclei alignment enables the appearance of this orientation to be interpreted. In analogy with particle suspensions in viscoelastic liquids, shish nuclei, after their formation in the polymer melt, align along the flow direction forming rows of shish nuclei. After the

cessation of the flow, at this stage of shearing, the aligned shish nuclei initiate secondary nucleation followed by crystal growth during crystallization. Since the crystals begin growing simultaneously along the whole row of shish nuclei, the neighbouring crystals impinge each other from the very beginning of crystallization causing directional growth of the lamellar stacks producing distorted spherulites similar to kebabs (**Figure 1.11 b**). It has to be pointed out that the concentration of shish nuclei induced by flow at this stage is low[84], and/or that the shish are very short, and thus undetectable during the flow by means of commonly-used techniques (optical methods, rheology or structural methods such as X-ray scattering). Therefore even if on-line SAXS measurements do not register any structural organization during the flow, the oriented morphology is detectable after the cessation of flow as the growing crystals of bulk material inherit the structural morphology of the aligned shish nuclei during the crystallization process. This structure generates SAXS patterns of the second type (**Figure 1.11 c**). The shish nuclei act in a homeopathic manner, that is leaving their imprint on the fluid whilst being essentially undetectable .

It has to be noted that the transition from stage 2 to stage 3 is rather tentative. Straight after the formation of the first shish nuclei in the polymer melt these nuclei tend to align under flow conditions and, therefore, stage 2 and stage 3 coexist together in the sheared material. Thus, time intervals of the two stages overlap and their effect on the crystallized material should be considered together (**Figure 1.11 b**). However, stage 3 cannot exist without stage 2 and the separation is clearly exemplified in optical micrographs of materials crystallised following a slot flow.[68]

(4) Fibrillation

If the shearing continues then the rows of aligned nuclei, in analogy with the suspension of particles in viscoelastic liquids[80], should accumulate into larger aggregates with the growing concentration of shish nuclei. This aggregation causes reduction of the free surface of separated nuclei making the aggregates energetically more favourable in comparison with rows of separated shish nuclei. While the particles in viscoelastic liquids remain as separated objects after aggregation, the phase boundary between

aggregated shish nuclei should disappear, transforming the aggregates into single elongated objects corresponding to the formation of fibrillar (shish) morphology (stage 4). Since the cross-section of the fibrils is larger than the shish nuclei and the total concentration of crystalline material is growing during shear, the formation of fibrillar morphology can be easily detected on-line by increasing birefringence[38, 66, 85] and/or by an streak oriented parallel to the flow in arising SAXS patterns[48, 70, 73]. It can be noted that the formation of elongated objects such as fibrils should significantly affect the rheological properties of the polymer melt[86]. A clear boundary observed between the fine grained layer (aligned shish nuclei) and the layer corresponding to highly oriented fibrillar morphology in the polymers after shear-induced crystallization in a slot flow is probably associated with a sudden change of rheological properties of the polymer melt when the fibrils (shishes) are formed (**Figure 1.12**)[68].

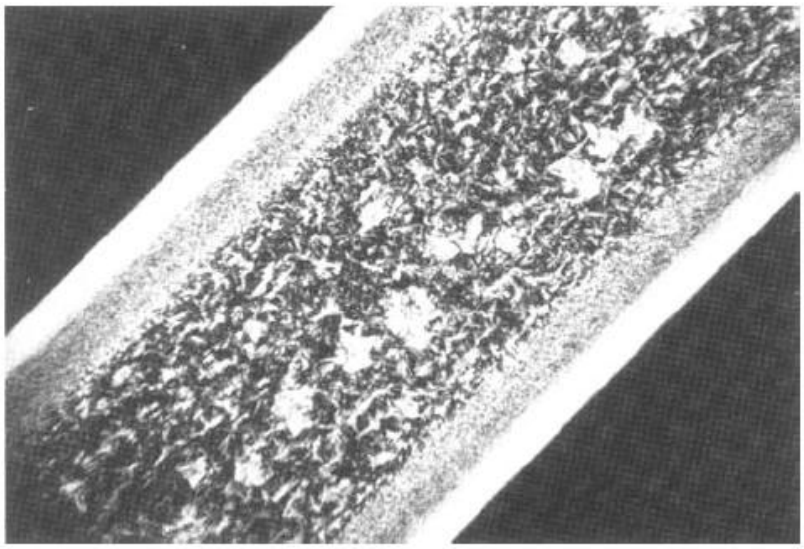

Figure 1.12. Cross-section through a quenched sample of an industrial polypropylene after short term extrusion at 150 °C.[68] (reproduced with permission)

After the cessation of the flow, the formed fibrils (shishes) work as nucleating agents for the rest of polymer melt causing crystallization of kebabs (**Figure 1.11b**). The final shish-kebab morphology can be identified by a SAXS pattern composed of two features: a streak parallel to the flow direction associated with the shishes and two reflections corresponding to lamellae with the layer normal parallel to the flow - kebabs

(**Figure 1.11 c**) and all three of these generic SAXS patterns can be observed if a x-ray beam is scanned across the vorticity direction in a slot flow.

1.5.3. Introduction of the idea of mechanical work

Following the discussion of the model for the formation of oriented structures two parameters have to be identified as responsible for the formation of the morphology indicated by stage 1 and stage 2 (together with stage 3) describing the stretching of the molecules and the formation of stable shish nuclei, respectively. The first parameter is associated with the Rouse time of the molecules and can be described as the minimum shear rate required for the molecules to be in a stretched state under flow conditions. This is the necessary condition for the formation of shish nuclei. Assuming that $De = \tau_R \dot{\gamma} = 1$, where *De* is the Deborah number[72], the minimum shear rate required for the stretching can be estimated as $\dot{\gamma}_{\min} = 1/\tau_R$. The second parameter describes the formation of stable shish nuclei. In accordance with the general concept of crystallization proposed by Willard Gibbs[87] the stability of a phase is related to the work that has to be done in order to create a critical nucleus of the new phase. Thus, the second parameter should be associated with the amount of work performed by the flow on the polymer system to build the nuclei from stretched segments of the molecules and stabilize the nuclei under certain thermodynamic conditions. It has been demonstrated that the number of nuclei tremendously increase with the amount of mechanical work applied to the system[74, 84], which can be expressed as a mechanical specific work $w = \int_0^{t_s} \eta[\dot{\gamma}(t)]\dot{\gamma}^2(t)dt$, where $\eta[\dot{\gamma}(t)]$ is the viscosity and $\dot{\gamma}(t)$ is the shear rate profile experienced by the polymer during shearing. If the shear rate is constant with time then the formula can be rewritten in a more simple version $w = \eta(\dot{\gamma})\dot{\gamma}^2 t_s$[70]. However, the shear rate used in experiments is not constant and has a certain acceleration (and deceleration) due to the capability of the motor used to apply the shear. The integral function to calculate the work can includes this acceleration and deceleration region of the used shear protocol.

The formation of an oriented morphology (stage 3) occurs straight after the formation of shish nuclei indicated by stage 2 (**Figure 1.11 a**). Coexistence of these two stages

during flow makes them indistinguishable from each other. It can be assumed that the orientation can be detected straight after the formation of point nuclei and, therefore, the work parameter can also be associated with the threshold conditions for the initial orientation. In this respect it is noteworthy to mention the discussion on the formation of shish precursors, where it has been suggested that long lasting deformations under low stresses can yield the same precursors as short term deformations under high loads. It can be concluded that that the applied specific work should be constant in both cases and be used as the universal parameter to describe the process[69]. This conclusion drawn for the precursors has found direct confirmation in the measurements of specific work for the onset of oriented morphology in the shear-induced polymer melts[61]. The direct measurements of the flow parameters for the onset of oriented morphology after shear-induced crystallization enable a diagram of parameters responsible for the formation of oriented morphology to be built (**Figure 1.13**) where the shear rate associated with the onset of orientation, $\dot{\gamma}_b(t)$, is plotted versus corresponding specific work

$$w_b = \int_0^{t_s} \eta[\dot{\gamma}_b(t)]\dot{\gamma}_b^2(t)dt .$$

This diagram has shown that two parameters can be used to describe the conditions for the formation of oriented morphology: the minimum shear rate associated with the reciprocal Rouse time of the long chains present in the polymer ensemble, $\dot{\gamma}_{min}$, and the critical specific work, w_c, which is constant at shear rates $\dot{\gamma} > \dot{\gamma}_{min}$. These two parameters can be used to calculate flow conditions, profile of shear or extensional flow rate and time of shearing under particular thermodynamic conditions (temperature and pressure) for the formation of oriented morphology in polymers under flow. This approach has been successfully applied in the analysis of flow-induced crystallization in geometries resembling elements of industrial polymer processing[88].

The diagram obtained for the bimodal polymer blends shows a clear threshold at a minimum shear rate below which the formation of oriented morphology is unlikely and the specific work tends to be infinite (**Figure 1.13 a**). The line of critical specific work should be associated with stage 2 (and stage 3) when the shish nuclei are formed. The oriented morphology caused by these nuclei, oriented along the flow direction, can be detected after crystallization. When the amount of work experienced by the polymer

melt increases, the shish nuclei become more numerous and the degree of orientation of the crystallized structure increases[61, 70]. At this point, stage 3 approaches stage 4 (**Figure 1.11 a**) as the high concentration of nuclei rows oriented along the flow directions transform into fibrillar (shish) morphology and the shish can be detected during the shear flow by the observation of meridional streak in SAXS (**Figure 1.11 c**) and/or by the irreversible increase of birefringence of the sheared polymer melt[38, 66, 85].

Polymers of broad polydispersity exhibit SIC behaviour similar to the model blends of controlled polydispersity (**Figure 1.13 b**)[70]. There is the same constant plateau of critical specific work within the wide range of shear rates; however, the threshold for the minimum shear rate is not as well defined as for the model blends. It is still possible to identify a minimum shear rate below which the specific work required for the formation of oriented morphology is not constant. The increase of the specific work at $\dot{\gamma} < \dot{\gamma}_{\min}$ is associated with the fact that the polydisperse system has a broad and continuous molecular weight distribution and there will always be some polymers long enough to initiate shish nuclei formation even at vanishing small shear rates. Since only longer molecules, characterized by a longer relaxation time, can be stretched at lower shear rates, the increase of the specific work at shear rates below $\dot{\gamma}_{\min}$ is associated with the concentration of long chain molecules available in the polymer ensemble for the stable nuclei formation. Thus, this increase should be related to the molecular weight distribution of the polymer. The minimum shear rate for polydisperse systems cannot be related to a Rouse time of particular molecules like in the bimodal blends, and should be rather considered as an averaged value characterising the ensemble of molecules present in the polymer.

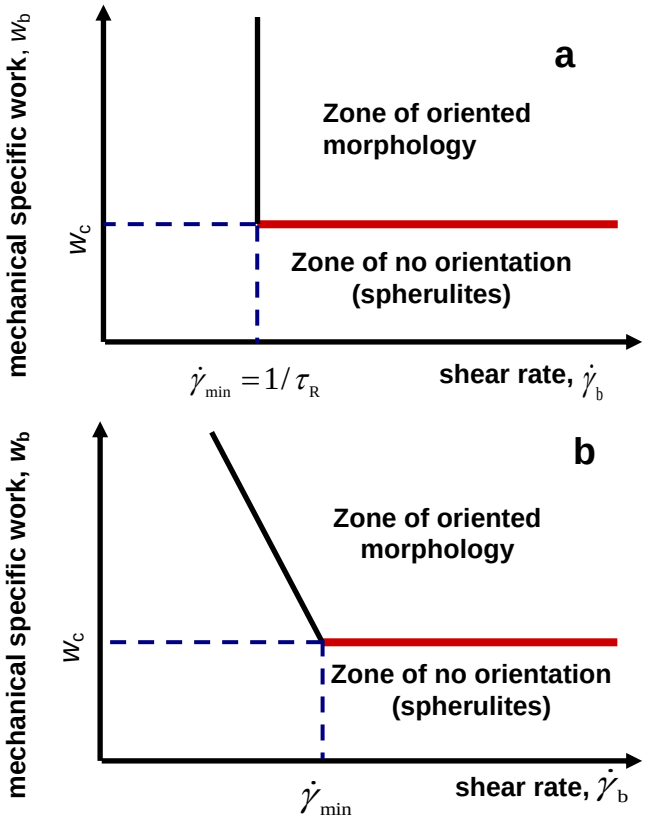

Figure 1.13. Schematic diagrams of threshold conditions for the formation of oriented morphology in the melts of bimodal polymer blends of long chain molecules in a short chain matrix (a) and polydisperse polymers (b) under flow conditions. The solid line dividing the diagram into two zones (a zone of orientation and a zone of no orientation) corresponds to a plot of the boundary specific work required for the formation of aligned shish nuclei (stage 2 and stage 3 in **Figure 1.11**), w_b, as a function of the boundary shear flow rate, $\dot{\gamma}_b$. The critical specific work, w_c, indicates the minimum amount of the specific work required for the formation of oriented nuclei at the chosen thermodynamic parameters. The minimum shear rate $\dot{\gamma}_{min}$ indicates the flow rate below which the concentration of molecules in a stretched state decreases.

1.6. Aim of this research

The understanding of the need for achieving $\dot{\gamma}_{min}$ in the formation of the oriented morphology in polymers is demonstrated by the reported research, thus far the link between the boundary flow conditions involving a required minimum strain between the bimodal blends and polydisperse polymers needs further consideration. In order to find the link between bimodal blends and polydisperse polymers, the most critical problem is

the interaction of many kinds of polymer chains with different molecular weight in polydisperse polymers.

The first aim of this study is to understand the interaction between long chains with different molecular weight in a model trimodal blend and illuminate how the interaction between polymer chains affects the boundary flow conditions in polydisperse polymers (**Figure 1.14, (1)**). The second aim of this study is to elucidate the effect of the molecular weight of a matrix in model bimodal blends on the specific work in order to identify the effect on the specific work by the long chains on its own (**Figure 1.14, (2)**).

1.7. Outline of the thesis

We investigate the flow induced crystallization in hydrogenated polybutadiene multi-modal blends. Commonly used experimental methods through the thesis such as sample preparation, differential scanning calorimetry, rheology, shear experiments, structural analysis and the calculation of specific work are summarized in Chapter 2.

The characterization of the low-polydispersity hydrogenated polybutadiene materials had been carried out before the experiments of the multi-modal blends were started. Relaxation times of the low polydisperse materials were obtained by the fitting of experimentally measured G' and G" by using the Linear theory, see Chapter 3.

The structural analysis of the sheared bimodal blend by using direct method was carried out in order to indicate the relationship between the flow conditions and oriented morphology further (Chapter 4).

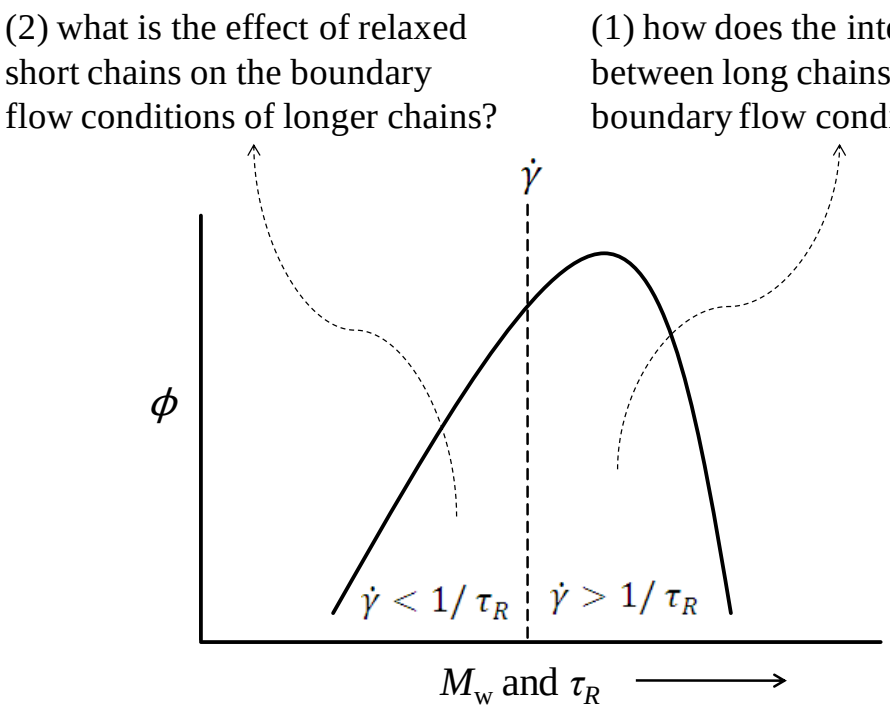

Figure 1.14. Explanation drawings of the open questions in this research. The curve in the figure shows molecular weight distribution of polydisperse polymers. A dashed line shows the magnitude of shear rate applying to the polydisperse polymer. The right area from the dashed line indicates long chains which can be stretched by the shear due to the relatively long relaxation times. The left area from the dashed line indicates short chains which cannot be stretched by the shear.

Experiments on the multi-modal blends can be divided into 2 parts. Firstly, the boundary conditions of hydrogenated polybutadiene trimodal blends were measured and compared to the conditions of the bimodal blends and polydisperse materials in order to elucidate the mechanism of flow induced crystallization in polydisperse polymers. This part mainly focused on the interaction between long chains with different molecular weight (Chapter 5). Secondly, bimodal blends having different length of short chains were prepared and the boundary conditions of them were measured in order to know the effect of viscosity of the blends on the boundary flow conditions (Chapter 6).

1.8. References

1. The Compelling Facts About Plastics 2007; An analysis of plastics production, demand and recovery for 2007 in Europe. http://www.plasticseurope.org/ (08/2009),
2. Warzelhan, V.; Brandstetter, F. *Macromol. Symp.* **2003,** 201, 291-300.
3. Arriola, D. J.; Carnahan, E. M.; Hustad, P. D.; Kuhlman, R. L.; Wenzel, T. T. *Science* **2006,** 312, 714-719.
4. Coates, G. W.; Waymouth, R. M. *Science* **1995,** 267, 217-219.
5. Guan, Z.; Cotts, P. M.; McCord, E. F.; McLain, S. J. *Science* **1999,** 283, 2059-2062.
6. Kageyama, K.; Tamazawa, J.-i.; Aida, T. *Science* **1999,** 285, 2113-2115.
7. Ziegler, K. *Angewandte Chemie* **1952,** 64, (12), 323-329.
8. Natta, G. *Journal of Polymer Science* **1955,** 16, (82), 143-154.
9. Natta, G.; Corradini, P. *Atti accad. nazl. Lincei, Mem.* **1955,** 8, 73-80.
10. Kaminsky, W. *Journal of Polymer Science Part A: Polymer Chemistry* **2004,** 42, (16), 3911-3921.
11. Natta, G. **1963**.
12. Szwarc, M. *Nature (London, U. K.)* **1956,** 178, 1168-9.
13. Hadjichristidis, N.; Iatrou, H.; Pispas, S.; Pitsikalis, M. *J. Polym. Sci: Part A: Polymer Chem.* **2000,** 38, 3211-3234.
14. Doi, Y.; Yano, A.; Soga, K.; Burfield, D. R. *Macromolecules* **1986,** 19, 2409.
15. Rachapudy, H.; Smith, G. G.; Raju, V. R.; Graessley, W. W. *J. Polym. Sci., Polym. Phys.* **1979,** 17, 1211.
16. Crist, B.; Howard, P. R. *Macromolecules* **1999,** 32, (9), 3057-3067.
17. Stevenson, J. F., 10 Extrusion of Rubber and Plastics. In *COMPREHENSIVE POLYMER SCIENCE, 7, Speciality Polymers & Polymer Processing*, Aggarwal, S. L., Ed. Pergamon Press: Oxford, UK, 1989; pp 303-354.
18. Morrison, F. A., *UNDERSTANDING Rheology*. Oxford University Press: Oxford, UK, 2001; p 382-392.
19. Blackadder, D. A.; Schleinitz, H. M. *Nature* **1963,** 200, 778-779.
20. Pennings, A. J.; Kiel, A. M. *Kolloid Z. Z. Polym.* **1965,** 205, 160-162.
21. Keller, A.; Machin, M. J. *J. Macromolec. Sci. B* **1967,** 1, 41-91.
22. Keller, A.; Kolnaar, H. W. H., Part II: Structure Development During Processing, 4 Flow-Induced Orienttion and Structure Formation In *Materials Science and Technology; A Comprehensive Treatment, Vol.18, Processing of Polymers*, Meijer, H. E. H., Ed. WILEY-VCH: Weinheim, Germany, 1997; pp 189-268.
23. Mykhaylyk, O. O.; Chambon, P.; Graham, R. S.; Fairclough, J. P. A.; Olmsted, P. D.; Ryan, A. J. *Macromolecules* **2008,** 41, 1901-1904.

24. Zuo, F.; Keum, J. K.; Yang, L.; Somani, R. H.; Hsiao, B. S. *Macromolecules* **2006,** 39, 2209-2218.

25. Coppola, S.; Grizzuti, N. *Macromolecules* **2001,** 34, 5030-5036.

26. Mykhaylyk, O. O.; Chambon, P.; Graham, R. S.; Fairclough, J. P. A.; Olmsted, P. D.; Ryan, A. J. *Macromolecules* **2008,** 41, 1901-1904.

27. Heeley, E. L.; Fernyhough, C. M.; Graham, R. S.; Olmsted, P. D.; Inkson, N. J.; Embery, J.; Groves, D. J.; McLeish, T. C. B.; Morgovan, A. C.; Meneau, F.; Bras, W.; Ryan, A. J. *Macromolecules* **2006,** 39, 5058-5071.

28. Yang, L.; Somani, R. H.; Sics, I.; Hsiao, B. S.; Kolb, R.; Fruitwala, H.; Ong, C. *Macromolecules* **2004,** 37, 4845-4859.

29. Hobbs, J. K.; Humphris, A. D. L.; Miles, M. J. *Macromolecules* **2001,** 34, 5508-5519.

30. Scelsi, L.; Mackley, M. R. *Rheol. Acta* **2008,** 47, 895-908.

31. Devaux, N.; Monasse, B.; Haudin, J.-M.; Moldenaers, P.; Vermant, J. *Rheol. Acta* **2004,** 43, (3), 210-222.

32. Janeschitz-Kriegl, H.; Eder, G. *J. Macromol. Sci., Part B: Phys.* **2007,** 46, (3), 591-601.

33. Jerschow, P.; Janeschitz-Kriegl, H. *Int. Polym. Process.* **1997,** 12, (1), 72-77.

34. Kumaraswamy, G.; Issaian, A. M.; Kornfield, J. A. *Macromolecules* **1999,** 32, (22), 7537-7547.

35. Muthukumar, M. *Adv. Chem. Phys.* **2003,** 128, 1-63.

36. Nogales, A.; Hsiao, B. S.; Somani, R. H.; Srinivas, S.; Tsou, A. H.; Balta-Calleja, F. J.; Ezquerra, T. A. *Polymer* **2001,** 42, (12), 5247-5256.

37. Pogodina, N. V.; Winter, H. H.; Srinivas, S. *J. Polym. Sci., Part B: Polym. Phys.* **1999,** 37, (24), 3512-3519.

38. Seki, M.; Thurman, D. W.; Oberhauser, J. P.; Kornfield, J. A. *Macromolecules* **2002,** 35, (7), 2583-2594.

39. Somani, R. H.; Yang, L.; Hsiao, B. S. *Physica A (Amsterdam, Neth.)* **2002,** 304, (1-2), 145-157.

40. Van der Beek, M. H. E.; Peters, G. W. M.; Meijer, H. E. H. *Macromolecules* **2006,** 39, (5), 1805-1814.

41. Yamazaki, S.; Watanabe, K.; Okada, K.; Yamada, K.; Tagashira, K.; Toda, A.; Hikosaka, M. *Polymer* **2005,** 46, (5), 1685-1692.

42. Ziabicki, A.; Alfonso, G. C. *Macromol. Symp.* **2002,** 185, (Flow-Induced Crystallization of Polymers), 211-231.

43. Zuidema, H.; Peters, G. W. M.; Meijer, H. E. H. *Macromol. Theory Simul.* **2001,** 10, (5), 447-460.

44. Fukushima, H.; Ogino, Y.; Matsuba, G.; Nishida, K.; Kanaya, T. *Polymer* **2005,** 46, 1878-1885.

45. Ogino, Y.; Fukushima, H.; Takahashi, N.; Matsuba, G.; Nishida, K.; Kanaya, T. *Macromolecules* **2006,** 39, 7617-7625.

46. Hill, M. J.; Barham, P. J.; Keller, A. *Colloid & Polymer Science* **1980,** 258, 1023-1037.

47. Seki, M.; Thurman, D. W.; Oberhauser, J. P.; Kornfield, J. A. *Macromolecules* **2002,** 2002, 2538-2594.

48. Keum, J. K.; Zuo, F.; Hsiao, B. S. *Macromolecules* **2008,** 41, (13), 4766-4776.

49. Hill, M. J.; Barham, P. J.; Keller, A. *Colloid & Polymer Science* **1983,** 261, 721-735.

50. Hill, M. J.; Keller, A. *Colloid & Polymer Science* **1981,** 281, 335-341.

51. Hobbs, J. K. *Polymer* **2006,** 47, 5566-5573.

52. Hermans, P. H., *Contribution to the Physics of Cellulose Fibres*. Elsevier: Amsterdam, Netherlands, 1946; p 221.

53. Ryan, A. J.; Fairclough, J. P. A.; Terrill, N. J.; Olmsted, P. D.; Poon, W. C. K. *Faraday Discuss.* **1999,** 112, 13-29.

54. Terrill, N. J.; Fairclough, P. A.; Towns-Andrews, E.; Komanschek, B. U.; Young, R. J.; Ryan, A. J. *Polymer* **1998,** 39, 2381-2385.

55. Bent, J.; Hutchings, L. R.; Richards, R. W.; Gough, T.; Spares, R.; Coates, P. D.; Grillo, I.; Harlen, O. G.; Read, D. J.; Graham, R. S.; Likhtman, A. E.; Groves, D. J.; Nicholson, T. M.; McLeish, T. C. B. *Science* **2003,** 301, 1961-1965.

56. Rouse, P. E. *Journal of Chemical Physics* **1953,** 21, (7), 1272-1280.

57. Doi, M.; Edwards, S. F., *The Theory of Polymer Dynamics*. Oxford University Press: Oxford, UK, 1986.

58. Larson, R. G.; Sridhar, T.; Leal, L. G.; McKinley, G. H.; Likhtman, A. E.; McLeish, T. C. B. *J. Rheol.* **2003,** 47, 809-818.

59. Kukalyekar, N.; Balzano, L.; Peters, G. W. M.; Rastogi, S.; Chadwick, J. C. *Macromolecular Reaction Engineering* **2009,** 3, (8), 448-454.

60. Heeley, E. L.; Fernyhough, C. M.; Graham, R. S.; Olmsted, P. D.; Inkson, N. J.; Embery, J.; Groves, D. J.; McLeish, T. C. B.; Morgovan, A. C.; Meneau, F.; Bras, W.; Ryan, A. J. *Macromolecules* **2006,** 39, (15), 5058-5071.

61. Mykhaylyk, O. O.; Chambon, P.; Graham, R. S.; Fairclough, J. P. A.; Olmsted, P. D.; Ryan, A. J. *Macromolecules* **2008,** 41, (6), 1901-1904.

62. Hill, M. J.; Keller, A. *Journal of Macromolecular Science-Physics* **1971,** B 5, (3), 591-&.

63. Keller, A. *Nature* **1954,** 174, (4437), 926-927.

64. Pennings, A. J.; Kiel, A. M. *Kolloid-Zeitschrift and Zeitschrift Fur Polymere* **1965,** 205, (2), 160-&.

65. Hill, M. J.; Keller, A. *Journal of Macromolecular Science-Physics* **1969,** B 3, (1), 153-&.

66. Eder, G.; Janeschitzkriegl, H.; Liedauer, S. *Progress in Polymer Science* **1990,** 15, (4), 629-714.

67. Keller, A.; Kolnaar, H. W., Flow induced orientation and structure formation. In *Materials Science and Technology, Processing of Polymers*, Meijer, H. E. M., Ed. Wiley-VCH: New York, 1997; pp 189-268.

68. Janeschitz-Kriegl, H. *Monatshefte Fur Chemie* **2007,** 138, (4), 327-335.

69. Janeschitz-Kriegl, H.; Eder, G. *Journal of Macromolecular Science Part B-Physics* **2007,** 46, (3), 591-601.

70. Mykhaylyk, O. O.; Chambon, P.; Impradice, C.; Fairclough, J. P. A.; Terrill, N. J.; Ryan, A. J. *Macromolecules* **2010,** 43, (5), 2389-2405.

71. Stadlbauer, M.; Janeschitz-Kriegl, H.; Eder, G.; Ratajski, E. *Journal of Rheology* **2004,** 48, (3), 631-639.

72. van Meerveld, J.; Peters, G. W. M.; Hutter, M. *Rheologica Acta* **2004,** 44, (2), 119-134.

73. Balzano, L.; Kukalyekar, N.; Rastogi, S.; Peters, G. W. M.; Chadwick, J. C. *Physical Review Letters* **2008,** 100, (4).

74. Janeschitz-Kriegel, H.; Ratajski, E. *Polymer* **2005,** 46, (11), 3856-3870.

75. Becker, R.; Doring, W. *Annalen Der Physik* **1935,** 24, (8), 719-752.

76. Coppola, S.; Grizzuti, N.; Maffettone, P. L. *Macromolecules* **2001,** 34, (14), 5030-5036.

77. Graham, R. S.; Olmsted, P. D. *Physical Review Letters* **2009,** 103, (11).

78. Metzner, A. B. *Journal of Rheology* **1985,** 29, (6), 739-775.

79. Michele, J.; Patzold, R.; Donis, R. *Rheologica Acta* **1977,** 16, (3), 317-321.

80. Scirocco, R.; Vermant, J.; Mewis, J. *Journal of Non-Newtonian Fluid Mechanics* **2004,** 117, (2-3), 183-192.

81. Housmans, J. W.; Steenbakkers, R. J. A.; Roozemond, P. C.; Peters, G. W. M.; Meijer, H. E. H. *Macromolecules* **2009,** 42, (15), 5728-5740.

82. Kumaraswamy, G.; Verma, R. K.; Kornfield, J. A.; Yeh, F. J.; Hsiao, B. S. *Macromolecules* **2004,** 37, (24), 9005-9017.

83. Ogino, Y.; Fukushima, H.; Takahashi, N.; Matsuba, G.; Nishida, K.; Kanaya, T. *Macromolecules* **2006,** 39, (22), 7617-7625.

84. Janeschitz-Kriegl, H.; Ratajski, E.; Stadlbauer, M. *Rheologica Acta* **2003,** 42, (4), 355-364.

85. Baert, J.; Van Puyvelde, P.; Langouche, F. *Macromolecules* **2006,** 39, (26), 9215-9222.

86. Macosko, C. W., In *Rheology: principles, measurements, and applications*, VCH Publishers, Inc.: New York, 1994; pp 83-92.

87. Gibbs, J. W., *The Scientific Papers of J. Willard Gibbs*. Dover Publications: New York, 1961; Vol. 1, p 434.

88. Scelsi, L.; Mackley, M. R.; Klein, H.; Olmsted, P. D.; Graham, R. S.; Harlen, O. G.; McLeish, T. C. B. *Journal of Rheology* **2009,** 53, (4), 859-876.

Chapter 2

Methodology

2.1. Introduction

The methodology of this study is quite important because the materials used and way to measure boundary flow conditions was inherent in this research. There are the following four key points in the methodology. Firstly, the materials used in this study were synthesized in our group and have well-controlled primary structure to control their crystallinity. Secondly, a parallel-plate geometry was used to apply a shear to the samples for "combinatorial approach" to measure the boundary flow conditions. Thirdly, polarized light imaging (PLI) techniques were used to distinguishing the boundary positions in the sheared samples conveniently. Finally, a boundary specific work and critical specific work were used to discuss the boundary flow conditions of the materials. The detail of them is mentioned in this chapter.

2.2. Low-polydispersity h-PBD samples

2.2.1. Synthesis

Polymer materials used in this research are hydrogenated polybutadiene (h-PBD) synthesized in our group. The synthesis method was based on the method reported by Fernyhough et al.[1] The h-PBD samples have some residue double bond units (less than 1 %) and 7 ethyl branch units per 100 butadiene units (**Figure 2.1**). A series of h-PBD samples have similar melting point in spite of their different molecular weight, because lamellae crystals which form in the samples have a homogeneous thickness due to the branches. In addition, the samples have a relatively high transparency because of the low crystallinity due to the 7 % of branches.

Table 2.1 indicates the molecular weight of the low-polydispersity h-PBD materials. Molecular weight measurements were carried out by DOW Benelux B.V. by using a high temperature size exclusion chromatography.[2] As shown in the list, all of them have adequately low polydispersity.

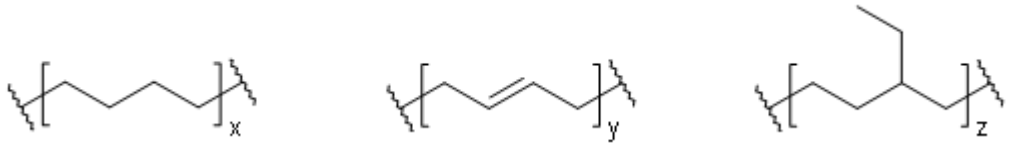

Figure 2.1. Structural information of synthesized h-PBD. The percentages under the chemical structure indicates the existing probability per a butadiene unit.

Table 2.1. The h-PBD samples used in this study.

Sample Label	M_n kDa	M_w kDa	Polydispersity (M_w / M_n)
7 kDa*1	7.20	7.25	-
18 kDa	-	18	-
52 kDa	46	52	1.13
147 kDa	136	147	1.08
442 kDa	398	442	1.11
1080 kDa*1	940	1080	1.15
1330 kDa	950	1330	1.40
1770 kDa	1200	1770	1.48

*1: The M_n and M_w value were measured before hydrogenation.

2.2.2. DSC measurement

Thermal properties are important in deciding a temperature to measure rheological parameters and a shearing temperature to perform shear crystallization measurements. The thermal properties such as melting point and crystallization temperature can be measured by using the DSC.

The PerkinElmer DSC was used to measure the thermal properties. Before the measurements, temperature and heat capacity are calibrated by the measurements of indium and zinc. Then the measurements were carried out under N_2 flow by using from 5 to 10 mg of sample. The measurement conditions are shown in the **Table 2.2**. The

data obtained by the 1st step was not used to avoid the effect of the thermal history at synthesis phase.

Table 2.2: The temperature protocol of the DSC measurements.

	initial temperature ºC	final temperature ºC	heating rate ºC / min	evaluated parameter
1st step	0	150	10	(T_m)
2nd step	150	0	-10	T_c
3rd step	0	150	10	T_m

2.2.3. Rheology measurements

There are two aims for rheology measurements of the low-polydispersity h-PBD samples.
Firstly, the relaxation times of the low-polydispersity h-PBD samples are calculated from their storage modulus and loss modulus obtained by the rheology measurements. Secondly, the viscosity of multi-modal blends is required to calculate the boundary specific work.

Rheometer AR-G2 is used to perform the rheology measurements. Although various geometries can be attached the rheometer, a cone-plate[3] or plate-plate geometry[4, 5] were used to measure the rheological parameters of the h-PBD samples in this study (**Figure 2.2**).

The diameter of the fixtures can be chosen from 8 mm and 25 mm. When the viscosity of the sample is low, it is required to use the 25 mm diameter to obtain enough torque to measure the viscosity precisely. The geometry with 8 mm diameter is used for viscous samples in order to save on the amount of material used.

Figure 2.2. Cone-plate geometry (a) and plate-plate geometry (b).

The principal of the rheometer is as follows. When a certain strain is applied to a loaded sample, a stress will be generated with a certain phase difference. The stress is measured as the torque by the rheometer. The **Figure 2.3** shows the relationship between the strain and stress. A storage modulus, *G*', can be calculated from the amplitude of the strain and stress. On the other hand, a loss modulus, *G*'', can be calculated from the phase difference and the amplitude of the strain and the stress. A complex viscosity, $|\eta^*|$, is indicated as follows by using angular frequency ω.

$$|\eta^*| = \sqrt{\left(\frac{G\prime}{\omega}\right)^2 + \left(\frac{G\prime\prime}{\omega}\right)^2} \qquad \textbf{Eq. 2.1}$$

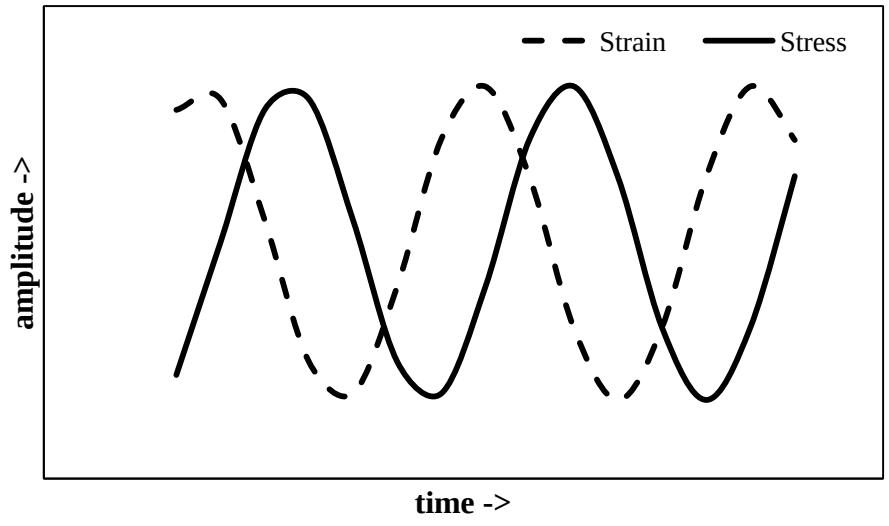

Figure 2.3. Relationship between an inputted strain and measured stress.

There are three measurement programs used in the rheology measurements in this study. The first program is a frequency sweep which is used to decide the relaxation times of the low-polydispersity polymers and complex viscosity of the blends by measuring the *G*', *G*" and complex viscosity toward angular frequency. The second program is a strain sweep program which is performed to decide a strain used for the frequency sweep. The third program is a start-up shear program which can be also used to decide the relaxation times by the viscosity measurements at a non-linear region.

In general, the frequency sweep is carried out at appropriate strain region which is called a linear region[6] (**Figure 2.4**). In this region, the rheology parameters such as *G*', *G*" and viscosity have linear relationship towards angular frequency and temperature. In a non-linear region, the viscosity starts to decrease with the increase of strain.

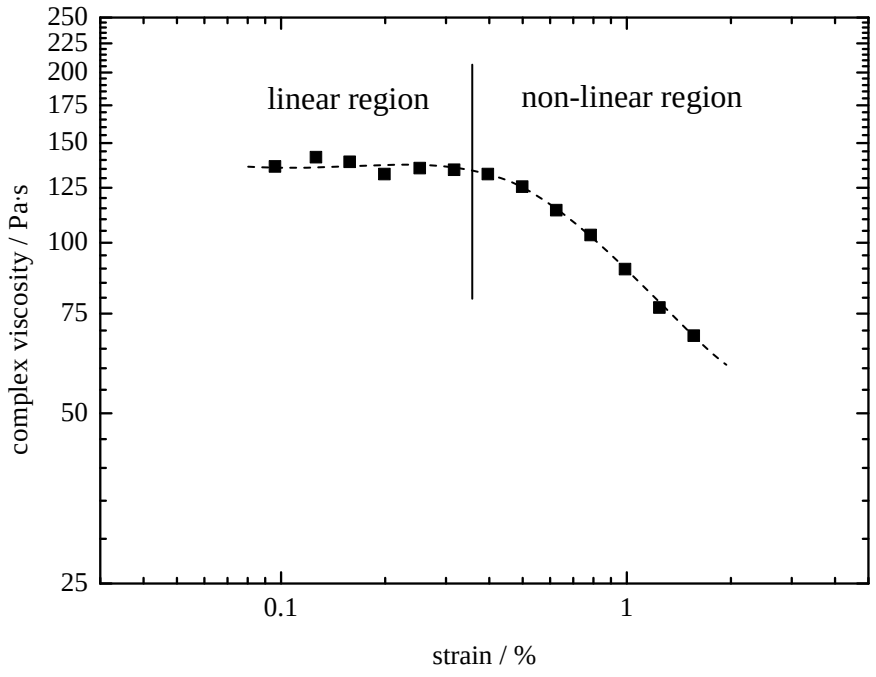

Figure 2.4. The example of linear region and non-linear region.

When the frequency sweep is performed, for the accuracy of the viscosity curve, at least three viscosity curves should be measured (**Figure 2.5 a**) at different temperatures and merged as a master curve (**Figure 2.5 b**) by the time-temperature superposition (TTS). The viscosity curve at the required temperature can also be calculated by the TTS of the master curve. The equation used for the TTS is the Williams-Landel-Ferry (WLF) equation.

$$\log_{10} a_{\mathrm{T}} = \frac{-C_1(T-T_{\mathrm{ref}})}{C_2(T-T_{\mathrm{ref}})} \qquad \textbf{Eq. 2.2}$$

The precise WLF parameters C_1, C_2 and T_{ref} can be obtained by optimizing of the TTS for the rheology data which was measured by using the frequency sweep. This procedure is quite popular and has been explained in many reference books.[7-10]

On the other hand, the start-up shear programs also can be used to calculate the relaxation times. The behaviour of the transition from non-steady shear to steady shear depends on relaxation time and shear rate. Therefore, a certain shear is applied to a sample continuously by using the cone-plate geometry. The transition from non-steady shear region to steady shear region is measured (**Figure 2.6**) and fitted by the Rolie-poly model[11]. In this thesis, the relaxation times of the h-PBD samples were estimated by both the linear and non-linear rheology for the comparison of the relaxation times.

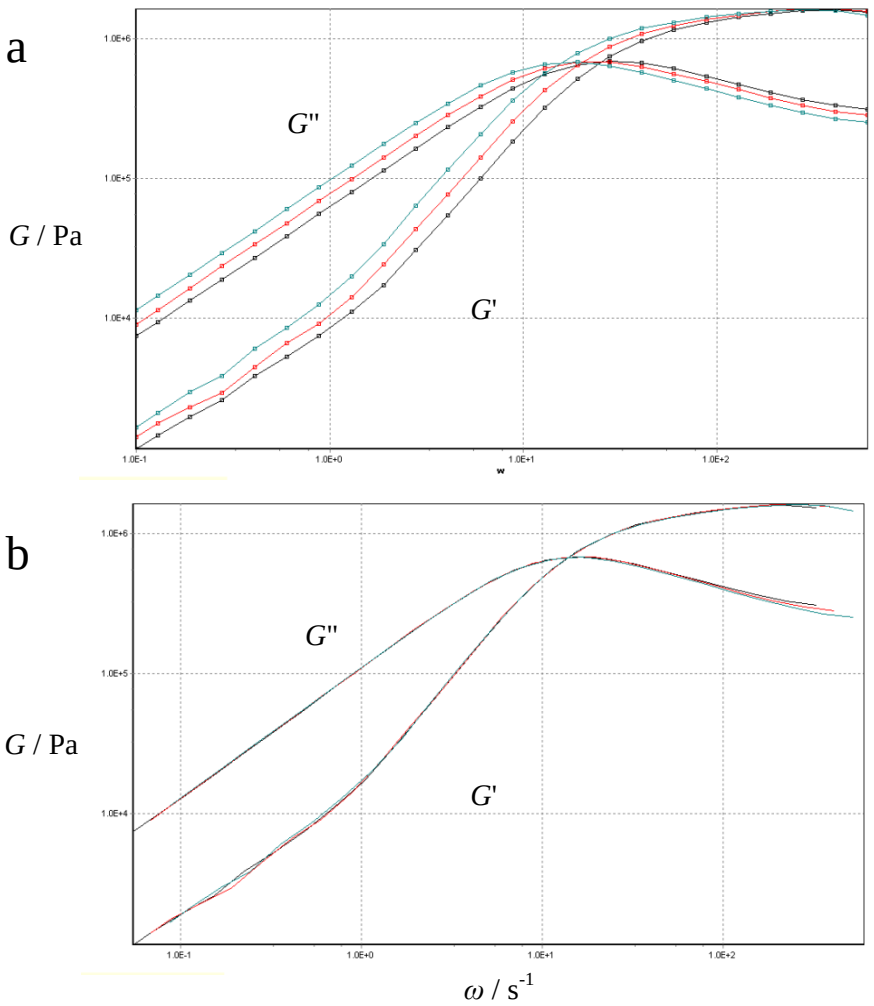

Figure 2.5. The example of time-temperature-superposition (TTS). The X-axis is angular frequency and the Y-axis is storage modulus, *G*', and loss modulus, *G*". The *G*' and *G*" curve of a sample were measured at three different temperatures (a). The master curve was created by the fitting using Williams-Landel-Ferry equation (b).

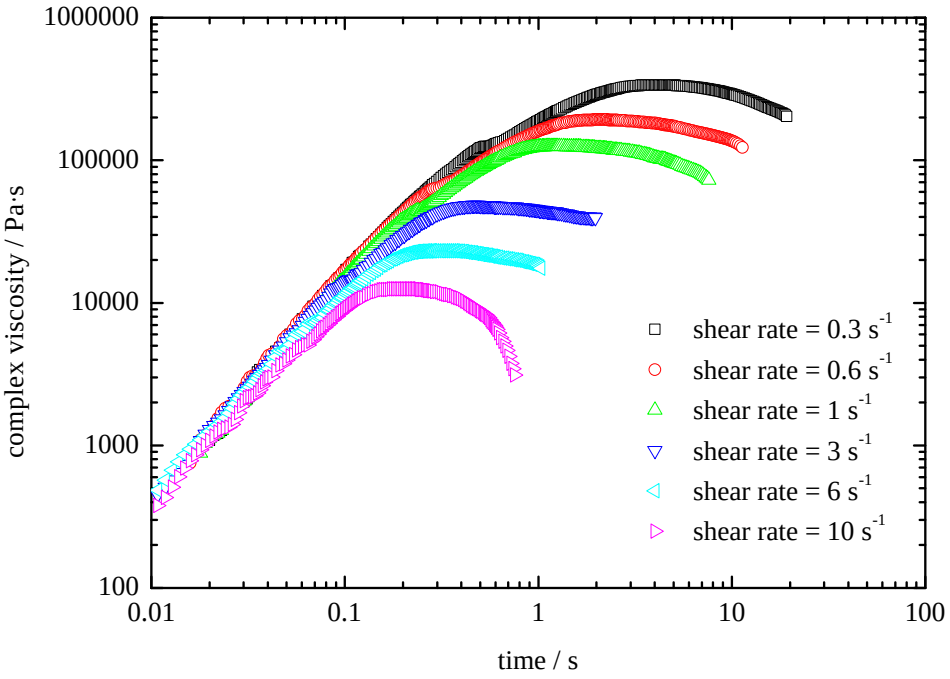

Figure 2.6. The example of the data measured by using start-up shear program.

2.2.4. Relaxation times

Relaxation times (equilibration time τ_e, Rouse time τ_R, reputation time τ_d) of the low-polydispersity h-PBD samples can be calculated from both linear and non-linear rheology measurements.

The Linear theory by Likhtman and McLeish is used to obtain the relaxation times from the fitting of the G' and G'' at the linear region.[12] The G' and G'' curves are fitted by the theory by changing four parameters τ_e, G_e, M_e, C_v (G_e: Plateau modulus, M_e: Entanglement molecular weight, C_v: Constraint release parameter). The first three parameters relate to the chemical structure of the polymer, and C_v indicates constrain-release events. The constraint-release is the effect that a constrained chain in the tube model can gain free motion when neighbour chains move away from the constrained chain (**Figure 2.7**).

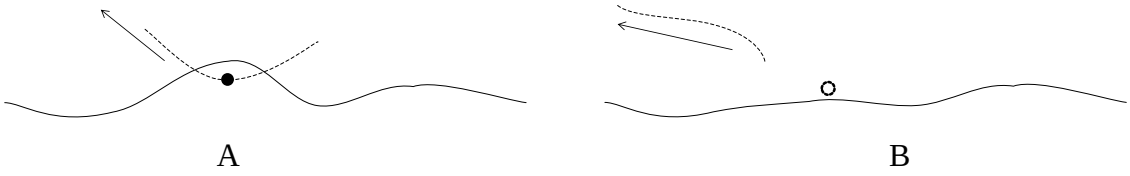

Figure 2.7. Constraint release effect. A; one of surrounding chains (dotted line) moves away from a constrained chain (solid line). B; the chain gains freedom from the constraint.

The Rolie-Poly model[11] is used to estimate the relaxation behaviour from the results taken at the non-linear region. The complex viscosity data against time are collected at different shear rate by using the start-up shear program with the cone-plate geometry, and then, the data are fitted by the Rolie-Poly model (**Eq. 2.3**),

$$\frac{d\sigma}{dt} = \kappa \cdot \sigma + \sigma \cdot \kappa^{T} - \frac{1}{\tau_d}(\sigma - I) - \frac{2\left(1-\sqrt{\left({}^{3}/_{tr\sigma}\right)}\right)}{\tau_R}\left(\sigma + \beta\left(\frac{tr\sigma}{3}\right)^{\delta}(\sigma - I)\right) \qquad \textbf{Eq. 2.3}$$

where σ is a polymer stress and β is a constraint release parameter.

2.3. Multi-modal h-PBD blends

2.3.1. Sample preparation

In this study, bimodal or trimodal blends comprised of long chains and matrix are used to measure the boundary flow conditions. The low-polydispersity h-PBD samples of the 1080, 1330 and 1770 kDa are used as long chains which have the role of creating the shish-nuclei in the blends because of their relatively small $1/\tau_R$ causing them to be stretched at the shearing temperature. In contrast, the low-polydispersity samples of the 7, 18, 52 and 147 kDa are used as a matrix. These samples used as the matrix have quite

fast relaxation times and they are not stretched and take no part in the shish nuclei but do crystallize effectively and report on the nuclei orientation.

The overlap concentration, c*, can be estimated by

$$c^* = \frac{M_w}{\langle R_g^2 \rangle^{3/2} \rho N_A} \qquad \textbf{Eq. 2.4}$$

where M_w is weight-average molecular weight, ρ is the density and N_A is the Avogadro number. Rg^2 is the radius of gyration whose relationship to M_w can be obtained by neutron scattering practically.[13]

The c* of the 1770 kDa chains and 1080 kDa chains are estimated to 1.1 % and 1.4 %, respectively. The concentration of the blends used in this study is higher than the c*, however, the effect on the viscosity caused by the overlap of the long chains can be considered to be negligible. Although c* is the critical concentration that molecular chains start to overlap each other, it does not mean the formation of full entanglements between the long chains. It can be considered that an extensive contact is required to make the full entanglement. One piece of evidence to support this is the research by Heo et al[14].

The preparation of the blends is as follows. At first, the low-polydispersity h-PBD samples have to be dried in a vacuum oven for a certain time. Then the prescribed amount of dried material and toluene are placed together in a flask. To dissolve the material in toluene, it is necessary to heat the toluene to approximately 95 °C. The flask is provided with nitrogen to prevent the oxidation and side reaction of the h-PBD. Each solution is made separately in advance, and then they are mixed and stirred for about 1-2 hours at 95 °C. Finally, a blend sample is obtained by using a precipitation method. The blend sample is washed repeatedly in methanol and dried in a vacuum oven before use.

A hot-press is used to prepare disc-shaped samples which have the appropriate thickness. A dried sample is placed between two flat stainless plates with a metal spacer.

And then, the sample is melted in the hot-press equipment and pressed at 0.7 N / cm^2. The sample is then cooled down to room temperature. Finally, the sample is removed from the heat press and punched to the disc-shape.

2.3.2. Viscosity measurements

The complex viscosity measurements of the blends are required to calculate the boundary specific work. The measurement process is as follows. At first, the complex viscosity is measured at different temperature by the same method which was used for the low-disperse h-PBD samples. And then, the master curve of viscosity at the temperature used for a shear experiment is obtained by the TTS technique.

In order to calculate the boundary specific work conveniently, the master curve is fitted by a modified Cross model. The modified model has a parameter, η_2, for describing the viscosity of a matrix. The fitting parameters obtained are used to calculate the boundary specific work. Some commercial software has the function of this non-linear fitting, for example Origin and Maple, and the example of such fittings is given in chapter 3.

$$|\eta^*(\omega)| = \frac{\eta_1}{1+(\omega/\omega_1)^{\alpha_1}} + \eta_2 \qquad \textbf{Eq. 2.5}$$

ω: angular frequency $\eta_1, \eta_2, \omega_1, \alpha_1$: fitting parameter

2.3.3. Shear experiments

The Linkam shear device (CSS450)[4, 15-17] is used to shear the blends. A plate-plate geometry is used in order that the shear rate $\dot{\gamma}$ is proportional to the radius of the sample disc (**Figure 2.8**). A motor to rotate the plate has been replaced to a more powerful and precise one than the original motor.

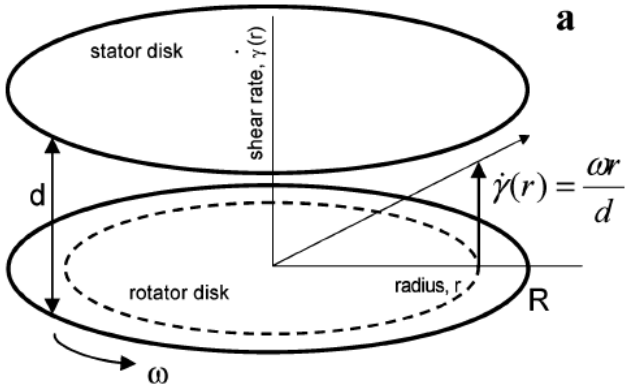

$\dot{\gamma}(r)$: shear rate ω: angular velocity r : radius d : thickness

Figure 2.8. Radial distribution of shear rate in a plate-plate geometry shearing device.

The temperature and shear profile which are used for shear experiments are as follows (**Figure 2.9**).

I – A sample disc is loaded into the shear equipment. Then temperature is increased above the melting point of the oriented nuclei. After the equilibration of temperature, the gap between two shear plates is adjusted to a certain distance (usually 0.5 mm). The required temperature is based on the research by Dalnoki-Veress et al.[18]

II – The sample is kept for a certain time to remove thermal history.

III – The temperature is decreased to a shearing temperature. This shearing temperature should be below the melting point of the oriented nuclei and above the melting point of un-oriented lamellae crystals. Then the shear is applied to the sample.

IV – The sample is maintained at the same temperature for from several minutes to hours to make the sample settled.

V – The temperature is decreased slowly. Rapid cooling may influence the crystal morphology.

VI – The sample is cooled down to a room temperature and unloaded from the equipment.

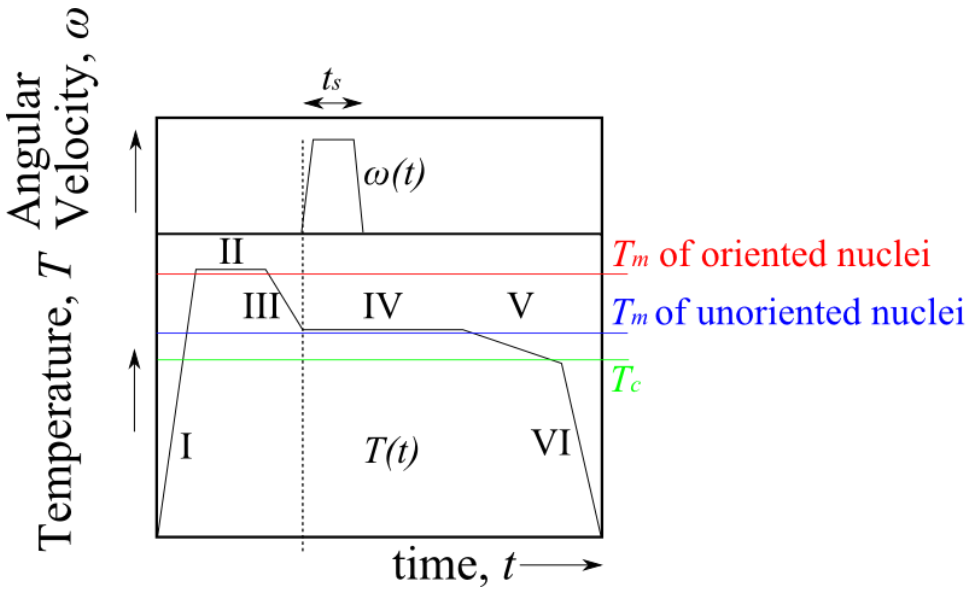

Figure 2.9. Temperature and shear profile of shearing experiment.

2.3.4. Detection of boundary positions

A boundary position is the position that the oriented morphology start to form in the sheared disc. It can be detected by both the polarized light imaging (PLI) and small angle X-ray scattering (SAXS) as follows.

The PLI is a useful method to study the oriented morphology in polymers. The PLI is the method to observe the retardation of incident light caused by the birefringence of oriented molecular chains. The incident light is separated to two different extraordinary rays due to the birefringence in samples. The retardation of samples can be indicated as follows by using refractive indices of each extraordinary rays, n_1 and n_2,

$$R = d \times (n_1 - n_2) \qquad \textbf{Eq. 2.6}$$

R; retardation, d; thickness of samples, n; refractive index

In this study, the sheared sample is placed between 90 ° crossed polarizer and analyzer (**Figure 2.10**). The picture is captured by using a CCD camera with a white light as an incident light.

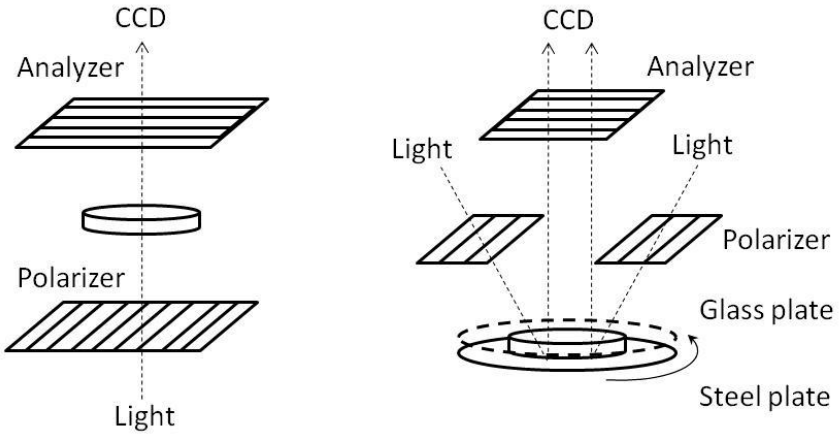

A B

Figure 2.10. Optical systems for Polarized light imaging. A: The basic method. B: The in-situ measurement method. The CCD camera detects the reflected light.

The **Figure 2.11** shows the illustration and image taken by the PLI technique of the sample having the boundary. Maltese cross can be observed at the outer area of the boundary. It means that the oriented morphology exists in the area.

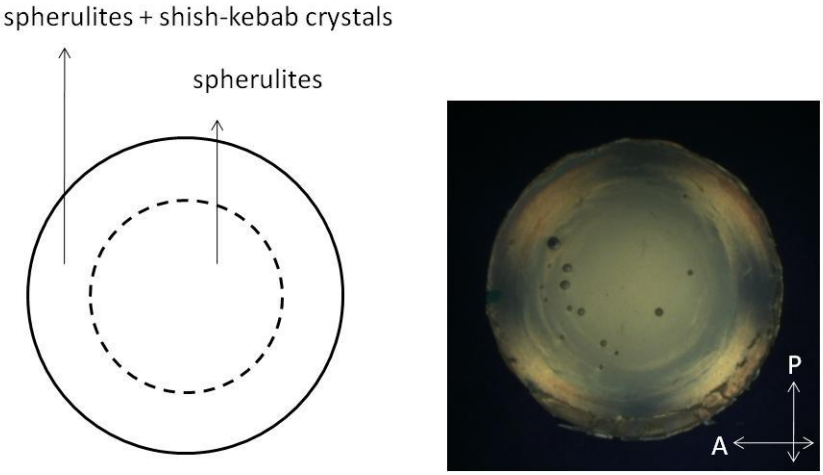

Figure 2.11. The relationship between morphology and PLI. Maltese cross can be seen only at the outer of boundary. The arrows in the right picture indicate the direction of the polarizers.

The morphology of the sheared samples also can be analysed by the SAXS (Bruker AXS Nanostar, Cu Kα radiation). Two-dimensional SAXS patterns were measured by

scanning on the line across the centre of the disks toward the diameter at 0.5 mm intervals by using a RAPID area detector. The degree of orientation which is used in this study is the Herman's orientation function P2[19]. The P2 can be defined as:

$$P_2 = \frac{3\langle cos^2\phi\rangle - 1}{2} \qquad \textbf{Eq. 2.7}$$

where the average angle of the lamellar orientation $\langle cos^2\phi\rangle$ is mentioned as follows.

$$\langle cos^2\phi\rangle = \frac{\int_0^{\pi/2} I(\phi) cos^2\phi \, sin\,\phi d\phi}{\int_0^{\pi/2} I(\phi)\, sin\,\phi d\phi} \qquad \textbf{Eq. 2.8}$$

The I(ϕ) indicates the intensity at the angle of direction, ϕ. The P2 shows inflection points if a sheared sample has a boundary (**Figure 2.12**) and they correspond to the boundary position.

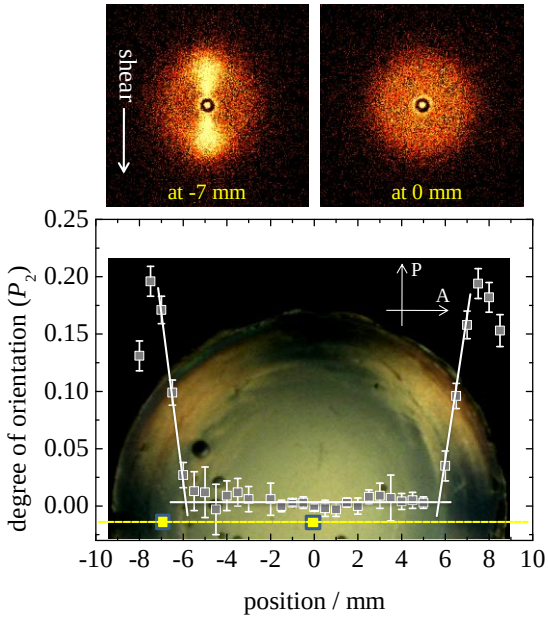

Figure 2.12. The example of the orientation function (P2) of the lamellae structure along the flow direction measured across the diameter of a sheared hydrogenated polybutadiene bimodal blend. The SAXS patterns for the calculation of the orientation function were scanned on the dotted line on the PLI of the sheared samples. The SAXS patterns at the top of the figure correspond to the areas marked by squares on the images in order of appearance from left to right.

2.3.5. The calculation of specific work

The boundary specific work which can be required to form the oriented morphology, w_b, can be calculated from following equation.[20]

$$w_b = \int_0^{t_s} \eta\,[\dot{\gamma}_b(t)]\dot{\gamma}_b{}^2(t)dt \qquad \textbf{Eq. 2.9}$$

By assuming the Cox-Merz rule, $\eta[\dot{\gamma}_b(t)]$ and $\dot{\gamma}$ can be replaced to $|\eta^*(\omega)|$ and ω respectively.[21] The validity of the rule for polyethylene has been reported by some researchers.[22-25] The shape of $\dot{\gamma}_b(t)$ is defined by the maximum shear rate, shearing duration t_s and acceleration rate.

Therefore, the calculation of this integral can be carried out by seven parameters which are η_1, η_2, ω_1, α_1, maximum shear rate, t_s and acceleration rate. The calculation can be carried out by using some commercial software which is typified by Maple and Mathematica.

The boundary specific work has a constant value at the condition of $\dot{\gamma}_b > 1/\tau_R$. This shear-rate independent constant value is defined as the critical specific work w_c.

2.4. References

1. Fernyhough, C. M.; Young, R. N.; Poche, D.; Degroot, A. W.; Bosscher, F. *Macromolecules* **2001,** 34, 7034-7041.
2. Chambon, P.; Fernyhough, C. M.; Ryan, A. J. *Polymer Preprints* **2008,** 49, 822-823.
3. Caputo, F. E.; Burghardt, W. R. *Macromolecules* **2001,** 34, (19), 6684-6694.
4. Mykhaylyk, O. O.; Chambon, P.; Graham, R. S.; Fairclough, J. P. A.; Olmsted, P. D.; Ryan, A. J. *Macromolecules* **2008,** 41, 1901-1904.
5. Nogales, A.; Hsiao, B. S.; Somani, R. H.; Srinivas, S.; Tsou, A. H.; Balta-Calleja, F. J.; Ezquerra, T. A. *Polymer* **2001,** 42, (12), 5247-5256.

6. Morrison, F. A., *UNDERSTANDING Rheology*. Oxford University Press: Oxford, UK, 2001; p 454.

7. Morrison, F. A., *UNDERSTANDING Rheology*. Oxford University Press: Oxford, UK, 2001; p 197-206.

8. Morrison, F. A., *UNDERSTANDING Rheology*. Oxford University Press: Oxford, UK, 2001; p 458.

9. Strobl, G., *The Physics of Polymers*. Springer: Berlin, Germany, 1996; p 214-217.

10. Van Krevelen, D. W., *Properties of Polymers*. Elsevier: New York, USA, 1990; p 402-405.

11. Likhtman, A. E.; Graham, R. S. *Journal of Non-Newtonian Fluid Mechanics* **2003,** 114, 1-12.

12. Likhtman, A. E.; McLeish, T. C. B. *Macromolecules* **2002,** 35, 6332-6343.

13. Ballard, D. G. H.; Cheshier, P.; Longman, G. W.; Schelten, J. *Polymer* **1978,** 19, 379-385.

14. Heo, Y.; Larson, R. G. *Journal of Rheology* **2005,** 49, 1117-1128.

15. Heeley, E. L.; Morgovan, A. C.; Bras, W.; Dolbnya, I. P.; Gleeson, A. J.; Ryan, A. J. *PhysChemComm* **2002,** 5, (23), 158-160.

16. Keum, J. K.; Zuo, F.; Hsiao, B. S. *Macromolecules* **2008,** 41, (13), 4766-4776.

17. Somani, R. H.; Hsiao, B. S.; Nogales, A.; Srinivas, S.; Tsou, A. H.; Sics, I.; Balta-Calleja, F. J.; Ezquerra, T. A. *Macromolecules* **2000,** 33, (25), 9385-9394.

18. Massa, M. V.; Lee, M. S. M.; Dalnoki-Veress, K. *Journal of Polymer Science: Part B: Polymer Physics* **2005,** 43, 3438-3443.

19. Hermans, P. H., *Contribution to the Physics of Cellulose Fibres*. Elsevier: Amsterdam, Netherlands, 1946; p 221.

20. Janeschitz-Kriegl, H.; Ratajski, E.; Stadlbauer, M. *Rheol. Acta.* **2003,** 42, 355-364.

21. Morrison, F. A., *UNDERSTANDING Rheology*. Oxford University Press: Oxford, UK, 2001; p 191-193.

22. Venkatraman, S.; Okano, M.; Nixon, A. *Polym. Eng. Sci.* **1990,** 30, 308-313.

23. Utracki, L. A. *J. Rheol.* **1984,** 28, 601-623.

24. Laun, H. M.; Aldhouse, S. T. E.; Coster, H.; Constantin, D.; Meissner, J.; Starita, J. M.; Fleissner, M.; Frank, D.; Groves, D. J.; Ajroldi, G.; Utracki, L. A.; White, J. L.; Yamane, H.; Ghijsels, A.; Winter, H. H. *Pure Appl. Chem.* **1987,** 59, 193-216.

25. Kalika, D.; Denn, M. M. *J. Rheol.* **1987,** 31, 815-834.

Chapter 3

Characterization of low-polydispersity hydrogenated polybutadiene

3.1. Introduction

The deformation of a molecular chain under flow is controlled by the flow rate and the relaxation time of the molecular chain[1]. The relaxation time of the molecular chain is therefore necessary for the study of flow induced crystallization. In this chapter, characterization of the low-polydispersity hydrogenated polybutadiene (h-PBD) samples is carried out by using thermal and rheological methods.

The aims of this chapter are as follows. Firstly, the thermal properties of h-PBD samples are measured by differential scanning calorimetry. The data obtained such as melting and crystallization temperature are significant[1] in choosing the shearing temperature in the following chapters. Secondly, linear rheology is measured to choose geometry for the rheology measurements and to calculate relaxation times by using the linear theory[2]. The relaxation times are also important to consider the orientation of polymer chains in the following chapters. Lastly, non-linear rheology is measured and fitted by the Rolie-Poly model[3] to calculate relaxation times. This is to confirm the validity of the rheological model used in subsequent calculations.

3.2. Molecular weight of h-PBD

The specially synthesized low-polydispersity h-PBD samples[4] were used in this study. The molecular weight, M_w, of each sample was measured by using high temperature gel permission chromatography (GPC), which is the DOW Benelux B.V. with a High Temperature SEC (HT-SEC, 3 mixed B columns; 145 °C in 1,2,4-trichlorobenzene; 1.1 ml / min; PS standard calibration) fitted out with a triple detector.[5]

The M_w of the low-polydispersity h-PBD samples are shown in **Table 3.1**.The results of the measurements for h-PBD samples having high molecular weight likely had the measurements error which is inherent in SEC detectors[5]; therefore the results of the precursor polybutadiene samples are indicated.

Table 3.1. Average molecular weight and its distribution of the h-PBD materials.

Sample name	M_n kDa	M_w kDa	PDI (M_w / M_n)
7 kDa*	7.20	7.25	1.01
18 kDa	-	18	-
52 kDa	46	52	1.13
147 kDa	136	147	1.08
442 kDa	398	442	1.11
1080 kDa*	940	1080	1.15
1330 kDa	950	1330	1.40
1770 kDa	1200	1770	1.48

* The data is the molecular weight of the polybutadiene before-hydrogenation material and was measured by using the GPC with a triple detection method using a Viscotek 200 SEC apparatus fitted with two PLgel mixed C 300×7.5 mm columns running at 30 °C with a THF flow rate of 1 ml / min having refractive index, viscometer, and Right Angle Laser Light Scattering detectors of 670 nm of wavelength.

3.3. Thermal properties

The thermal properties of h-PBD samples were measured by using differential scanning calorimetry (DSC). The heat flow curves of the cooling step of the all samples indicated the exothermic peaks which are attributed to the crystallization (**Figure 3.1**). The 7 and 18 kDa sample has relatively high T_c whose onsets are 99.6 and 101.7 °C respectively. Other samples show their onsets of T_c between 91.8 and 97.4 °C. The exothermic peaks in the curves of the heating step can be ascribed to the melting of crystals (**Figure 3.2**). Also the 7 and 18 kDa sample have higher T_m than others and this was the expected result from their high T_c. The 18 kDa sample has the highest T_m whose end is 113.8 °C. The temperature for the rheology measurements needs to be above the melting point to remove memory of previous treatments.[1] Also, the temperature used for shearing should be above the melting point measured in quiescent state in order to neglect the effect of the growth of spherulites while shearing.[1]

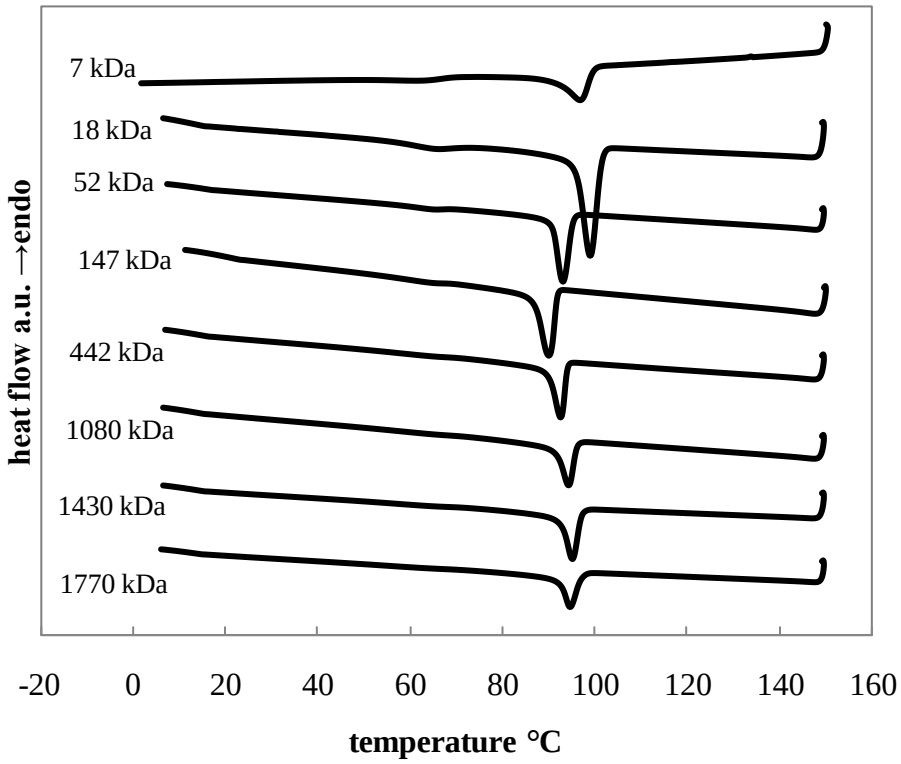

Figure 3.1. DSC diagram of h-PBD, cooling step. Cooling rate is 10 °C / min.

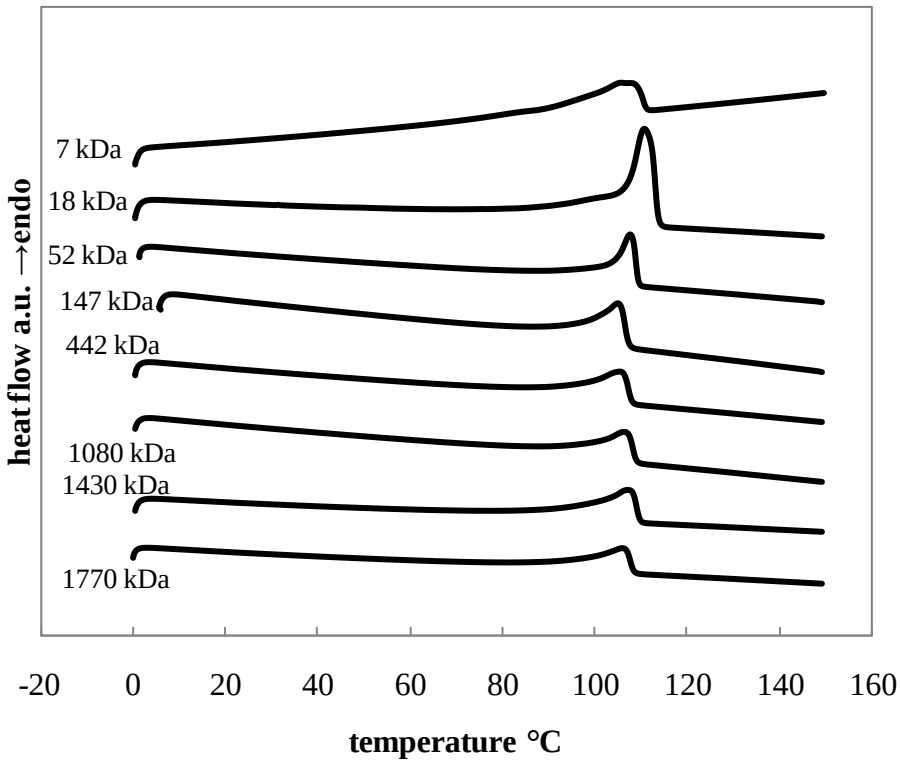

Figure 3.2. DSC diagram of h-PBD, second heating step. Heating rate is 10 °C / min.

3.4. Rheology measurements

3.4.1. Sample preparation

Low M_w h-PBD samples whose M_w are 18, 52 and 147 kDa, were kept in the vacuum oven for 3 hours at 140 °C to remove bubbles. The reason to use this temperature is that the sample turns yellow due to the cleavage of the residual double bonds existing in chemical structure at higher temperature. Then, they were melted and pressed in heat press equipment at 140 °C. The thickness of the samples was controlled to 0.5 mm by metal spacers. After the heat press, the samples were cut into disk shapes which have appropriate diameter to apply rheology measurements. The duration that the samples were maintained at 140 °C in the heat press was approximately 10 minutes in total.

3.4.2. Rheology measurements conditions

Before turning into the rheology measurements for the calculation of relaxation times, the conditions for rheology measurements were decided by some preparatory measurements. The preparatory measurements consist of three parts; (1) the effect of different geometry, (2) the selection of strain and (3) the selection of measurement temperature.

(1) Effect of geometry

The geometries used in this study are cone-plate and plate-plate geometry with 25 mm diameter and cone-plate and plate-plate geometry with 8 mm diameter. In order to check the effect of the difference of geometry for the rheology measurements, the viscosity of the 18 kDa sample was measured by using different geometries. The viscosity was measured against angular frequency at 120, 130 and 140 °C, and then the data at different temperatures were shifted to 112 °C by using Time-Temperature-Superposition (TTS) technique. No significant difference was seen in the viscosities measured by different geometries (**Figure 3.3**).

When the plate-plate geometry is used, gap size may give an effect to the result due to the difference of the shape of the sample at the edge, 'edge-effect'. Therefore, the effect of the gap between two plates of the plate-plate geometry on the rheology measurements was investigated as follows. The viscosity of 18 kDa at 120, 130 and 140 °C was measured by using the plate-plate geometry with different gaps which were 0.5, 0.3 and 0.1 mm. The data at the different temperatures were also shifted to 112 °C by the TTS technique. Similarly, there was no significant change in the viscosities measured by the plate-plate geometry with different gaps (**Figure 3.4**).

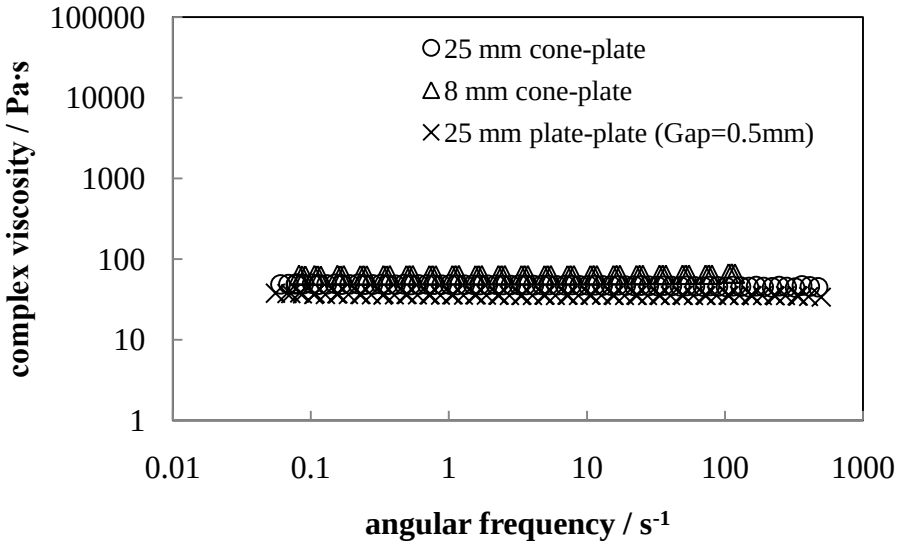

Figure 3.3. The complex viscosity of h-PBD (18 kDa) at 112 °C by different geometries. The data at 112 °C were obtained by time-temperature shift from the measurement data at 120, 130 and 140 °C. The 20 % of strain was used.

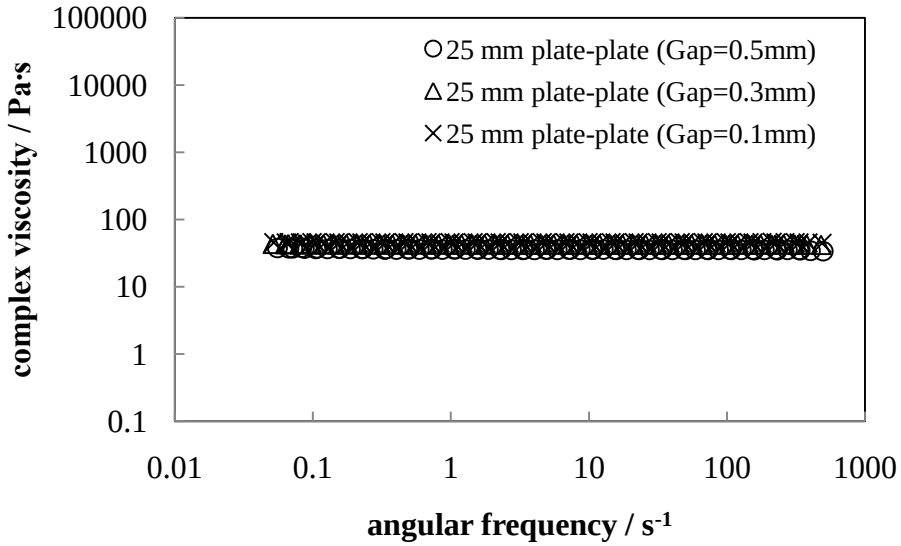

Figure 3.4. The complex viscosity of h-PBD (18 kDa) at 112 °C by a plate-plate geometry with different gap values. The data at 112 °C were obtained by time-temperature shift from measurement data at 120 °C, 130 °C and 140 °C. The 20 % of strain was used.

The *G*' of the low-viscosity samples measured by the 8 mm geometry tended to be noisy at low frequency due to a low torque. Therefore larger 25 mm cone-plate geometry was used to measure the rheology of the low-viscosity samples such as 7 kDa, and higher M_w samples were measured by the 8 mm plate-plate geometry in order to adjust the torque range of the measurements to the right range and save the amount of samples (**Table 3.2**).

(2) Strain sweep tests

The rheology parameters for the calculation of relaxation times by linear theory have to be measured in the linear viscoelastic region (LVE)[6] where the rheology parameters indicate constant value against a strain. In this section, strain sweep tests were performed to clarify the strain which is used for frequency sweep tests.

The strain sweep tests for the low-polydispersity h-PBD samples were performed at different angular frequency ω = 6.3, 100, 300 s^{-1}. The measured viscosity of the 7 kDa h-PBD was noisy at low strain due to low torque and showed constant viscosity in the

strain range used (**Figure 3.5**). A constant viscosity against the strain means that the strain is within the linear region. Thus, the strain for the rheology measurements for the calculation of relaxation times can be chosen from anywhere in this region. Although higher strain is preferred due to the greater torque, 0.3 % strain was chosen for the rheology measurements because the 7 kDa sample is quite liquid and leakage of the sample was observed.

The strain sweep result of 1080 kDa was carried out from 0.01 to 1 % strain (**Figure 3.10**). In this case, the measured viscosity was not noisy at lower strain in spite of the 8 mm plate-plate being used. This is because the sample has higher viscosity; therefore, enough torque can be obtained from the low strain region. The measurement was stopped at 1 % strain, because the sample was quite viscous and it may be damaged in the high strain region. The 0.3 % strain was chosen for the rheology measurements since the viscosity at lower strain was slightly noisy at low angular frequency.

The strain sweep results and chosen strains are shown in **Figure 3.6-9**.

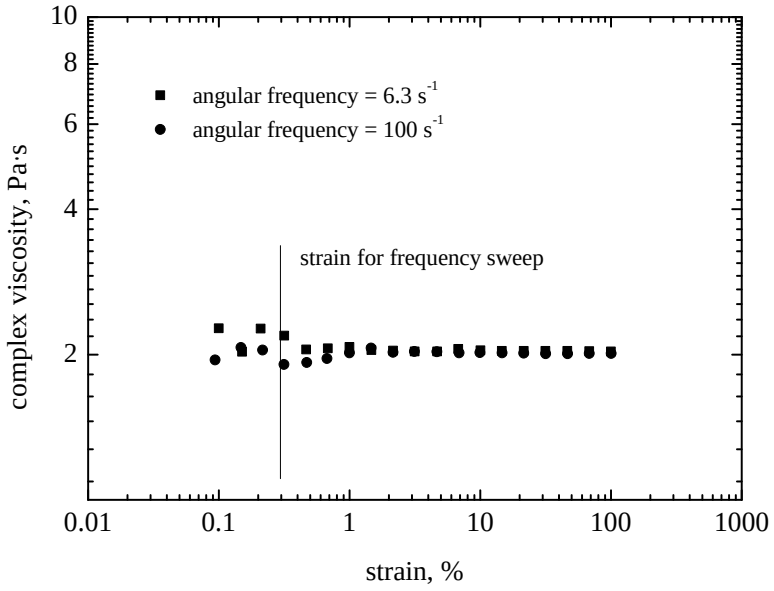

Figure 3.5. Strain sweep measurement for the low-polydispersity h-PBD 7 kDa at 120 °C by 25 mm cone-plate geometry (cone angle = 6:36:00) at angular frequency = 6.3 and 100 s^{-1}.

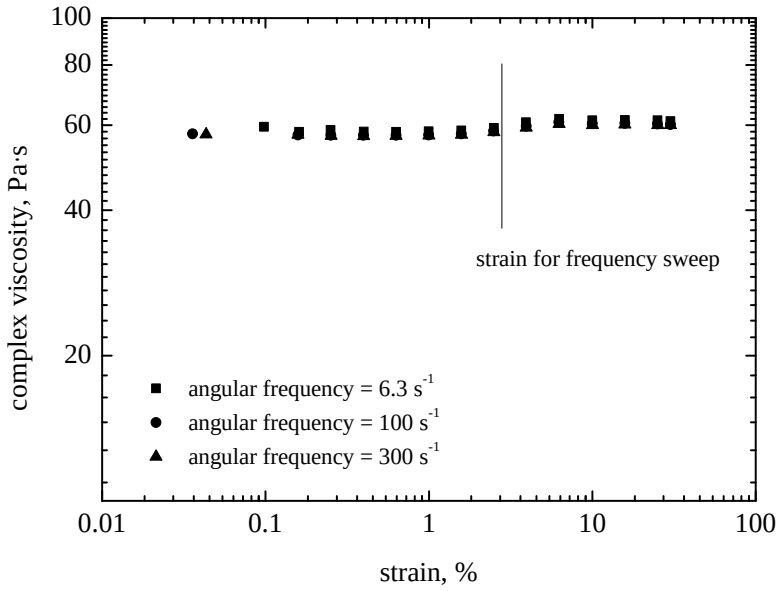

Figure 3.6. Strain sweep measurement for the low-polydispersity h-PBD 18 kDa at 120 °C by 25 mm cone-plate geometry (cone angle = 6:36:00) at angular frequency = 6.3, 100 and 300 s^{-1}.

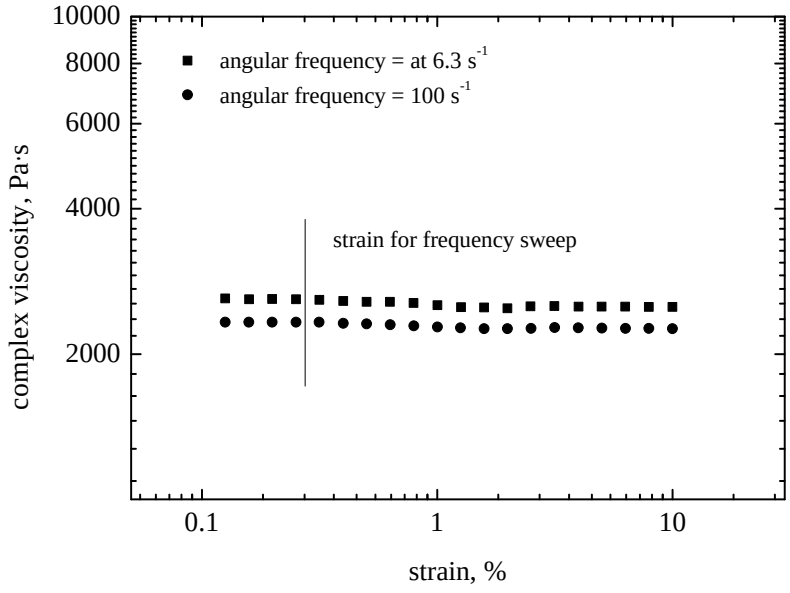

Figure 3.7. Strain sweep measurement for low-polydispersity h-PBD 52 kDa at 120 °C by 8 mm plate-plate geometry (gap = 0.5 mm) at angular frequency = 6.3 and 100 s^{-1}.

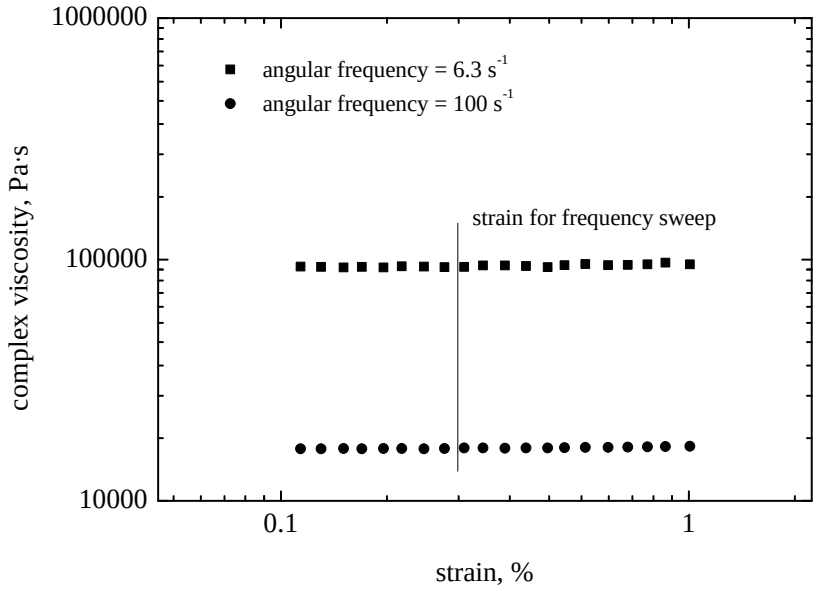

Figure 3.8. Strain sweep measurement for the low-polydispersity h-PBD 147 kDa at 120 °C by 8 mm plate-plate geometry (gap = 0.5 mm) at angular frequency = 6.3 and 100 s^{-1}.

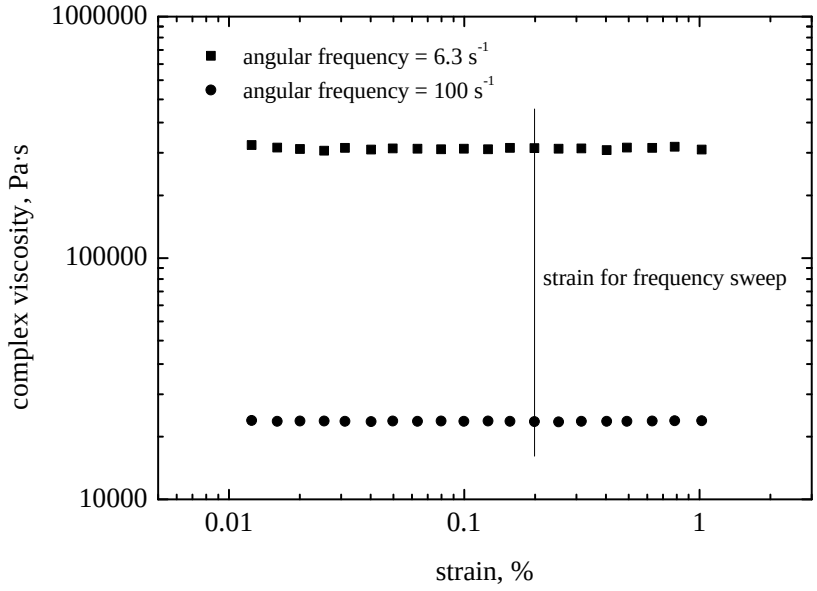

Figure 3.9. Strain sweep measurement for the low-polydispersity h-PBD 442 kDa at 120 °C by 8 mm plate-plate geometry (gap = 0.5 mm) at angular frequency = 6.3 and 100 s^{-1}.

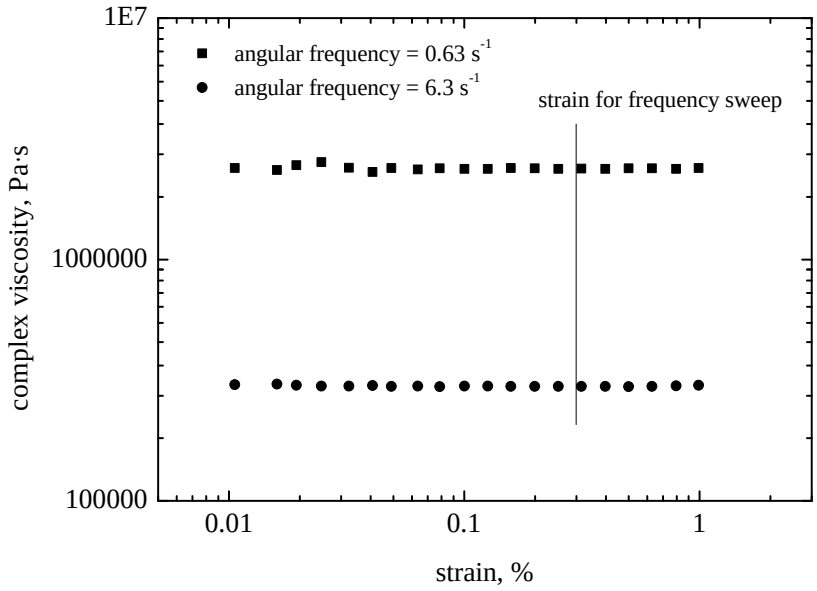

Figure 3.10. Strain sweep measurement for the low-polydispersity h-PBD 1080 kDa at 120 °C by 8 mm plate-plate geometry (gap = 0.5 mm) at angular frequency = 0.63 and 6.3 s^{-1}.

(3) Temperature

The last preparatory measurement for frequency sweep tests is thermal stability tests in order to decide the temperature used for frequency sweep tests. The thermal stability was checked by measuring the time dependence of the *G*' and complex viscosity of h-PBD samples at different temperatures. Then, the temperature which was used for rheology measurements was selected.

The viscosity of hydrogenated polybutadiene samples used in this study tends to increase if they are maintained at relatively high temperature for a long time. The viscosity increase is problematic because it makes the TTS shift of the viscosity curve difficult and causes large error in calculating the specific work. Therefore, the viscosity of the samples needs to be measured at the temperature when the increase of viscosity is negligible.

In order to check the thermal stability of the h-PBD samples, the complex viscosity of the 52 kDa sample was measured by the frequency sweep test (strain = 0.2 %) by using

the cone-plate geometry with 8 mm diameter after holding the sample at different temperatures. When the sample was held at 170 °C, the complex viscosity of the sample which was held there for 120 min had 50 times higher complex viscosity than un-annealed material, and the viscosity of a sample held at 170 °C for 210 min was 100 times higher than the un-annealed sample (**Figure 3.11**). The *G*' of the sample also increased with time. The increase of both the complex viscosity and *G*' was remarkable at low angular frequency.

On the other hand, the complex viscosity of 52 kDa measured by the same geometry and conditions but at 140 °C did not indicate the significant increase of the *G*' and complex viscosity (**Figure 3.12**). Even after holding at this temperature for 60 min, the change of the *G*' and viscosity from the un-annealed material was in the range of measurement error. After 140 min, a slight increase of the *G*' and viscosity could be seen; however, it was much less than the change after holding at 170 °C. Since the duration of the rheology measurements to measure the viscosity is for 20 min at one temperature, it was considered that the effect of the viscosity increase is insignificant to perform the TTS if the rheology measurements are carried out at temperature below 140 °C.

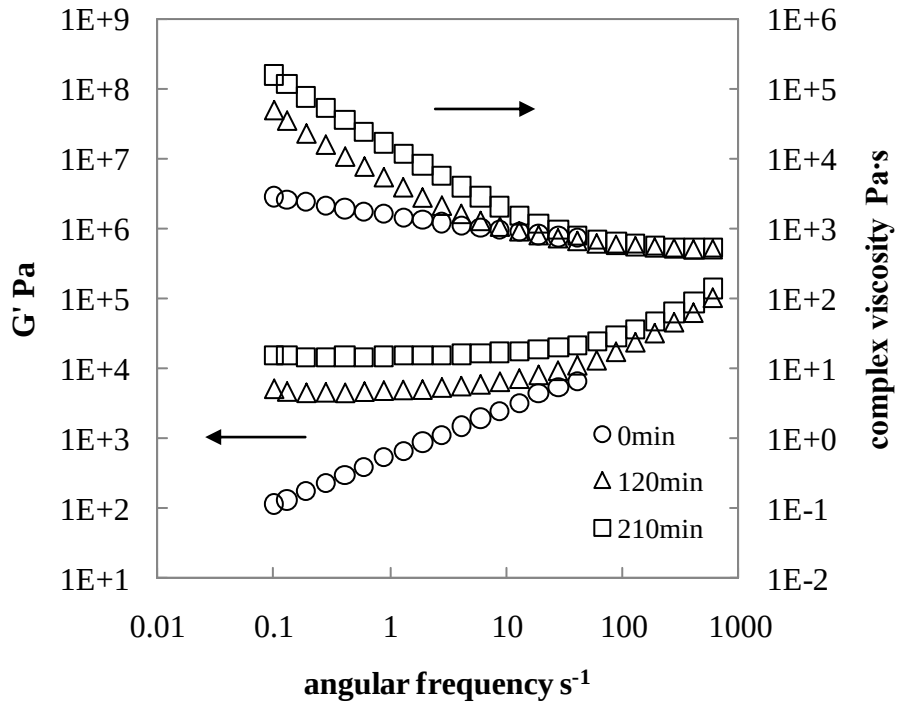

Figure 3.11. The time dependence of *G*' and complex viscosity of h-PBD (52 kDa) after maintained at 170 °C. The 8 mm cone-plate (angle = 6:36:00) and 0.2 % strain were used.

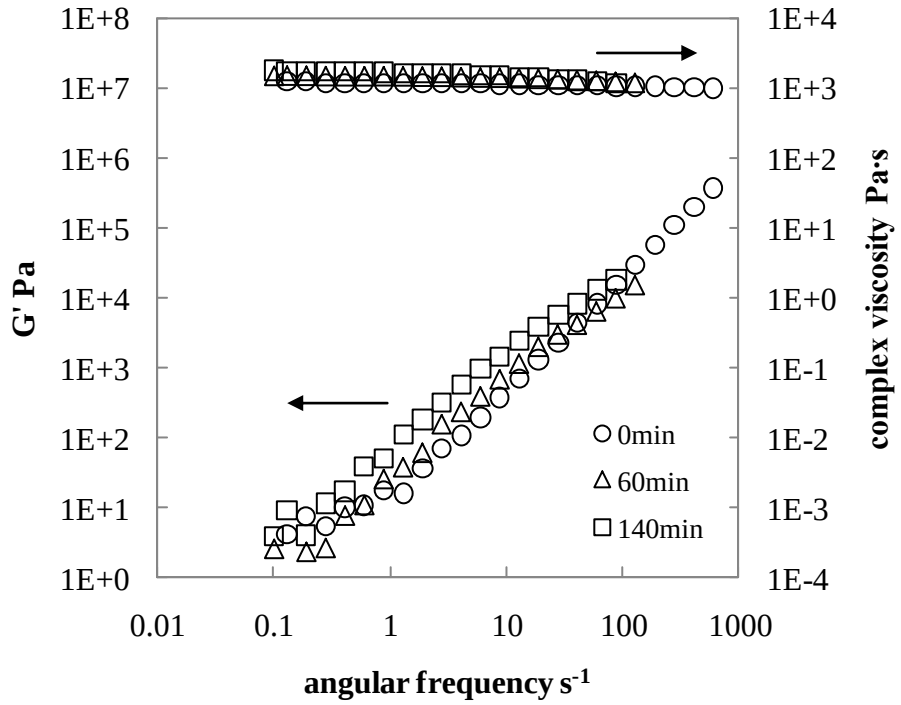

Figure 3.12. The time dependence of *G*' and complex viscosity of h-PBD (52 kDa) after maintained at 140 °C. The 8 mm cone-plate (angle = 6:36:00) and 0.2 % strain were used.

The reason that the 52 kDa sample was chosen to evaluate the time dependence of the viscosity is as follows. Although the increase of the viscosity is observed for all h-PBD samples used in this study, the viscosity increase of the 52 kDa sample is the most pronounced. It is most likely due to it having the highest proportion of residual unsaturation. Therefore, the temperature condition that the 52 kDa sample does not indicate the significant increase of the viscosity can be used for the all other samples.

The reason of the viscosity increase has not been fully understood; however it can be considered that it is due to the crosslink by the cleavage of the double bonds slightly existing in the h-PBD samples. Kruliš and Fortelný reported about the relationship between the rheology and degree of crosslink for polypropylene/ethylene-propylene elastomer blends.[7] In the same way to the results of h-PBD blend samples, it was reported that the viscosity and storage modulus *G*' increase with the increase of ethylene-propylene elastomer content and the differences are also large at low angular frequency.

From the all preparatory experiments mentioned above, the measurement conditions (geometry, strain and temperature) for the rheology measurements for a series of the low-polydispersity h-PBD samples were chosen as shown in **Table 3.2**.

3.5. Linear rheology

The *G*' and *G*" were measured at 140, 130 and 120 ºC (for 18 kDa, at 125, 120 and 115 ºC). The conditions for rheology measurements are summarized in **Table 3.2**. The data was measured from high to low temperature to minimise the thermal history caused by the each steps of the rheology measurements. And then the master curves of *G*' and *G*" at 115 ºC were created by using the TTS technique (**Figure 3.13**). Although the *G*' and *G*" of the 7 kDa were measured, the data were quite noisy due to the low viscosity of the 7 kDa. Therefore, it is not shown in the figure.

Table 3.2. Conditions used for rheology measurements.

	geometry	temperature ºC	angular frequency s^{-1}	strain %
7 kDa	25 mm cone-plate	140, 130, 120	600 to 0.1	0.3
18 kDa	25 mm cone-plate	125, 120, 115	600 to 0.1	2.0
52 kDa	8 mm plate-plate	140, 130, 120	600 to 0.1	0.3
147 kDa	8 mm plate-plate	140, 130, 120	600 to 0.1	0.3
442 kDa	8 mm plate-plate	140, 130, 120	600 to 0.1	0.2
1080 kDa	8 mm plate-plate	140, 130, 120	10 to 0.5	0.3

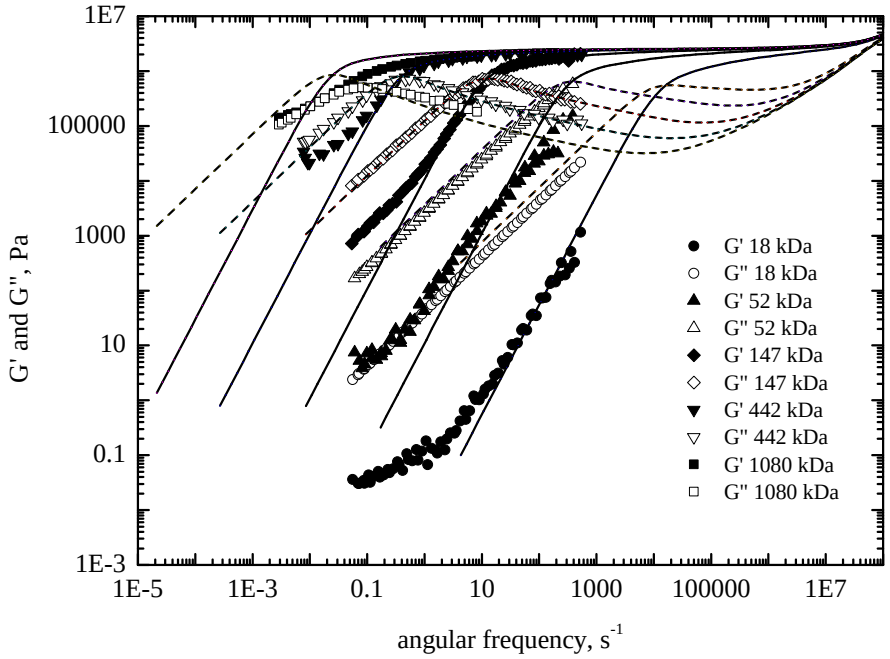

Figure 3.13. *G*' and *G*'' of the h-PBD samples at 115 °C. The *G*' and *G*'' were measured by a rheometer at 140, 130 and 120 °C (for 18 kDa, at 125, 120 and 115 °C) and then the data were shifted to 115 °C by using time-temperature superposition technique. The *G*' and *G*'' were fitted by the linear theory[2] (*G*'; solid lines, *G*''; dotted lines).

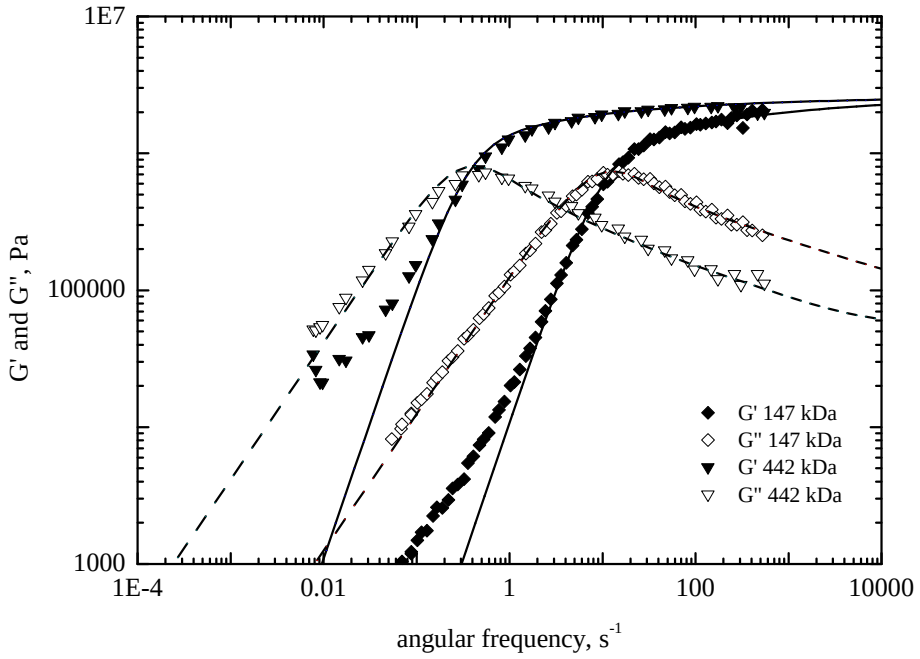

Figure 3.14. The results of 147 and 442 kDa extracted from **Figure 3.13**.

The linear theory was used to fit the G' and G'' (**Figure 3.13, lines**) by using the same procedure previously reported[8]. The cross-points, which correspond to the magnitude of the relaxation times, of the measured data and the fitted curves are consistent (**Figure 3.14**). The fitting parameters of the Linear theory were the Rouse time of one entanglement segment; $\tau_e = 3.1371 \times 10^{-8}$, plateau modulus; $G_e = 3.2024 \times 10^6$, a mass between cross-links; $M_e = 1.2723$ kg mol^{-1} and the constraint release parameter; $c_\nu = 0.1$.

The Rouse time τ_R and reptation time τ_d at 115 °C were obtained from fitting results (**Table 3.3**). The Rouse time was compared to the Rouse time calculated from the τ_e[9] and WLF parameters[8] taken from the previous research. The Rouse time obtained from the rheology data of newly-synthesized hydrogenated polybutadiene samples was close to the value of the Rouse time calculated by the parameters in previous research.

Table 3.3. Relaxation times of the low-polydispersity h-PBD samples at 115 °C. The relaxation times were obtained by the fitting of the G' and G'' of the samples by the linear theory. Reference Rouse time was calculated from τ_e[9] and WLF parameters[8] taken from the previous research.

M_w, kDa	τ_R, s	τ_R (ref), s	τ_d, s	1 / τ_R, s^{-1}
7	9.50×10^{-7}	1.26×10^{-6}	3.09×10^{-6}	1052632
18	6.28×10^{-6}	8.32×10^{-6}	9.78×10^{-5}	159235
52	5.24×10^{-5}	6.94×10^{-5}	3.65×10^{-3}	19084
147	4.19×10^{-4}	5.55×10^{-4}	1.05	2387
442	3.79×10^{-3}	5.01×10^{-3}	3.28	264
1080	2.26×10^{-2}	2.99×10^{-2}	51.2	44
1430	3.96×10^{-2}	5.25×10^{-2}	121	25
1770	6.14×10^{-2}	8.04×10^{-2}	235	16

The viscosities of samples were calculated from the *G*' and *G*" at 115 ºC (**Figure 3.15**). The series of low-polydispersity hydrogenated polybutadiene samples has discrete viscosity. The viscosity estimated by using linear theory is consistent with the measured viscosity in spite of the parameters were obtained from the fitting of only the 147 and 442 kDa samples. This means that the parameters obtained by the fitting were reasonable and the linear theory can simulate wide range of viscosity because of the consideration of the constraint release[2].

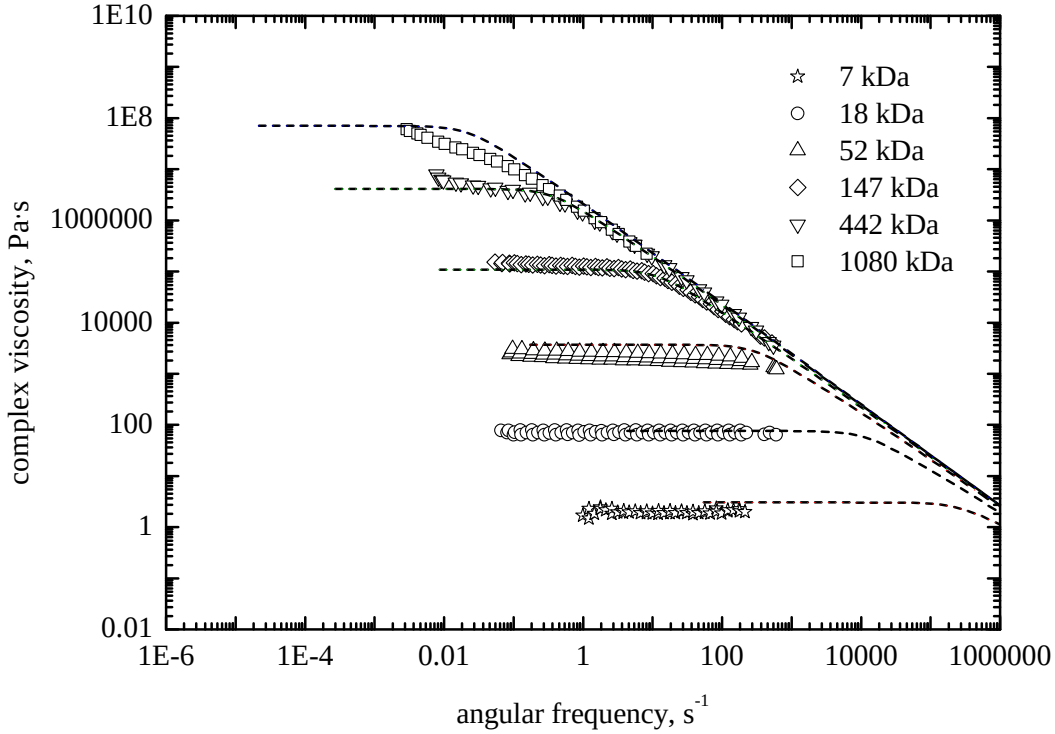

Figure 3.15. Complex viscosity of the low-polydispersity h-PBD samples at 115 °C. The *G*' and *G*" were measured by a rheometer at 140, 130 and 120 °C (for 18 kDa, at 125, 120 and 115 °C) and then the data were shifted to 115 °C by using time-temperature superposition technique. Then, the complex viscosity was calculated from the *G*' and *G*". The dotted lines indicate the complex viscosity which is simulated by the linear theory by using the fitting parameter obtained from the fitting of the *G*' and *G*" by the linear theory.

3.6. Non-linear rheology

The relaxation times can be also estimated from non-steady shear viscosity data by using the Rolie-Poly model.[3] The time required for reaching steady shear flow depends on relaxation times of the polymer. Therefore, the complex viscosity was measured against time and then the viscosity was fitted by using the theory in order to calculate the relaxation times. The Rouse times of h-PBD 1080 kDa was estimated and compared with the Rouse time obtained by the linear theory.

The complex viscosities of 1080 kDa sample were measured at 140 °C at different shear rates (**Figure 3.16**) with 8 mm cone-plate geometry by using a peak hold step program of the rheometer. The shear rate was chosen from 0.3 to 10 s^{-1}. Although the measurements above 10 s^{-1} were tried, satisfactory data was not obtained because of the decrease of the viscosity which arises from destruction of the sample due to high strain ratio. The viscosity at 0.3 s^{-1} increases with time until 3 s and then decreases slightly. On the other hand, the viscosity at 10 s^{-1} stops increasing viscosity at 0.1 s and then decreases rapidly.

The Rolie-Poly model was applied to the viscosity data; however, the calculation of the relaxation time by using fitting did not work for the following reasons. Firstly, the fitting of the viscosity measured at high shear rate was not good enough. It is considered that the viscosity measured at high shear rate such as at 10 s^{-1} has already been compromised and indicates a lower viscosity. Another reason for the poor fit in can be that slip is occurring between bulk and surface of the sample, which contacts with the rheometer plate. Secondly, the shear rate used was not high enough compared to the relaxation time of the sample. Although only the viscosity at 10 s^{-1} has shown rapid decrease in the data, it did not seem enough. This rapid decrease is quite effective in the fitting process; therefore, it can be fitted if few more data can be obtained at higher shear rate.

Although the fitting by the theory was difficult, the non-linear viscosity data of the h-PBD 1080 kDa sample was simulated by the theory by assuming the Rouse time = 1, 0.1, 0.01 and 0.001 s in order to estimate the magnitude of the Rouse time and compare with the Rouse time by linear theory. When the Rouse time = 1 s, the simulated

viscosity does not match the measured data (**Figure 3.16**). The simulated points that the viscosity tends to equilibrium are much longer than the measured data. It means that the sample has shorter Rouse time than 1 s. The viscosities were also simulated at Rouse time = 0.1, 0.01, and 0.001 s (**Figure 3.17-19**). The simulated viscosity becomes closer to the measured data with decreasing Rouse time. The simulated viscosities at Rouse time = 0.01 and 0.001 s indicated similar result. It can be suggested that the used shear rate is not high enough to estimate Rouse time shorter than 0.01 s. From above results, it can be suggested that the magnitude of the Rouse time of low-polydispersity h-PBD 1080 kDa is below 0.1 s. This estimation of the magnitude is consistent with the Rouse time = 0.013 s of the h-PBD 1080 kDa at 140 °C, which can be calculated from the linear rheology measurements by the linear theory.

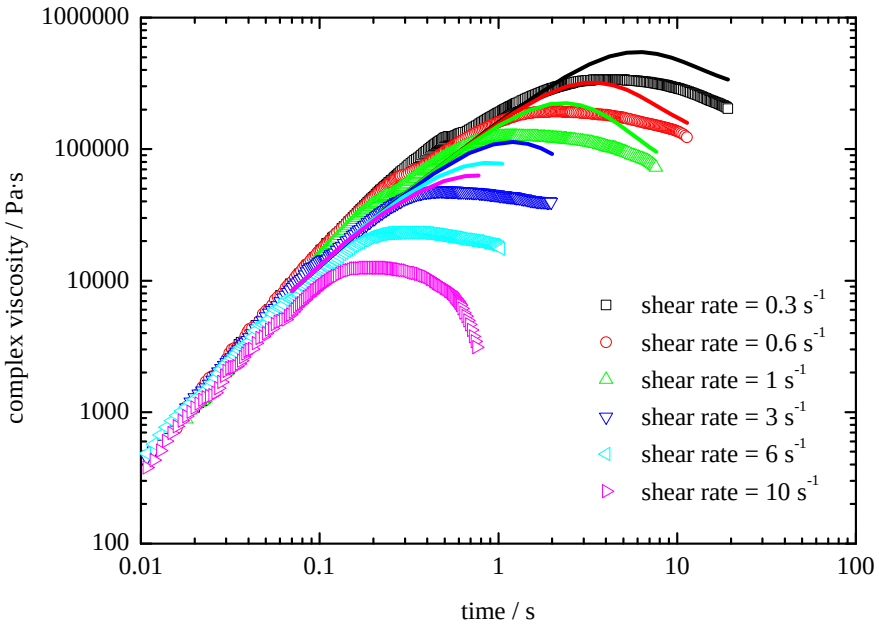

Figure 3.16. The non-linear rheology of low polydisperse h-PBD 1080 kDa sample (markers). The viscosities were measured at 140 °C at different shear rates. The lines show the result of the simulation by the Rolie-Poly model. The Rouse time = 1 s was used as the parameter. The simulation was carried out by using Reptate software. Other parameters were, adjust G = 0.1175, delay = 0.02, beta = 0, delta = -0.5 and Imax = 10.

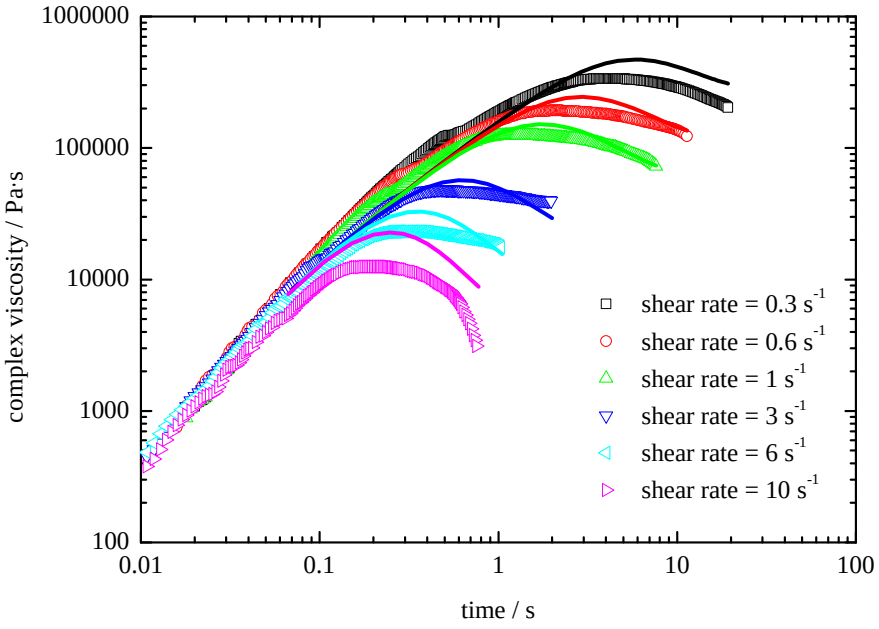

Figure 3.17. Same as **Figure 3.16** but the lines for the Rouse time = 0.1 s.

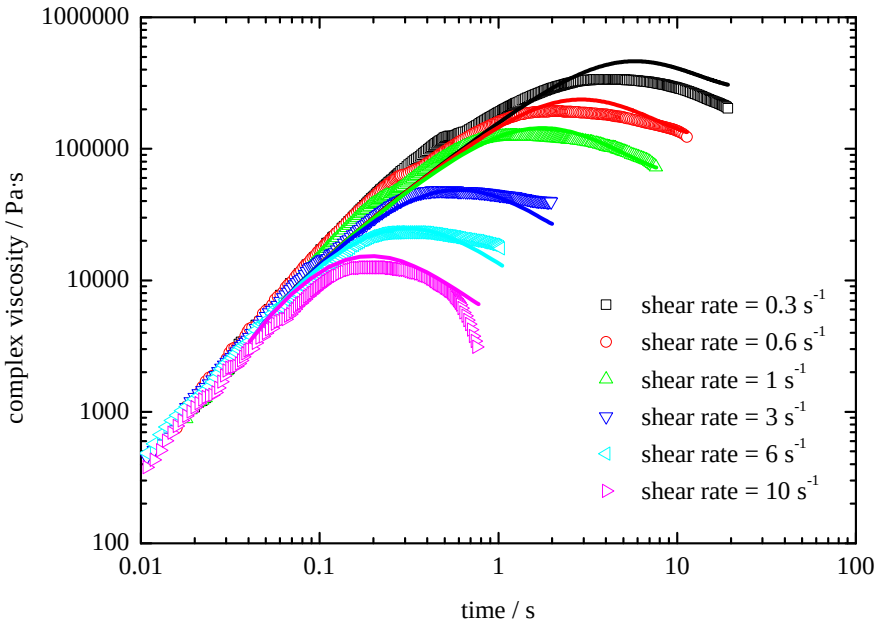

Figure 3.18. Same as **Figure 3.16** but the lines for the Rouse time = 0.01 s.

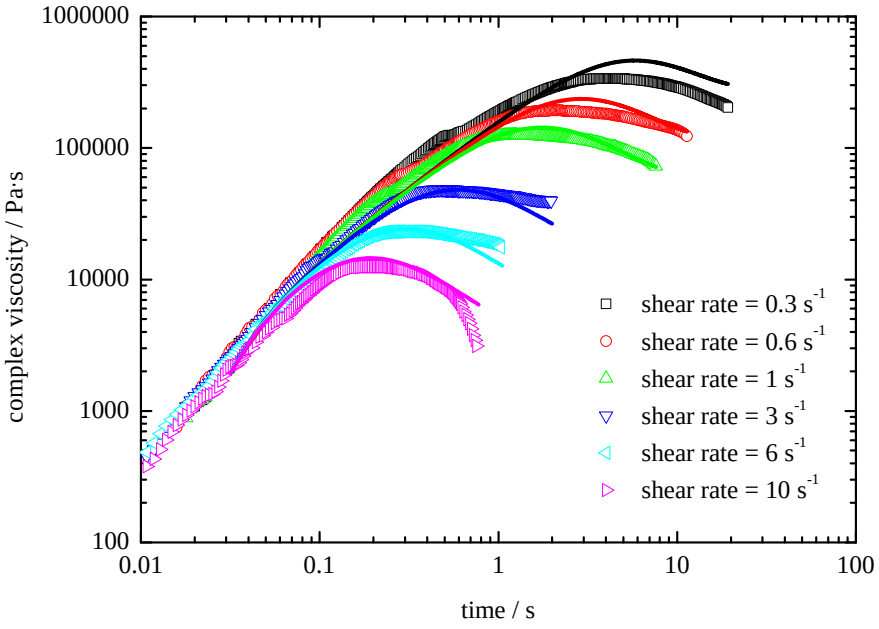

Figure 3.19. Same as **Figure 3.16** but the lines for the Rouse time = 0.001 s.

3.7. Conclusions

The relaxation times of synthesized low-polydispersity h-PBD samples were measured from the *G*' and *G*" by the linear theory and they were consistent with the result of the previous research. The viscosity simulated by the linear theory reproduced measured viscosity of low-polydispersity h-PBD with wide range of M_w. Although the Rouse time of low-polydispersity h-PBD whose M_w is 1080 kDa could not be calculated by Rolie-Poly model, roughly estimated Rouse time had similar magnitude with the Rouse time obtained by the linear theory.

3.8. References

1. Mykhaylyk, O. O.; Chambon, P.; Impradice, C.; Fairclough, J. P. A.; Terrill, N. J.; Ryan, A. J. *Macromolecules* **2010,** 43, (5), 2389-2405.

2. Likhtman, A. E.; McLeish, T. C. B. *Macromolecules* **2002,** 35, 6332-6343.

3. Likhtman, A. E.; Graham, R. S. *Journal of Non-Newtonian Fluid Mechanics* **2003,** 114, 1-12.

4. Fernyhough, C. M.; Young, R. N.; Poche, D.; Degroot, A. W.; Bosscher, F. *Macromolecules* **2001,** 34, 7034-7041.

5. Chambon, P.; Fernyhough, C. M.; Ryan, A. J. *Polymer Preprints* **2008,** 49, 822-823.

6. Morrison, F. A., *UNDERSTANDING Rheology*. Oxford University Press: Oxford, UK, 2001; p 382-392.

7. Krulis, Z.; Fortelny, I. *Eur. Polym. J* **1997,** 33, (4), 513-518.

8. Heeley, E. L.; Fernyhough, C. M.; Graham, R. S.; Olmsted, P. D.; Inkson, N. J.; Embery, J.; Groves, D. J.; McLeish, T. C. B.; Morgovan, A. C.; Meneau, F.; Bras, W.; Ryan, A. J. *Macromolecules* **2006,** 39, 5058-5071.

9. Likhtman, A. E. *Macromolecules* **2005,** 38, (14), 6128-6139.

Chapter 4

Structural Analysis of Sheared Hydrogenated Polybutadiene Blends

4.1. Introduction

The processing conditions vary the crystal morphology formed in semi-crystalline polymers from isotropic spherulites crystallized under quiescent conditions to highly oriented shish kebab structure[1-3] formed under melt flow conditions. Furthermore, the formation of oriented structure greatly affects to the mechanical property of polymers[2-5]. Therefore, the investigation and control of the flow induced crystallization is a significant subject to control both the structure and property of polymer products.

The quantitative studies of the amount of flow necessary to form oriented morphology in polymers were carried out.[6, 7] The specific work[8] was introduced as the criterion for the necessary mechanical work of the formation of the oriented morphology. The specific work has been measured for the model polyethylene[6] [hydrogenated polybutadiene (h-PBD) bimodal blend comprised of long chains in matrix] and commercial polyolefins[7] with high polydispersity. The mechanism of the flow induced crystallization of polydisperse polymers was also studied in this thesis by using multimodal h-PBD blends.

Although the necessary amount of work for the formation of the oriented morphology has been well studied, the structural analysis in the previous studies[6, 7] whilst compaling is not enough. Only indirect analytical methods were applied to assess the oriented morphology in sheared polymers such as the polarized light imaging (PLI) and X-ray scattering in the studies. It is significant to apply a direct method such as optical microscopy (OM) for the sheared polymers in order to understand the relationship between the flow conditions and formed morphology.

The main aim of this chapter is to carry out the structural analysis by using OM, PLI and X-ray scattering in sheared model polyethylene.

4.2. Experimental

4.2.1. Materials

A linear hydrogenated polybutadiene (h-PBD) bimodal blend was prepared from low-polydispersity polymers[9] whose molecular weights are 1770 and 18 kDa (the latter is used as a matrix). The blend contains 2 wt % of 1770 kDa chains in the matrix. A commercial low density polyethylene[7] (LDPE, Lupolen 1840H, Basell) was also used in the optimization of microtome conditions.

4.2.2. Shear experiments

A modified Linkam CSS-450 shear device[6, 7] with a parallel disks geometry was used to apply a shear flow. The geometry and temperature profile for shearing experiments were based on the methodology reported previously.[6, 7, 10] The shearing temperature used is higher than the melting point of the sample. The shear rate $\dot{\gamma}(r)$ which is applied to the samples by the parallel disks geometry is proportional to the radius r and represented as $\dot{\gamma}(r) = \Omega r/d$, where Ω is an angular speed and d is the gap between two parallel disks (0.5 mm was used). Consequently, one sheared sample disk has variant shear conditions of the $\dot{\gamma}(r)$ and strain $[\dot{\gamma}(r) \cdot \mathrm{t}]$ in the radius of the sample disk.

The procedures to apply the shear to samples were as follows. The sample was loaded between the parallel disks and was maintained for 10 min at 438 K to erase its thermal history[11] before being cooled to a shearing temperature (388 K for the h-PBD bimodal blend and 385 K for the LDPE) at a rate of -0.333 K / s. After a shear pulse was applied, the sample was maintained for 10 min at the shearing temperature. Afterward, the sample was further cooled to 363 K at 0.0167 K / s below the peak of crystallisation temperature and then it was quenched to lower temperature. The sample was unloaded from the shear device at room temperature and was analyzed. The sheared sample disks had thickness of 0.5 mm and diameter of approximately 16 mm.

4.2.3. Structural analysis

Polarized light imaging (PLI) technique is a useful method to observe the orientation state of crystals in the whole sheared sample disk in one time through the birefringent state. The sheared disk was placed between a 90 °crossed polarizer and analyzer and then the photographs of the sample were taken by a CCD camera with using a white light as the incident light.

X-ray scattering (Bruker AXS Nanostar, Cu Kα radiation) was used to evaluate the arrangements of the crystals in the sample. Two-dimensional small angle X-ray scattering (SAXS) and wide angle X-ray diffraction (WAXD) patterns were scanned on the line across the diameter of the disks.

Thin slices for the observation by optical microscopy (OM) were prepared by using a microtome technique. The sheared disc was sliced at room temperature (Reichert-Jung Ultracut E) or at 113 K (Leica EM UC6 with cryo-unit) by using a glass and diamond knife. Thickness was controlled from 0.1 to 5 micron. Thin slices created were observed by using OM (Olympus BX50) with 90 degree crossed polarizer and analyser.

4.3. Result and discussion

4.3.1. Polarized light imaging

The polarized light imaging (PLI) of the h-PBD bimodal blend (2 wt % 1770 kDa in 18 kDa) sheared at 388 K at Ω = 3.3 rad / s for t_s = 40 s was taken under 90 ° crossed polarizers (**Figure 4.1 a**). A single boundary, which can be considered the point where the oriented morphology starts to form, is observed as the change of the contrast of the birefringence in the PLI as already reported in the previous paper[6, 7]. The Maltese cross[12] (as the result of a circumferentially-aligned birefringence axis) seen in only outside of the circular boundary can be explained that the oriented morphology has been formed in the area outside of the circular boundary and the isotropic spherulites have been formed in the inside of the boundary.[6, 7]

4.3.2. X-ray scattering

The small angle X-ray scattering (SAXS) and wide angle X-ray diffraction (WAXD) patterns were scanned across the diameter of the same sheared blend in order to confirm the formation of the oriented morphology and spherulites.

The SAXS patterns are consistent with the boundary decided by the PLI (**Figure 4.1 b**). The pattern taken at the edge of the sheared disk indicates the orientation of morphology. The pattern is the combination of the lobes on the meridian and the isotropic ring. The lobes arise from the kebabs forming perpendicular to the shish and the isotropic ring can be explained that the isotropic lamellae structure (spherulites) exists in the space between shish-kebabs. [7] The scattering from the shish[13] cannot be observed in the pattern due to the low concentration of the long chains.[7, 14, 15] The orientation becomes weaker at the area closer to the boundary but outside of the boundary. At last, the orientation disappears and only the isotropic ring from the lamellae in the spherulites is shown.

The WAXD patterns are also consistent with the PLI and SAXS (**Figure 4.1 c**). The WAXD patterns are composed of reflections as the diffraction from the crystallographic planes[16]. The intense area of the ring corresponding to 200 is indicated by Miller indices at meridian and 110 on the azimuth angle of 30 degree from equator. The reflections, 110 and 200, shown in the patterns are typical diffraction pattern for polyethylene with orthorhombic cell[16]. The b-axis of the unit cell in the sheared disk is therefore considered to be aligned perpendicular to the flow direction and parallel to the kebabs. The six reflections indicate that the a-axis and c-axis is twisting around the b-axis and therefore it suggests the formation of the twisted lamellae structure[17] as the kebabs. The broad reflections in the patterns mean that the direction of the b-axis (in the kebabs) is not perfectly perpendicular to the flow direction and it has the distribution of angle. At the area closer to the boundary but outside of the boundary, the orientation is weaker than the edge as shown in the reflection 110 on meridian. The orientation is no longer seen at the inside area of the boundary and it is considered that the unit cell of the crystals are randomly aligned.

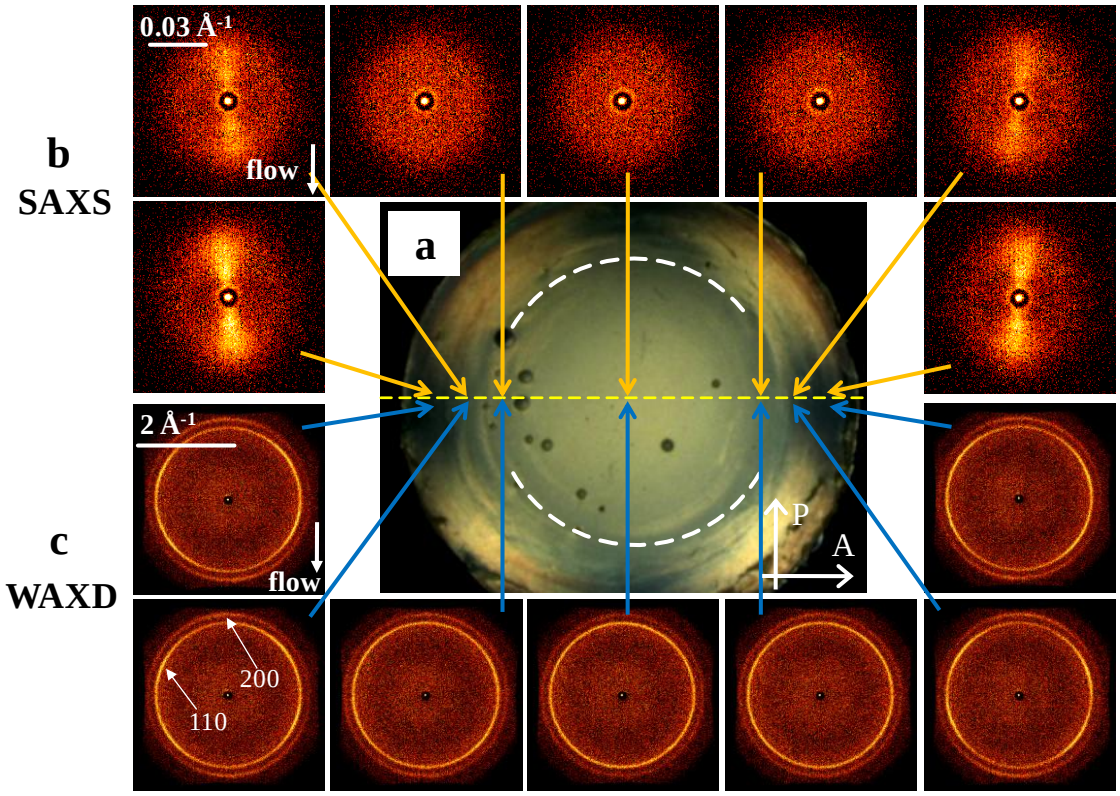

Figure 4.1. A polarized light image (PLI) of the bimodal blend (2 wt % 1770 kDa in 18 kDa) sheared at 388 K at Ω = 3.3 rad / s for t_s = 40 s taken under 90 ° crossed polarizers (a) SAXS patterns taken perpendicular to flow direction (b) and WAXD patterns taken perpendicular to flow direction (c). The directions of the polarizer and analyser are indicated by the arrows in the image. The dashed semi-circle indicates the boundary positions which correspond to the change of morphologies from an un-oriented to oriented morphology. The SAXS and WAXD patterns were scanned on the dotted line on the image. The SAXS and WAXD patterns correspond to the areas marked by arrows on the images. The white bars on the patterns indicate q-scale.

The SAXS and WAXD pattern were also taken from the direction parallel to the flow in the oriented area and they were also consistent with the suggested morphology. The SAXS pattern was similar to the pattern taken in the un-oriented area and shows no orientation (**Figure 4.2 b**). This suggests that the scattering is caused by the kebab crystals which are grown random directions around shish structure orthogonal to the

plane of the page. The WAXD pattern also indicates no orientation (**Figure 4.2 c**) and it can be explained by the same way with the SAXS pattern.

The both SAXS and WAXD patterns have a scattering on an equatorial line. It is due to the form factor of the sample. Since the thickness of the sheared disc (0.5 mm) and the size of the beam spot (0.4 mm) are close, the scattering occurs at the surface of the sample.

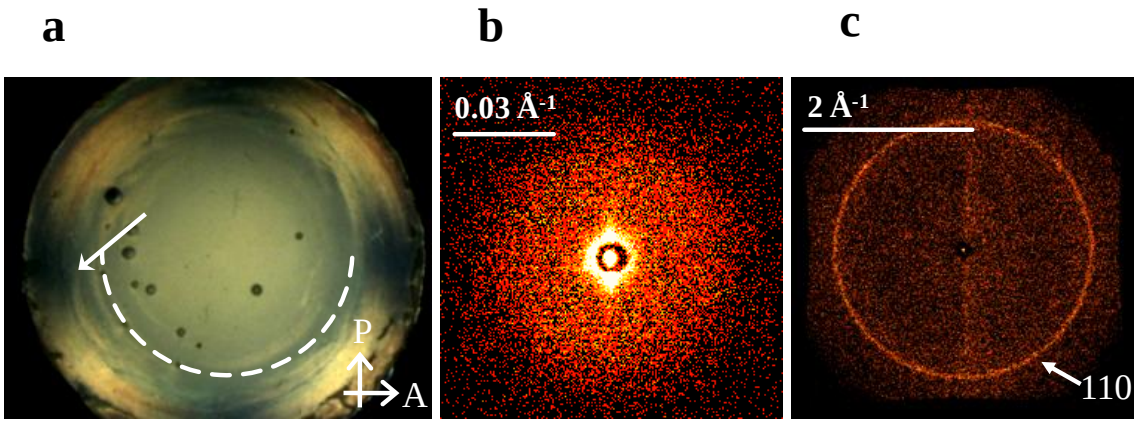

Figure 4.2. A polarized light image (PLI) of the bimodal blend (2 wt % 1770 kDa in 18 kDa) sheared 388 K at Ω = 3.3 rad / s for t_s = 40 s taken under 90 ° crossed polarizers (a) SAXS pattern of the oriented part of the blend taken from the direction parallel to flow and (c) SAXS pattern of the oriented part of the blend taken from direction. The directions of the polarizer (P) and analyser (A) are indicated by the arrows on the PLI. The dashed curve line on the PLI indicates the position of a boundary. A diagonal arrow on the PLI shows the positions that the SAXS and WAXD pattern were taken. The white bars on the patterns indicate q-scale.

4.3.3. Optimising microtome conditions

The aim of this section is to find out the conditions for the preparation of polyethylene thin slices for morphology observation. The sheared commercial polyethylene disc has a boundary between un-oriented and oriented morphology at about a radius, r = 4 mm. The centre part (un-oriented part) of the sheared disc was sliced by using microtome with different settings.

The best method for the preparation of thin slice to observe transverse morphology was 5 μm of thickness by using a diamond knife at room temperature. The micrograph taken under 90 ° crossed polarizer and analyser was full of contrast and there were fewer knife marks on the thin slice (**Figure 4.3 a**). The diamond knife was effective to avoid the knife marks. The thin slice of 0.1 μm thickness prepared by the diamond knife has only few knife marks (**d**). The thin slice of 1 μm cut by glass knife at room temperature has plenty of knife marks toward parallel to cutting direction (**b**). This can be derived from poor flatness of the glass knife blade. Also, no morphology could be observed by optical microscopy with crossed polarizer and analyser. The contrast under crossed polarizer and analyser can be represented by retardation, $R = t \cdot \Delta n$, where t is the thickness and Δn is the birefringence per unit thickness of the sample. Therefore, the reason of low contrast is considered that the thickness of the slice was too thin compared to the birefringence. The cutting at 113 K by using cryo-microtome with glass knife was also tried (**c**). However, the thin slice was curly compared to the slice cut at room temperature. Also, distinctive pattern perpendicular to the cutting direction is observed in micrographs taken under crossed polarizer and analyser (**Figure 4.4**). The pattern is considered to be the result of flexure stress in the thin slice caused by compression by the glass knife. A pronounced pattern can be seen around the knife mark where the more compression is emphasized in the thin slice. The pattern can be observed under crossed polarizer and analyser because the flexure of the slice is thicker than the flat area and it makes enough contrast of retardation, R. In contrast, crystal morphology (spherulites and streaks) can be observed in thin slice of 5 μm thickness created by diamond knife at room temperature (**Figure 4.5**).

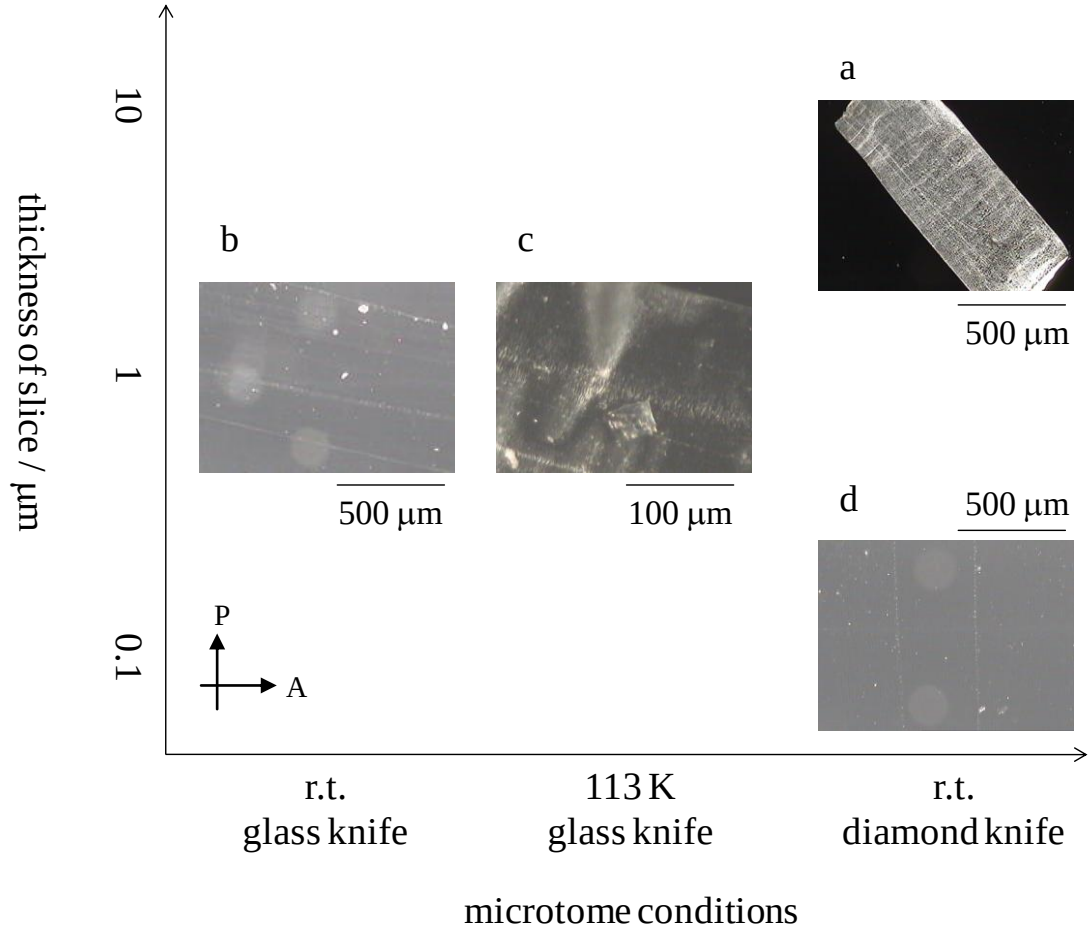

Figure 4.3. Optical micrographs of thin slices of centre part of sheared polyethylene cut under different conditions. The thin slices were cut parallel to longer direction. Pictures were taken by using a 90 ° crossed polarizer and analyser and their directions are indicated by the arrows in the image.

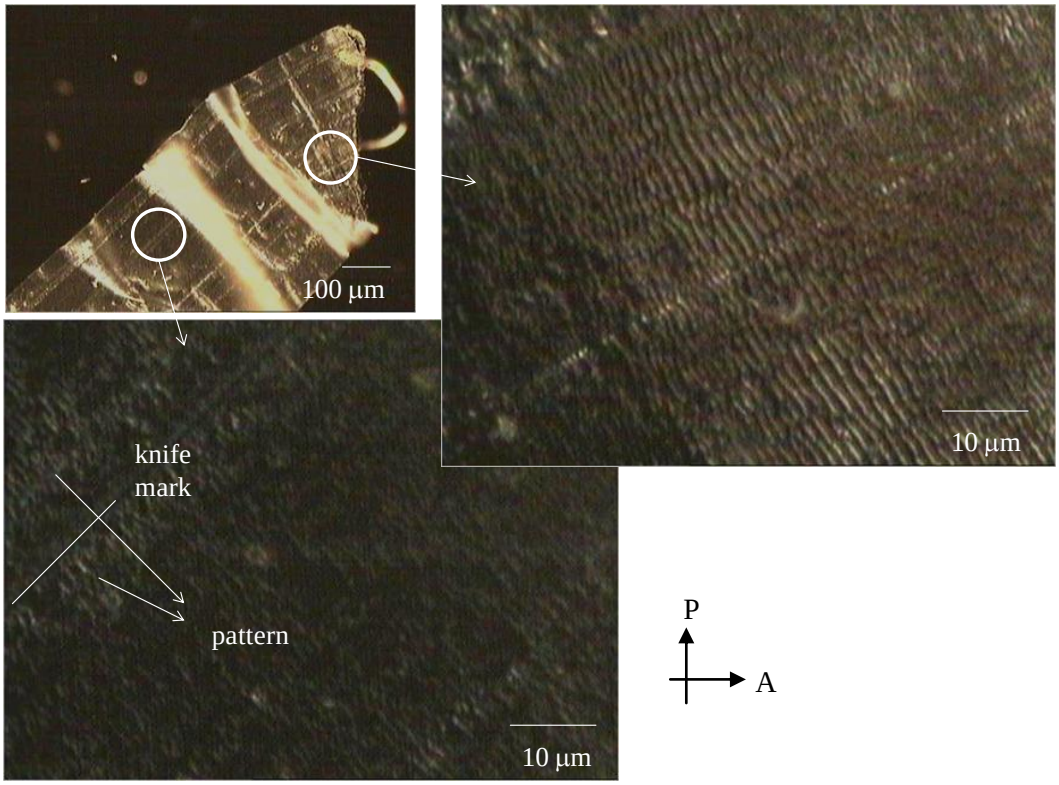

Figure 4.4. Optical micrographs of 1 μm thin slice of centre part of sheared polyethylene cut by glass knife at 113 K. The micrographs were taken by using a 90 ° crossed polarizer and analyser and their directions are indicated by the arrows in the image.

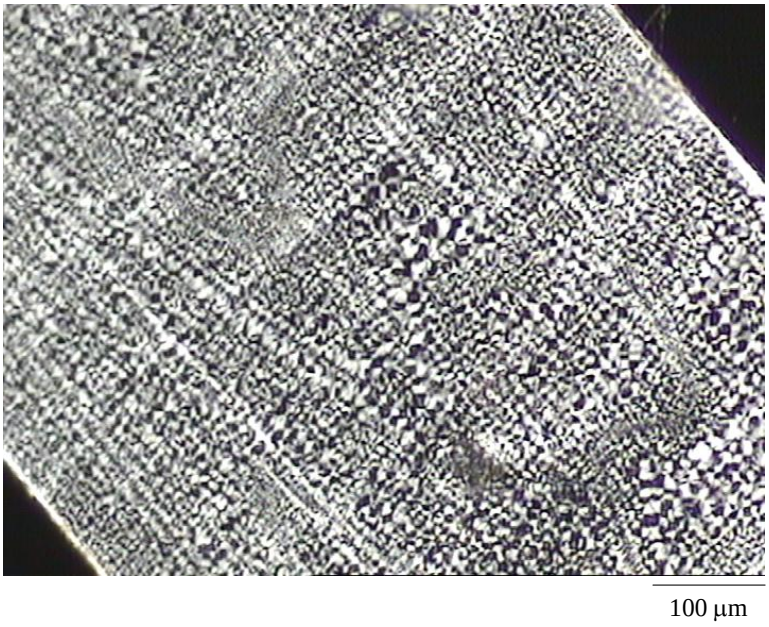

Figure 4.5. An optical micrograph of 5 μm thin slice of centre part of sheared polyethylene cut by diamond knife at room temperature. The micrograph was taken by using a 90 ° crossed polarizer and analyser.

4.3.4. Morphology by optical microscopy

The morphology of the h-PBD bimodal blend comprised of the 2 wt % 1770 kDa in 18 kDa matrix sheared at 388K at Ω = 3.3 rad /s for t_s = 40 s was checked by the optical microscopy (OM). Crystal morphology of the centre part of the disk, where the shear rate is zero, is an isotropic spherulitic morphology (**Figure 4.6 b**) similar to the morphology which can be shown in polyethylene crystallised under quiescent condition. An anisotropic morphology was observed at the outer area of the disk sliced parallel to flow direction (**Figure 4.6 c**). The long crystals (shish) aligned parallel to the flow direction are observed. The kebabs, which are detected by the SAXS scattering, cannot be distinguished in the image because the thickness of the kebabs is too thin to observe by OM (the thickness of the lamellar crystals has been controlled to few nm by the number of branches per chain[9]). The morphology of the thin strip sliced perpendicular to the flow direction (**Figure 4.6 d**) is isotropic. It is considered that the shish structure is aligned parallel to the eye direction. In summary, the results of the morphology observation by OM were consistent to the expectation by the PLI and X-ray scattering.

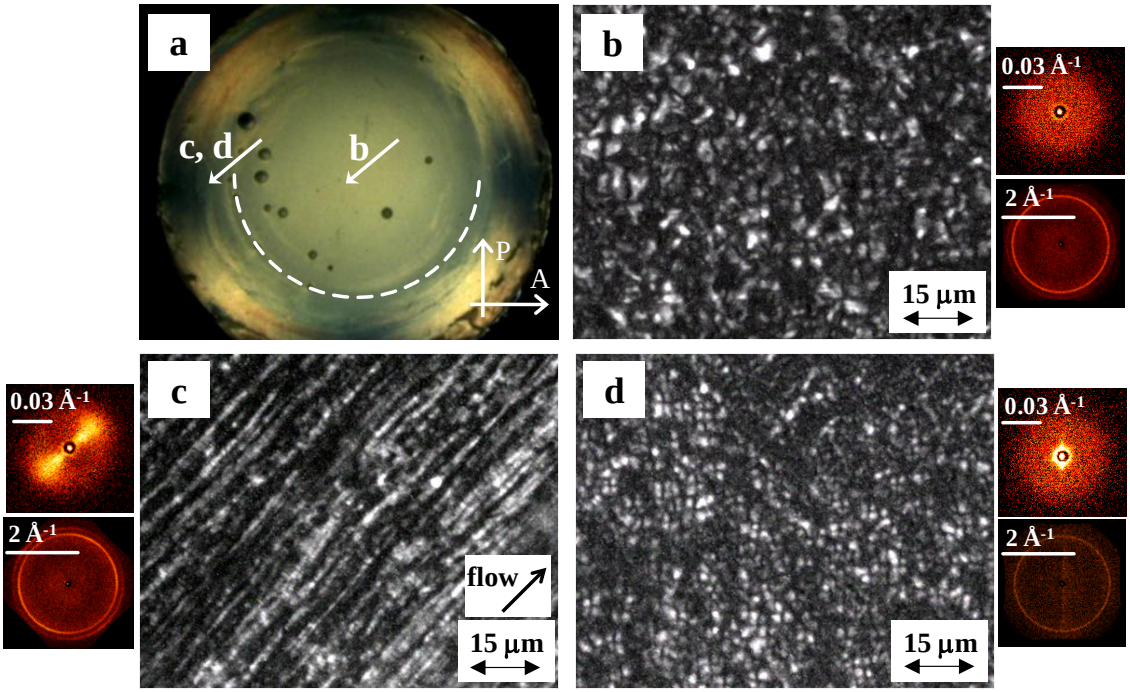

Figure 4.6. A polarized light image (PLI) of the bimodal blend (2 wt % 1770 kDa in 18 kDa) sheared 388 K at Ω = 3.3 rad / s for t_s = 40 s taken under 90 ° crossed polarizers (a) and morphology of the cross section of the centre of the sheared disk (b), sliced parallel to flow direction at the outside area of boundary position (c) or sliced perpendicular to flow direction at the outside are of boundary position (d) taken by using optical microscopy (OM) with crossed polarizers. The directions of the polarizer (P) and analyser (A) are indicated by the arrows in on the PLI. The directions of polarizer and analyser in (b), (c) and (d) are same with the PLI. The diameter and the thickness of the sheared sample are 16 mm and 0.5 mm respectively. The dashed curve line on the PLI indicates the position of a boundary. Diagonal arrows on the PLI show the positions that thin strips for morphology observation were prepared. The SAXS and WAXD patterns in the images were taken at the areas corresponding to the same areas and directions used for the OM observation. The white bars on the patterns indicate q-scale.

4.4. Conclusions

The structural information of sheared hydrogenated polybutadiene blends was checked by polarised light imaging (PLI), X-ray scattering and optical microscopy (OM). The boundary position where an oriented morphology starts to form was distinguished on

the PLI as the boundary between isotropic birefringence and anisotropic birefringence. The small angle X-ray scattering (SAXS) and wide angle X-ray diffraction (WAXD) patterns scanned across the diameter of the sample parallel to a flow direction indicated the oriented scattering patterns at the area of outside of the boundary and un-oriented scattering patterns at the inside of the boundary. The SAXS and WAXD patterns were also taken at the oriented area perpendicular to the flow direction and did not indicate the orientation.

The morphology observed by the optical microscopy (OM) was also consistent with the results by PLI and X-ray scattering patterns. The morphologies of oriented part and un-oriented part of the blend were observed by the OM in the cross-section, sliced at the conditions decided by preparatory experiments by using commercial polyethylene. No oriented morphology was observed in the OM images taken from the un-oriented area and the oriented area observed perpendicular to the flow direction. On the other hand, shish structure was observed parallel to flow direction taken from the oriented area, observed perpendicular to the flow direction.

4.5. References

1. Blackadder, D. A.; Schleinitz, H. M. *Nature* **1963,** 200, 778-779.
2. Pennings, A. J.; Kiel, A. M. *Kolloid Z. Z. Polym.* **1965,** 205, 160-162.
3. Keller, A.; Machin, M. J. *J. Macromolec. Sci. B* **1967,** 1, 41-91.
4. Hill, M. J.; Barham, P. J.; Keller, A. *Colloid & Polymer Science* **1980,** 258, 1023-1037.
5. Zuo, F.; Keum, J. K.; Yang, L.; Somani, R. H.; Hsiao, B. S. *Macromolecules* **2006,** 39, 2209-2218.
6. Mykhaylyk, O. O.; Chambon, P.; Graham, R. S.; Fairclough, J. P. A.; Olmsted, P. D.; Ryan, A. J. *Macromolecules* **2008,** 41, 1901-1904.
7. Mykhaylyk, O. O.; Chambon, P.; Impradice, C.; Fairclough, J. P. A.; Terrill, N. J.; Ryan, A. J. *Macromolecules* **2010,** 43, (5), 2389-2405.
8. Janeschitz-Kriegl, H.; Ratajski, E.; Stadlbauer, M. *Rheol. Acta.* **2003,** 42, 355-364.
9. Fernyhough, C. M.; Young, R. N.; Poche, D.; Degroot, A. W.; Bosscher, F. *Macromolecules* **2001,** 34, 7034-7041.
10. Nogales, A.; Hsiao, B. S.; Somani, R. H.; Srinivas, S.; Tsou, A. H.; Balta-Calleja, F. J.; Ezquerra, T. A. *Polymer* **2001,** 42, (12), 5247-5256.

11. Massa, M. V.; Lee, M. S. M.; Dalnoki-Veress, K. *Journal of Polymer Science: Part B: Polymer Physics* **2005,** 43, 3438-3443.

12. Saville, B. P., *Polarized Light: Qualitative Microscopy.* Elsevier Applied Science: London, 1989.

13. Keum, J. K.; Zuo, F.; Hsiao, B. S. *Macromolecules* **2008,** 41, (13), 4766-4776.

14. Ogino, Y.; Fukushima, H.; Matsuba, G.; Takahashi, N.; Nishida, K.; Kanaya, T. *Polymer* **2006,** 47, (15), 5669-5677.

15. Somani, R. H.; Hsiao, B. S.; Nogales, A.; Srinivas, S.; Tsou, A. H.; Sics, I.; Balta-Calleja, F. J.; Ezquerra, T. A. *Macromolecules* **2000,** 33, (25), 9385-9394.

16. Ward, I. M., *Structure and Properties of Oriented Polymers*. Applied Science Publishers: London, 1975; p 500.

17. Keith, H. D.; Padden, F. J. *Journal of Polymer Science* **1958,** 31, (123), 415-421.

18. Eder, G.; Janeschitz-Kriegl, H.; Liedauer, S. *Progress in Polymer Science* **1990,** 15, (4), 629-714.

Chapter 5

Using Multi-modal Blends to Elucidate the Mechanism of Flow-induced Crystallisation in Polymers

This chapter has partially reproduced in part from the paper submitted to Macromolecules.

5.1. Introduction

Polyolefins are the most widely used polymer nowadays due to their excellent cost-benefit performance. The typical processing methods for semi-crystalline polyolefins take a melt and shape it by means of either an extrusion or moulding technique and the shape stabilisation process is crystallisation by cooling.[1] The flow conditions in the extruder, and die or mould system has a profound effect on the morphology of the crystalline material and introduces different crystal types from isotropic spherulites to highly oriented "shish-kebab structure" in the polyolefin with the significant effect on materials through their mechanical, thermal and optical properties.[2] Therefore using appropriate processing conditions is important to obtain better performance out of the polyolefin products.

The shish-kebab structure produced by flow-induced crystallization was first observed in agitated dilute polyethylene solution[3, 4] and then a similar oriented morphology was also observed in sheared bulk polyolefin.[5] It is commonly held that the mechanism of formation of the oriented morphology is that the shish nuclei are firstly created in the direction of flow and then kebab crystals grow on the shish nuclei.[2] Consequently, the creation of the shish nuclei is a key element to form the oriented morphology.

It is generally considered that the shear rate needs to surpass critical values for shish nuclei formation.[6] Various attempts have been made to clarify the critical shear rate, $\dot{\gamma}_{\min}$, which is required to develop the oriented morphology. Although a number of the studies have focused on the issue that the $\dot{\gamma}_{\min}$ relates to a specific relaxation time, the reptation time τ_{d} or the Rouse time τ_{R},[7-9] it was recently confirmed experimentally[10] that the $\dot{\gamma}_{\min}$ correlates the inverse of τ_{R}.

When polymer chains are sheared above $\dot{\gamma}_{\min}$, it is well established that the polymer chains are locally stretched and create precursors of the shish nuclei. These precursors can develop into shish nuclei by the growth of the precursors in the direction of the flow[11] or by aggregation of the precursors.[12] The total amount of flow applied to the polymer chains is also considered to affect the development process from precursors to shish nuclei. So both the shear rate and total strain are important factors in the formation of the shish nuclei and oriented morphology. In this study, boundary flow conditions are

used as a term which describes the required flow conditions involving both the shear rate and strain to form the oriented morphology.

Boundary flow conditions have been established for bimodal blends of hydrogenated polybutadiene prepared from low-polydispersity short and long chains.[10] The blends were sheared at different shear rates and strains by using a torsional flow created by parallel disks. The flow geometry allowed a wide range of shear rates and total strain to be studied in a single experiment and the boundary flow conditions for the formation of an oriented morphology were measured by using small angle X-ray scattering (SAXS) and polarized light imaging (PLI) technique. The results clearly demonstrated that the bimodal blends have a single boundary flow conditions corresponding to the τ_R of the long chains.

Analogous measurement of the boundary flow conditions of industrial polydisperse polymers have also been published.[13] The boundary flow conditions of industrial polydisperse polymers such as polyethylene and polypropylene were measured by using combinatorial methods developed described above and it was shown that polydisperse polymers also have a single boundary flow conditions corresponding to the longest τ_R of the polymers.

Although the understanding about the $\dot{\gamma}_{min}$ for the formation of the oriented morphology is well established, the link between the boundary flow conditions involving a required minimum strain for both the bimodal blends and polydisperse polymers needs further consideration. In order to uncover the underlying link between bimodal blends and polydisperse polymers, the most critical problem is the interaction of many kinds of long chains with different molecular weight in polydisperse polymers. The aim of this study is to understand the interaction between two kinds of long chains with different molecular weight in a model trimodal blend and illustrate how the interaction between long chains affects the boundary flow conditions in polydisperse polymers.

5.2. Experimental

5.2.1. Materials

A linear hydrogenated polybutadiene trimodal blend was prepared from low-polydispersity polymers[14] whose molecular weights are 1770, 1080 and 18 kDa (the latter is used as a matrix). The blend contains 2 wt % of 1770 kDa chains and 2 wt % of 1080 kDa chains in the matrix. Bimodal blends were also prepared from 2 wt % 1770 kDa chains or 2 wt % 1080 kDa chains in the same matrix.

5.2.2. Thermal properties

Crystallization temperature and melting temperature of the bimodal blend (2 wt % 1080 kDa in 18 kDa) and the trimodal blend (2 wt % 1770 kDa and 2 wt % 1080 kDa in 18 kDa) were measured by using differential scanning calorimetry (**Figure 5.1 and 5.2**). The melting point of the bimodal blend, 387 K, and trimodal blend, 385 K are similar to the melting point of h-PBD bimodal blend, 388 K, reported previously[10].

The crystallization and melting temperature are important information in selecting the temperature used for rheology measurements and shearing experiments. The lowest temperature used in the rheology measurements were 393 K and it is above the melting temperature. Although the lowest temperature used for shearing experiments (383 K) is below the end of melting peak of the blend, it is still 8 K higher than the temperature that the crystallization starts and it can be considered that the effect of the formation of spherulite during the shear experiments is negligible.

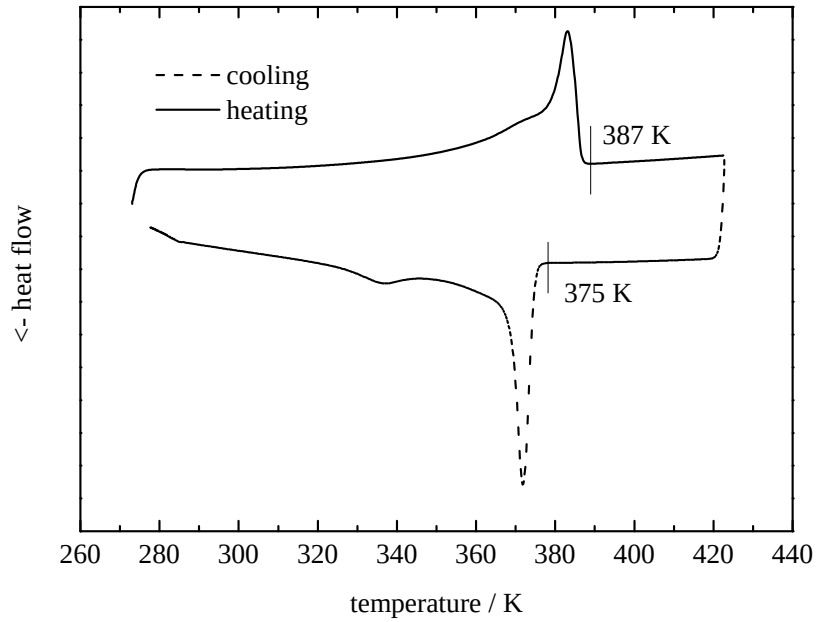

Figure 5.1. DSC result of the bimodal blend (2 wt % 1080 kDa in 18 kDa). Cooling step (dotted line) was measured first at -10 K/min and then heating step (solid line) was measured at 10 K/min.

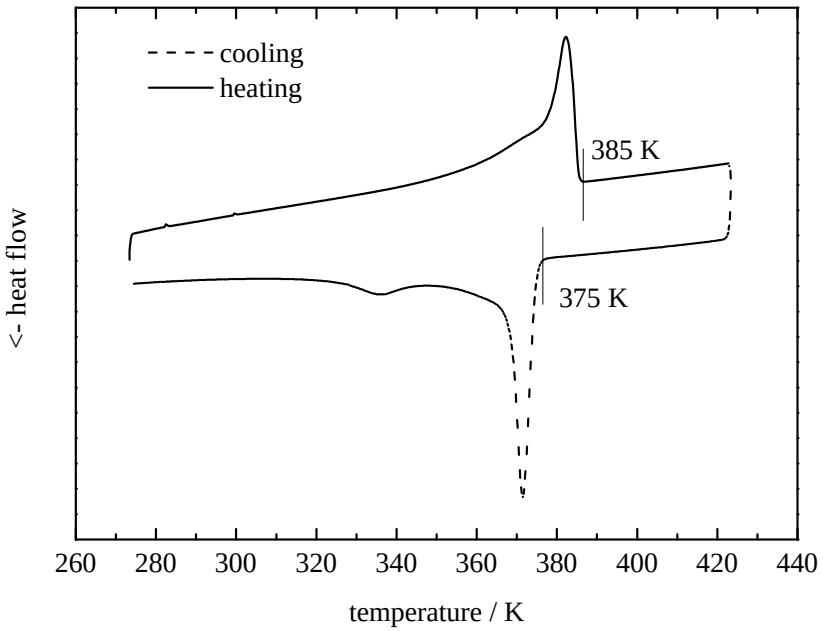

Figure 5.2. DSC result of the trimodal blend (2 wt % 1770 kDa and 2 wt % 1080 kDa in 18 kDa). Cooling step (dotted line) was measured first at -10 K/min and then heating step (solid line) was measured at 10 K/min.

5.2.3. Relaxation times of low-polydispersity polymers

The relaxation times of the low-polydispersity polymers were obtained from a storage modulus, *G*', and loss modulus, *G*", measured by a rheometer (see chapter 3). The relaxation times of the materials used here were extracted from the previous chapter (**Table 5.1**).

Table 5.1. Relaxation times of the low-polydispersity hydrogenated polybutadiene samples at 388 K used in this study.

M_w, kDa	τ_R, s	τ_d, s	$\dot{\gamma}_{min} = 1/\tau_R$, s^{-1}
18	6.28×10^{-6}	9.78×10^{-5}	159240
1080	2.26×10^{-2}	51	44
1770	6.07×10^{-2}	231	16

5.2.4. Shear experiments

The procedures to apply the shear to samples were similar to the chapter 4. The used shearing temperature was 383, 385, 388 or 391 K. After the shear procedure, the sample was unloaded from the shear device at room temperature and was analyzed. The sheared sample disks had thickness of 0.5 mm and diameter of approximately 16 mm.

Small angle X-ray scattering (SAXS, Bruker AXS Nanostar, Cu Kα radiation) was used to evaluate the oriented morphology of the sheared disks as reported previously.[10, 13, 15] Two-dimensional SAXS patterns were scanned at 0.5 mm intervals on the line across the diameter of the disks. The Herman's orientation function P_2[16] was used as the criterion for the lamellae orientation across the diameter of the sheared disks:

$$P_2 = \frac{3\langle cos^2\phi \rangle - 1}{2} \qquad \textbf{Eq. 5.1}$$

P2 was calculated from intensity patterns $I(\phi)$ by SAXS. The average angle of the lamellar orientation $\langle cos^2\phi \rangle$ is expressed by the following.

$$\langle cos^2\phi \rangle = \frac{\int_0^{\pi/2} I(\phi) cos^2\phi \, sin\, \phi d\phi}{\int_0^{\pi/2} I(\phi) \, sin\, \phi d\phi} \quad \textbf{Eq. 5.2}$$

Polarized light imaging (PLI) is a useful method to observe the orientation state of crystals in the whole sheared sample disk in one time. The sheared disk was placed between a 90 °crossed polarizer and analyzer and then a photograph of the sample was taken by a CCD camera with using a white light as the incident light.

A boundary position, which is the radius that the oriented morphology starts to form in the sheared disks, can be detected by both the PLI and orientation function by SAXS. The boundary position by the PLI was calculated by using the average of the boundary position in the whole sample. Conversely the boundary position assessed from the degree of orientation P2 by SAXS was the result of the scan on only one line across the diameter of the sheared disk and, therefore, the boundary positions determined by the PLI tend to have smaller deviation than those determined by SAXS.

Then a boundary specific work w_b [10, 12, 13] was calculated from the boundary position of each sample. The w_b is defined as follows:

$$w_\mathrm{b} = \int_0^{t_s} \eta[\dot{\gamma}_\mathrm{b}(t)] \, \dot{\gamma}_\mathrm{b}{}^2(t)\mathrm{d}t \quad \textbf{Eq. 5.3}$$

where t_s is a shearing duration, $\dot{\gamma}_\mathrm{b}(t)$ is a boundary shear rate which can be calculated from the boundary position and η is the shear rate dependent viscosity.

When the shear is applied to the sample in this study, the shear rate is not constant through the shear duration. The function of the shear rate against the shear duration is a

trapezoidal shape which has a certain acceleration and deceleration zone. The equation for the boundary specific work includes a shear rate dependent viscosity $\eta[\dot{\gamma}(t)]$; therefore it must be measured separately.

5.2.5. Viscosity fitting of the blend

Firstly, a complex viscosity was measured against strain to investigate the linear region and decide the strain used for the viscosity measurements against angular frequency (**Figure 5.3-5)**.

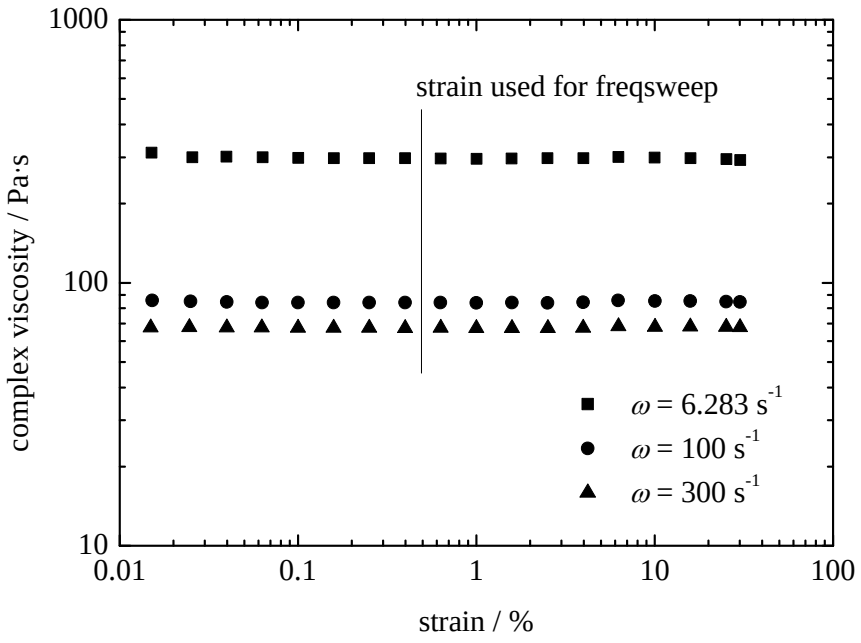

Figure 5.3. Strain sweep measurement for the h-PBD trimodal blend (2 wt % 1770 kDa and 2 wt % 1080 kDa in 18 kDa) at 403 K by 25 mm cone-plate geometry (cone angle = 6:36:00) at angular frequency = 6.3, 100 and 300 s^{-1}.

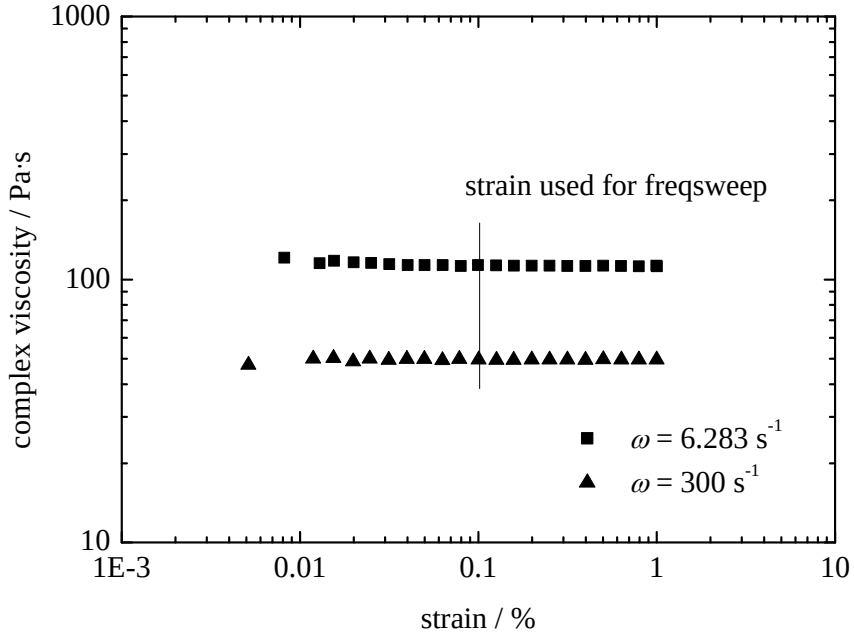

Figure 5.4. Strain sweep measurement for the h-PBD bimodal blend (2 wt % 1770 kDa in 18 kDa) at 413 K by 25 mm cone-plate geometry (cone angle = 6:36:00) at angular frequency = 6.3 and 300 s^{-1}.

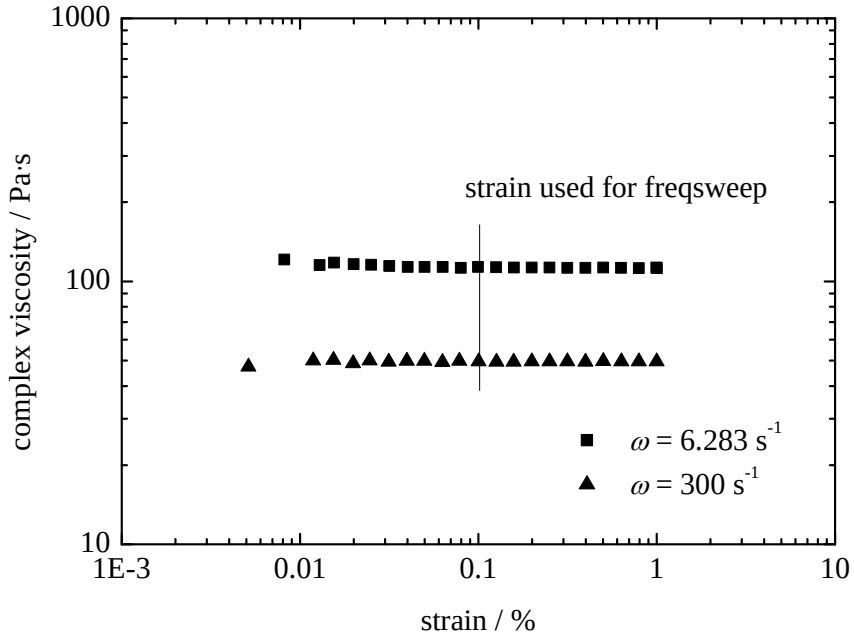

Figure 5.5. Strain sweep measurement for the h-PBD bimodal blend (2 wt % 1080 kDa in 18 kDa) at 413 K by 25 mm cone-plate geometry (cone angle = 6:36:00) at angular frequency = 6.3 and 300 s^{-1}.

The complex viscosity $\eta^*(\omega)$ which is equivalent to $\eta[\dot{\gamma}(t)]$ by considering the Cox-Merz rule $\eta(\dot{\gamma}) = |\eta^*(\omega)|$, was measured at 393, 403 and 413 K by frequency sweep rheology measurements using the strain decided above. Then, the $\eta^*(\omega)$ at the shearing temperature was calculated by using the time-temperature-superposition technique (**Figure 5.6 - 5.9, symbols**). The $\eta^*(\omega)$ curve can be represented by the following modified Cross model equation that a linear term η_2 has been added to account for a less frequency-dependent component originating from a low molecular weight matrix.

$$|\eta^*(\omega)| = \frac{\eta_1}{1+(\omega/\omega_1)^{\alpha_1}} + \eta_2 \qquad \textbf{Eq. 5.6}$$

where η_1, η_2, ω_1 and α_1 are fitting parameters.

The $\eta^*(\omega)$ of the trimodal blend and bimodal blends at 383, 385, 388 and 391 K was fitted by the equation and the parameters of the fitting were acquired. The trimodal blend has a higher $\eta^*(\omega)$ than the bimodal blend (1770 kDa) at 388 K (**Figure 5.6**) due to the concentration of the long chains. Since the Eq. 4.3 includes the $\eta^*(\omega)$ as the parameter, the difference of $\eta^*(\omega)$ affects the boundary specific work calculated later. The difference of $\eta^*(\omega)$ at the range of the shear rate used for shearing (30-300 s^{-1}) is up to twice.

The $\eta^*(\omega)$ of the bimodal blend (1080 kDa) was also compared with the $\eta^*(\omega)$ of the trimodal blend at 383 K (**Figure 5.7**). Since the $\eta^*(\omega)$ of the bimodal blend (1080 kDa) is lower than the bimodal blend (1770 kDa), the $\eta^*(\omega)$ difference at the range of the shear rate used for shearing (30-300 s^{-1}) is up to 2.5 times.

The $\eta^*(\omega)$ curves and fitting result at different temperature are shown in **Figure 5.8 and 5.9**. The fitting parameters obtained were summarised in Table **5.2 – 5.5**.

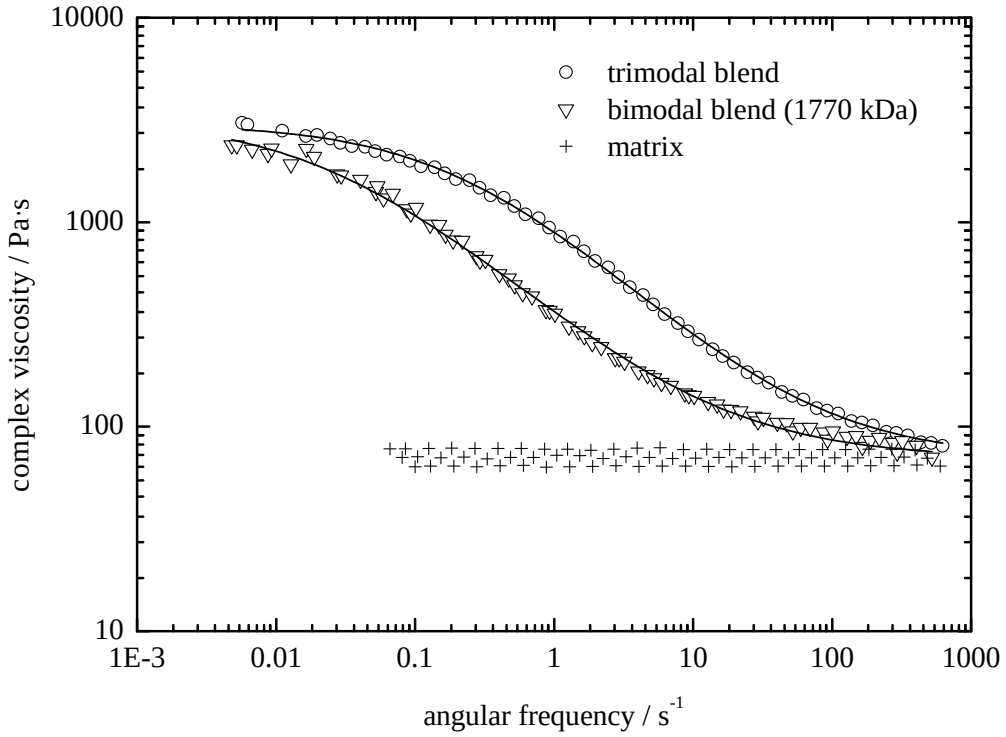

Figure 5.6. The measured shear-rate dependent complex viscosity of the blends and 18 kDa matrix (symbols) and fitting curves (lines). The viscosity of the hydrogenated polybutadiene trimodal blend (2 wt % 1770 kDa and 2 wt % 1080 kDa in 18 kDa), the bimodal blend (2 wt % 1770 kDa in 18 kDa) and matrix were measured by a rheometer. The viscosity were measured at 393, 403 and 413 K and then were shifted to T = 388 K by using time-temperature superposition. The modified Cross model was used to fit the data.

Table 5.2. The fitting parameters (T = 388 K).

	η_1	η_2 &	ω_1	α_1
trimodal blend (2 wt % 1770 and 1080 kDa in 18 kDa)	3070	71	0.22	0.67
bimodal blend (2 wt % 1770 kDa in 18 kDa)	2862	71	0.05	0.70

&: the viscosity curves were fitted all together (including matrix) with a constraint that η_2 is a common parameters.

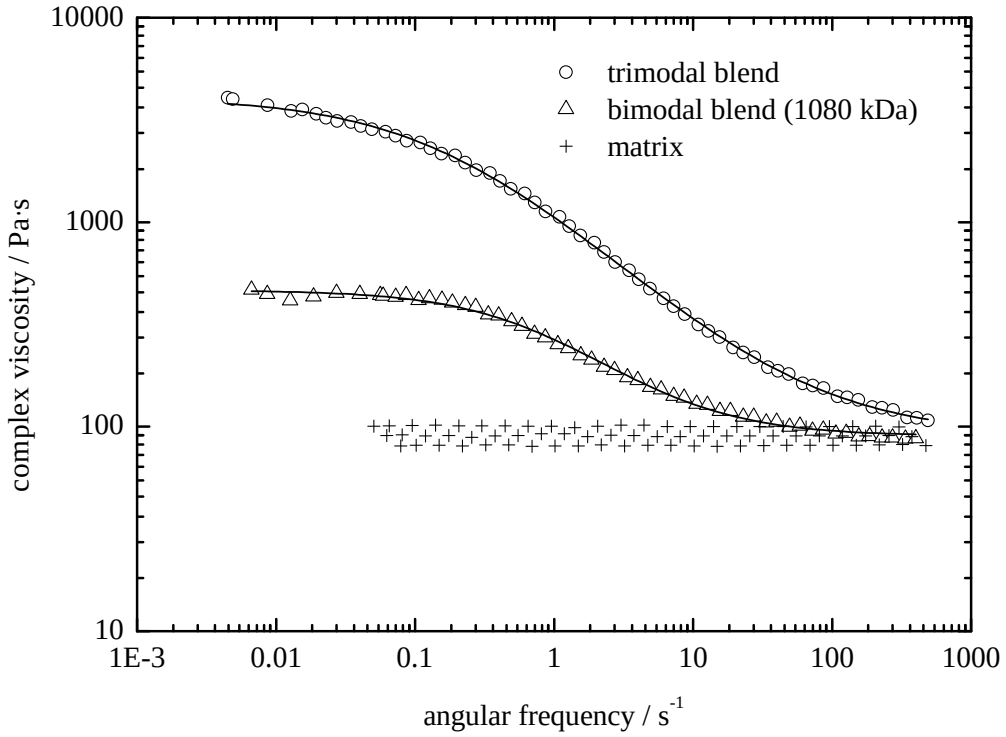

Figure 5.7. The measured shear-rate dependent complex viscosity of the blends and 18 kDa matrix (symbols) and fitting curves (lines). The viscosity of the hydrogenated polybutadiene trimodal blend (2 wt % 1770 kDa and 2 wt % 1080 kDa in 18 kDa), the bimodal blend (2 wt % 1770 kDa in 18 kDa) and matrix were measured by a rheometer. The viscosity were measured at 393, 403 and 413 K and then were shifted to T = 383 K by using time-temperature superposition. The modified Cross model was used to fit the data.

Table 5.3. The fitting parameters (T = 383 K).

	η_1	η_2 [&]	ω_1	α_1
trimodal blend (2 wt % 1770 and 1080 kDa in 18 kDa)	3994	90	0.19	0.68
bimodal blend (2 wt % 1080 kDa in 18 kDa)	375	90	0.88	0.89

&: the viscosity curves were fitted all together (including matrix) with a constraint that η_2 is a common parameters.

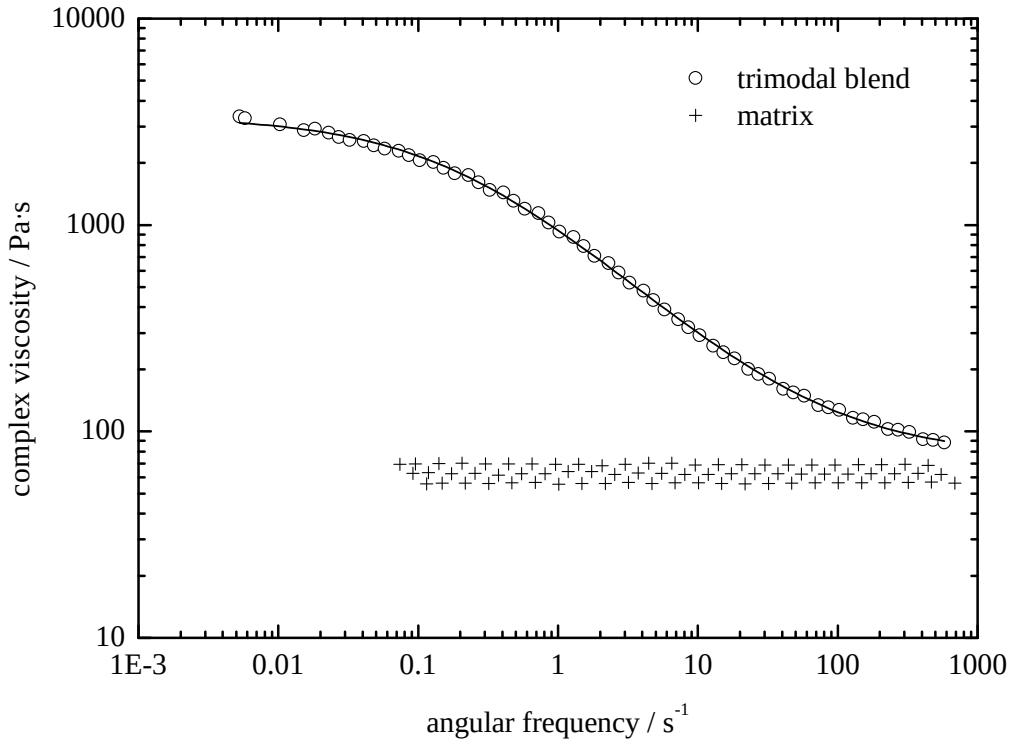

Figure 5.8. The measured shear-rate dependent complex viscosity of the blends and 18 kDa matrix (symbols) and fitting curves (lines). The viscosity of the hydrogenated polybutadiene trimodal blend (2 wt % 1770 kDa and 2 wt % 1080 kDa in 18 kDa) and matrix were measured by a rheometer. The viscosity were measured at 393, 403 and 413 K and then were shifted to T = 391 K by using time-temperature superposition. The modified Cross model was used to fit the data.

Table 5.4. The fitting parameters (T = 391 K).

	η_1	η_2 &	ω_1	α_1
trimodal blend (2 wt % 1770 and 1080 kDa in 18 kDa)	3281	75	0.22	0.69

&: the viscosity curves were fitted all together (including matrix) with a constraint that η_2 is a common parameters.

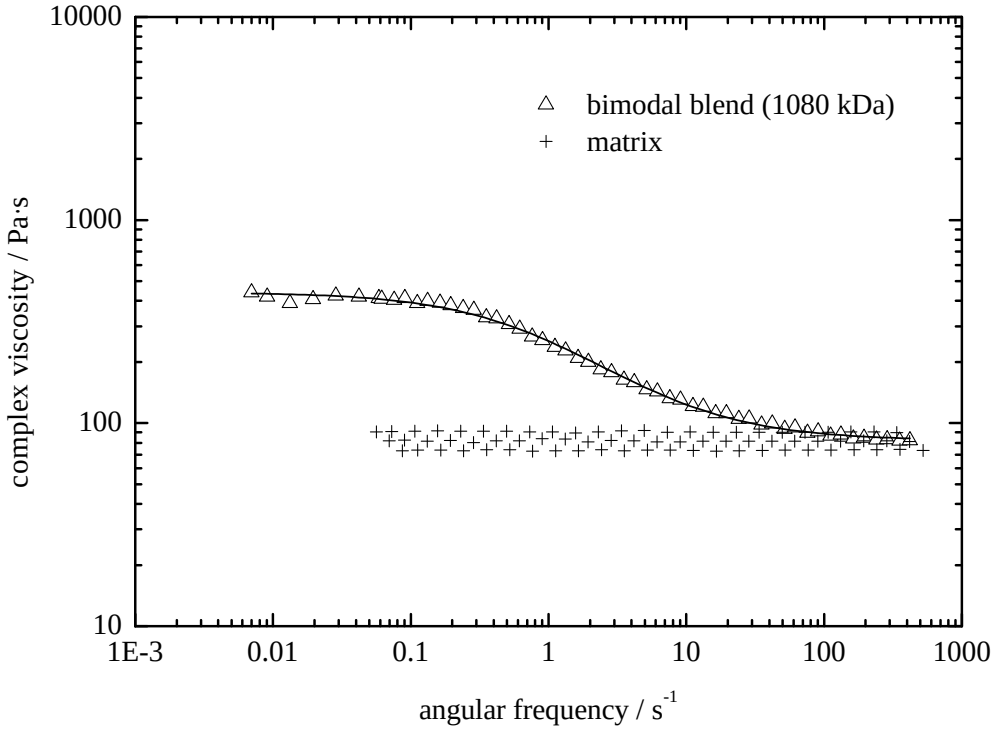

Figure 5.9. The measured shear-rate dependent complex viscosity of the blends and 18 kDa matrix (symbols) and fitting curves (lines). The viscosity of the hydrogenated polybutadiene bimodal blend (2 wt % 1080 kDa in 18 kDa) and matrix were measured by a rheometer. The viscosity were measured at 393, 403 and 413 K and then were shifted to T = 385 K by using time-temperature superposition. The modified Cross model was used to fit the data.

Table 5.5. The fitting parameters (T = 385 K).

	η_1	η_2 &	ω_1	α_1
bimodal blend (2 wt % 1080 kDa in 18 kDa)	359	82	0.90	0.85

&: the viscosity curves were fitted all together (including matrix) with a constraint that η_2 is a common parameters.

5.3. Results and discussion

The boundary flow conditions of the sheared bimodal blend comprised of 2 wt % 1770 kDa chains in the 18 kDa chains was remeasured (**Figure 5.10 a**) in order to check the reproducibility of the previous research[10]. A single circular boundary is observed by the change of the contrast in the PLI image and the orientation function P2[16] ,calculated from scattering patterns which were scanned across the diameter of the sample, shows a single inflexion point about a 6 mm radius. These results concerning the position of the single boundary in the bimodal blend are commensurate with the previously published results[10].

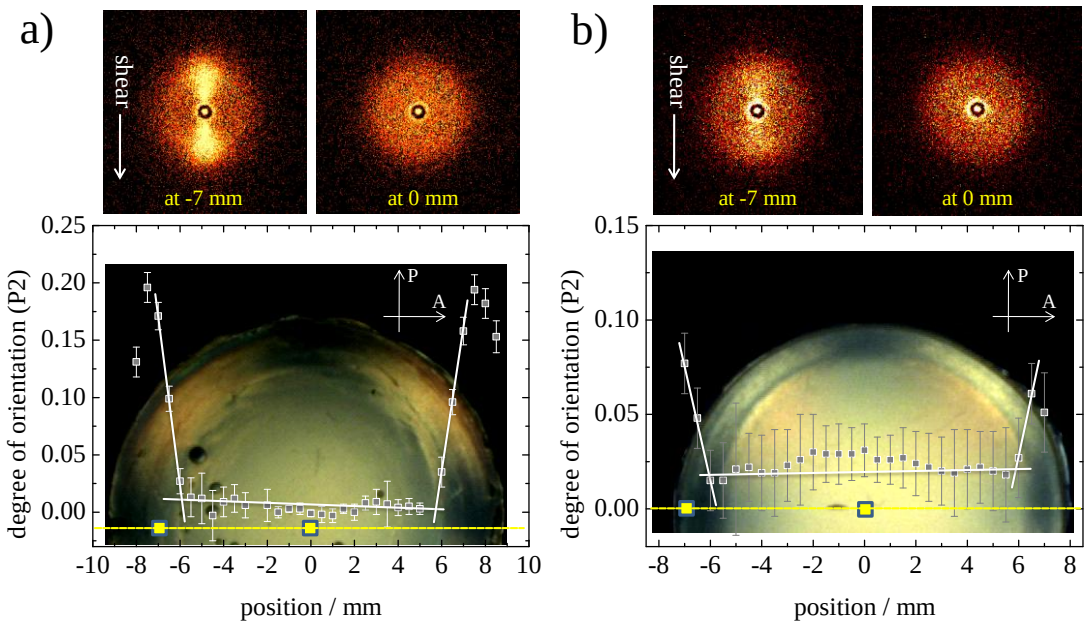

Figure 5.10. The orientation function (P2) of the lamellae structure along the flow direction measured across the diameter of a hydrogenated polybutadiene bimodal blend (2 wt % 1770 kDa in 18 kDa) sheared at 388 K at ω = 3.3 rad / s for t_s = 40 s (a) and the bimodal blend (2 wt % 1080 kDa in 18 kDa) sheared at 385 K at ω = 2.3 rad / s for t_s = 1,650 s (b). The images in the graphs were taken by using a 90 ° crossed polarizer and analyser. The directions of the polarizer and analyser are indicated by the arrows in the images. The SAXS patterns for the calculation of the orientation function were scanned at 0.5 mm intervals on the dotted line on the images of the sheared samples. The SAXS patterns at the top of the figure correspond to the areas marked by squares on the images in order of appearance from left to right.

The difference between the results herein and those reported previously is the magnitude of the boundary specific work w_b (**Figure 5.11**). The present data show the average w_b, calculated from the boundary positions detected by the PLI of the bimodal blend sheared at $\dot{\gamma}_b > \dot{\gamma}_{min}^{1770\,kDa}$ $(= 1/\tau_{R(1770\text{ kDa})})$, to be 6.0 ± 0.9 MPa and significantly greater than the value of w_b which was previously reported to be, 2.38 ± 0.07 MPa. This difference can be explained by the sensitivity of the boundary flow conditions to the viscosities of the blends. The equation to calculate the w_b includes the viscosity as a parameter. It means that the transmittance of the energy of flow to long chains in the blends to stretch them depends on the viscosity of the blends. That is that the long chains in a blend having higher viscosity can be more greatly stretched than the chains in lower viscosity blend if a same amount of flow is applied to the blends.

The bimodal blend in this study has higher viscosity than the previous blend (**Figure 5.11, small figure**). The bimodal blend with the 18 kDa matrix has more than twice the viscosity than the blend with the 15 kDa matrix at $\dot{\gamma}$ = 30 ~ 100 which is the range of $\dot{\gamma}$ used for the measurement of w_b. This viscosity difference is a factor of 2.5 which is the difference between the w_b of the blend with the 18 kDa matrix and the w_b of the blend with the 15 kDa matrix.

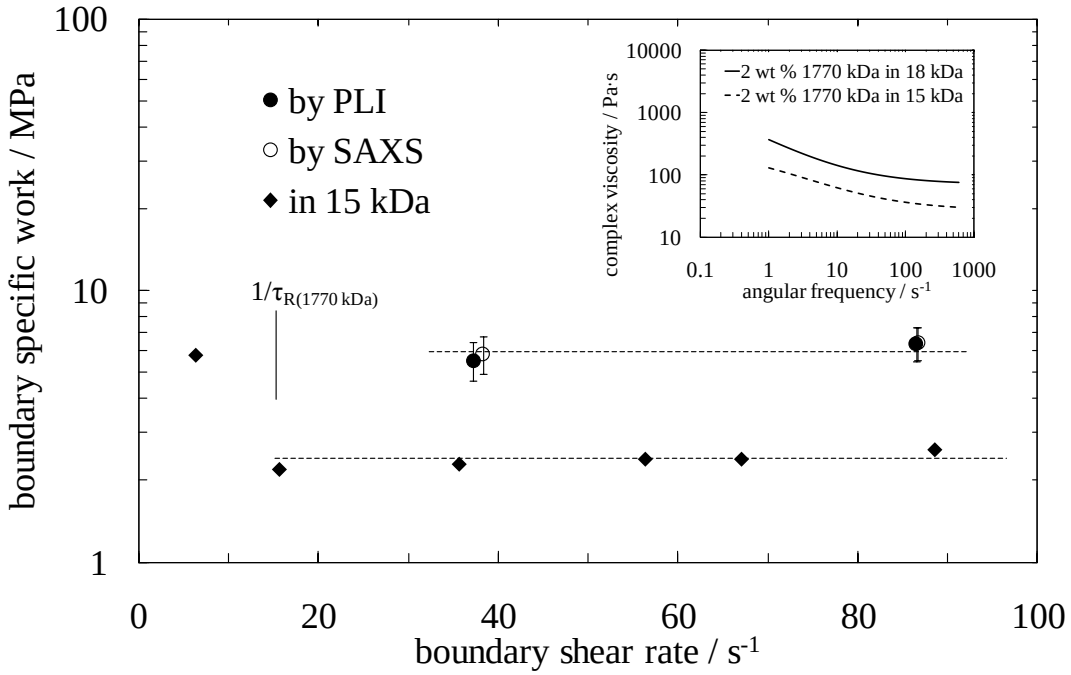

Figure 5.11. The plots of the boundary specific work w_b of the hydrogenated polybutadiene bimodal blend (2 wt % 1770 kDa in 18 kDa) measured at different boundary shear rates $\dot{\gamma}_b$ at shearing temperature 388 K. The w_b was calculated from both results by the PLI and degree of orientation by SAXS separately, and they are plotted as black (by PLI) and white markers (by SAXS), respectively. The rhombuses show the w_b of the hydrogenated polybutadiene bimodal blend (2 wt % 1770 kDa in 15 kDa) sheared at 388 K, which was referred from the previous research. The critical specific work w_c (the average of the w_b by PLI at $\dot{\gamma}_b > \dot{\gamma}_{min}$) is shown by the dashed lines. The small figure shows the viscosities of the hydrogenated polybutadiene bimodal blends composed by 2 wt % 1770 kDa in 18 kDa (line) and 2 wt % 1770 kDa in 15 kDa (dashed line) at 388 K.

The boundary position of the bimodal blend comprising of the 2 wt % 1080 kDa chains in the matrix sheared at 385 K was also detected in the same way (**Figure 5.10 b**). Similar to the bimodal blend comprised of the 1770 kDa chains, the single boundary was detected by the PLI and degree of orientation. The bimodal blend sheared above 388 K did not, however, exhibit a clear boundary despite the fact that the blend was sheared at $\dot{\gamma}_b > \dot{\gamma}_{min}^{1080\ kDa}$ $(= 1/\tau_{R(1080\ kDa)})$ for a long time. One possible reason for this could be as follows. As the temperature increases the critical nucleus size becomes

larger, therefore more stretched segments need to come together to form a nucleus. A larger chain contains more connected stretched segments and is more likely to take part in a stable nucleus than a shorter chain at the same temperature. Therefore the required work strongly depends on temperature and it can be considered that the formation of the oriented morphology in the 1080 kDa blend requires extremely long shear duration at 388 K.

The w_b of the bimodal blends were measured by using different shear rates at 385 K and 383 K (**Figure 5.12**). Both bimodal blends comprising of the 2 wt % long chains in the matrix have a constant w_b at $\dot{\gamma}_b > \dot{\gamma}_{min}^{1080\ kDa}$ and $\dot{\gamma}_b > \dot{\gamma}_{min}^{1770\ kDa}$ respectively. The sensitivity of the formation of oriented morphology is best exemplified by the fact that no boundary could be observed below $\dot{\gamma}_b$ = 25 s^{-1} at 385 K for the blend comprising 1080 kDa long chains. This is because $\dot{\gamma}_b$ is below the $\dot{\gamma}_{min}^{1080\ kDa}$ at this point (**Table 5.1**), it is considered that the oriented morphology does not form because the 1080 kDa chains are not sufficiently stretched below this shear rate.

The average w_b of the bimodal blend at $\dot{\gamma}_b > \dot{\gamma}_{min}^{1080\ kDa}$ was calculated to 130.5 ± 20.6 MPa at 385 K and 12.9 ± 1.9 MPa at 383 K using the results from the PLI. These w_b are much higher than the w_b of the bimodal blend comprised of the 1770 kDa chains, 6.0 ± 0.9 MPa, despite the lower shearing temperature being used. This suggests that the formation of shish nuclei by the 1080 kDa chains requires more energy than the formation of shish nuclei by the 1770 kDa chains.

The w_b calculated from the results by the PLI and SAXS were consistent each other. When comparing the w_b by SAXS and PLI the data from the former looks more scattered than the latter due to the difference of the accumulation methods, collecting information along a line and over an area respectively. For detecting the boundary position, the measurement by the PLI has the advantage that the whole boundary in the sample can be detected at once without scanning.

In summary, the hydrogenated polybutadiene bimodal blends comprising of the 2 wt % long chains in the short chain matrix also has a single boundary and constant w_b at $\dot{\gamma}_b > \dot{\gamma}_{min} = 1/\tau_R$. The boundary flow conditions by the PLI and SAXS were self-consistent, and as a method for measuring the boundary positions in the sheared disk, the PLI method is more time-efficient than SAXS.

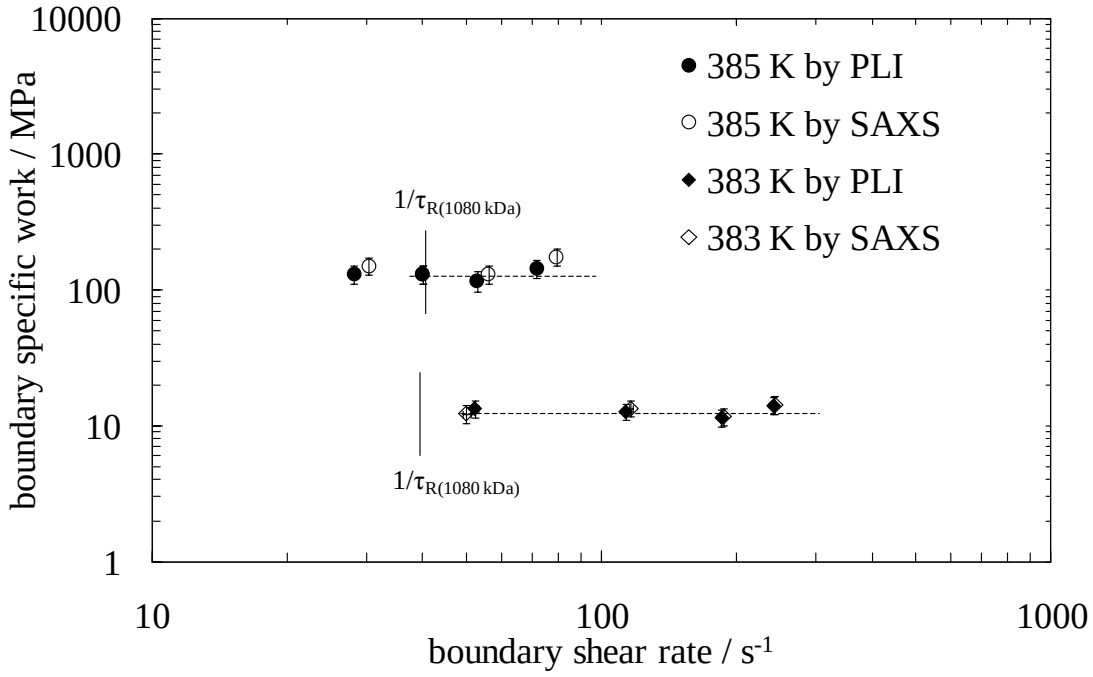

Figure 5.12. The plots of the boundary specific work w_b of the hydrogenated polybutadiene bimodal blend (2 wt % 1080 kDa in 18 kDa) measured at different boundary shear rates $\dot{\gamma}_b$. The circles and rhombuses show the w_b at shearing temperature 385 K and 383 K, respectively. The w_b was calculated from both results by the PLI and degree of orientation by SAXS separately, and they are plotted as black (by PLI) and white markers (by SAXS), respectively. The critical specific work w_c (the average of the w_b by PLI at $\dot{\gamma}_b > \dot{\gamma}_{min}$) is shown by the dashed lines.

PLI images of the sheared trimodal blend sample (2 wt % 1770 kDa and 2 wt % 1080 kDa in the matrix) disks were taken in order to investigate morphology changes in the disks (**Figure 5.13**). The images were analogous to the case of bimodal blends except for the number of boundaries observed. Two boundaries are identified as the change of the contrast in the sheared trimodal disks. Since the bimodal blends had a single boundary, the reason for the formation of two boundaries can be logically thought of as having its origin in the separated effect of having two kinds of long chains with different lengths (and hence relaxation times) in the trimodal blend.

The two boundaries of the trimodal blends can be interpreted as follows. Firstly the inner boundaries, which are indicated by dashed semi-circles in **Figure 5.13**, are the boundary positions where the 1770 kDa chains in the trimodal blend start to be stretched and make the oriented morphology. The 1080 kDa chains cannot be stretched at this position and shear rate because of their short relaxation time. Secondly, outer boundaries which are shown by solid semi-circles in the **Figure 5.13** are the boundary positions that the 1080 kDa chains start to participate the formation of the oriented morphology by nucleating an additional population of crystals.

The orientation function P2 was calculated from scattering patterns which were scanned across the diameter of the sample (**Figure 5.14**). The profile of the orientation function was also analogous to the bimodal blends except that it has two inflexion points associated with each boundary. At the centre of the disk, the orientation function is nearly zero and it indicates that no oriented morphology is formed. Inner inflexion points are the inner boundary and these points are consistent with the boundary position of the inner boundary obtained by the PLI technique. Outer inflexion points are the outer boundary and these points are also consistent with the boundary position of the outer boundary by the PLI.

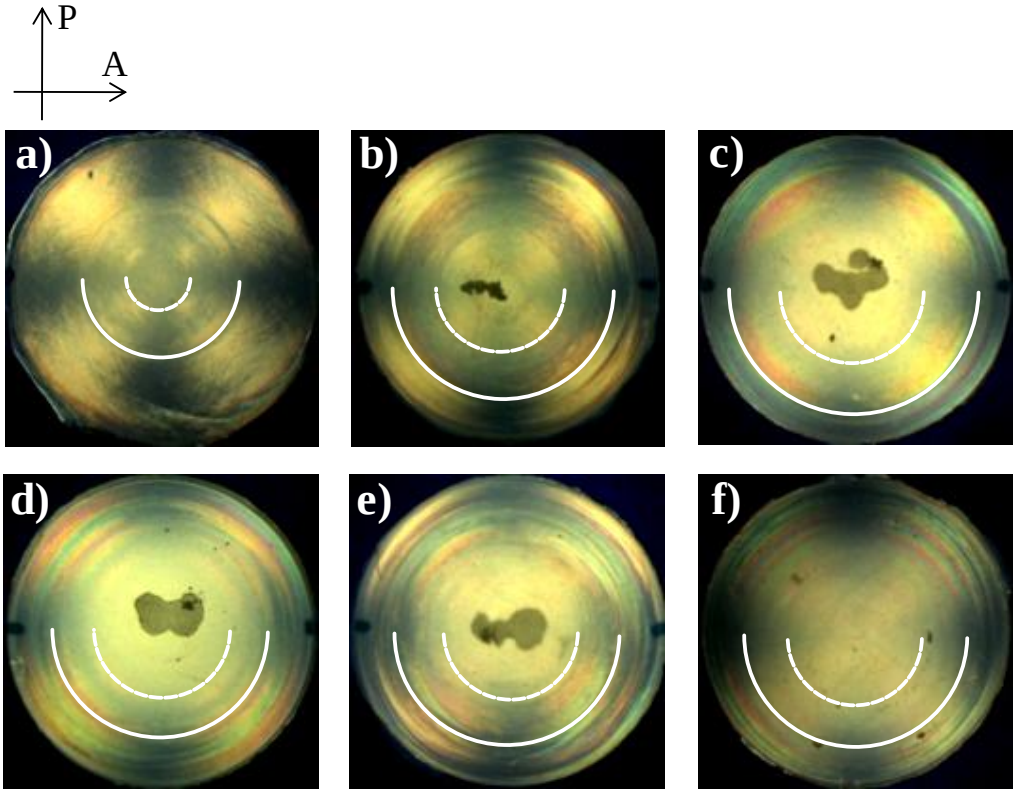

Figure 5.13. Images of the sheared hydrogenated polybutadiene trimodal blend (2 wt % 1770 kDa and 2 wt % 1080 kDa in 18 kDa) taken by using a 90 ° crossed polarizer and analyser. The directions of the polarizer and analyser are indicated by the arrows above the images. The shear conditions were ω = 0.7 rad / s, t_s = 2000 s (a); ω = 3.3 rad / s, t_s = 40 s (b); ω = 6.7 rad / s, t_s = 10 s (c); ω = 10.0 rad / s, t_s = 6 s (d); ω = 13.3 rad / s, t_s = 4 s (e); ω = 16.7 rad / s, t_s = 1 s (f) at 388 K. The diameter and the thickness of the sheared samples are 16 mm and 0.5 mm respectively. The dashed semi-circles indicate the boundary positions of inner boundaries which correspond to the change of morphologies from an un-oriented to oriented morphology and the solid semi-circles indicate the boundary positions of outer boundaries from the oriented morphology to a further oriented morphology.

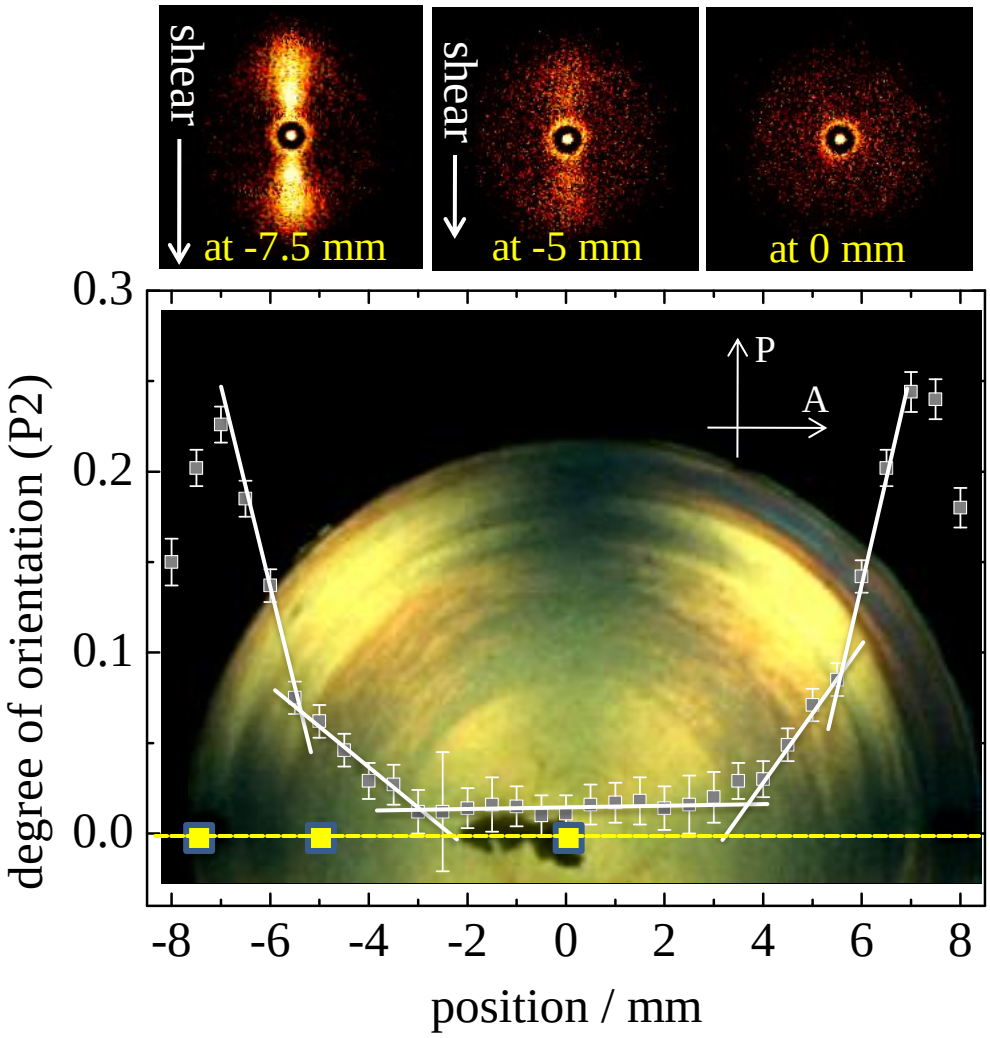

Figure 5.14. The orientation function (P2) of the lamellae structure along the flow direction measured across the diameter of the hydrogenated polybutadiene trimodal blend (2 wt % 1770 kDa and 2 wt % 1080 kDa in 18 kDa) sample sheared at 388 K at ω = 3.3 rad / s for t_s = 40 s. The SAXS patterns for the calculation of the orientation function were scanned at 0.5 mm intervals on the dotted line on the image of the sheared sample. The SAXS patterns at the top of the figure correspond to the areas marked by squares on the image in order of appearance from left to right.

Then the boundary specific work w_b was calculated from the boundary positions obtained by the PLI and SAXS in order to estimate the amount of flow which is required to form oriented morphology in the trimodal blend (**Figure 5.15**). As indicated by the previous results, w_b is a constant at $\dot{\gamma}_b > 1/\tau_R$. The constant w_b is defined as a critical specific work, w_c,[10] which is independent of the shear rate and shearing duration under the conditions that $\dot{\gamma}_b > 1/\tau_R$. Each w_c for the inner and outer boundary was calculated to 4.4 ± 1.0 and 10.4 ± 1.5 MPa respectively from the average of w_b by the PLI at $\dot{\gamma}_b > 1/\tau_R$.

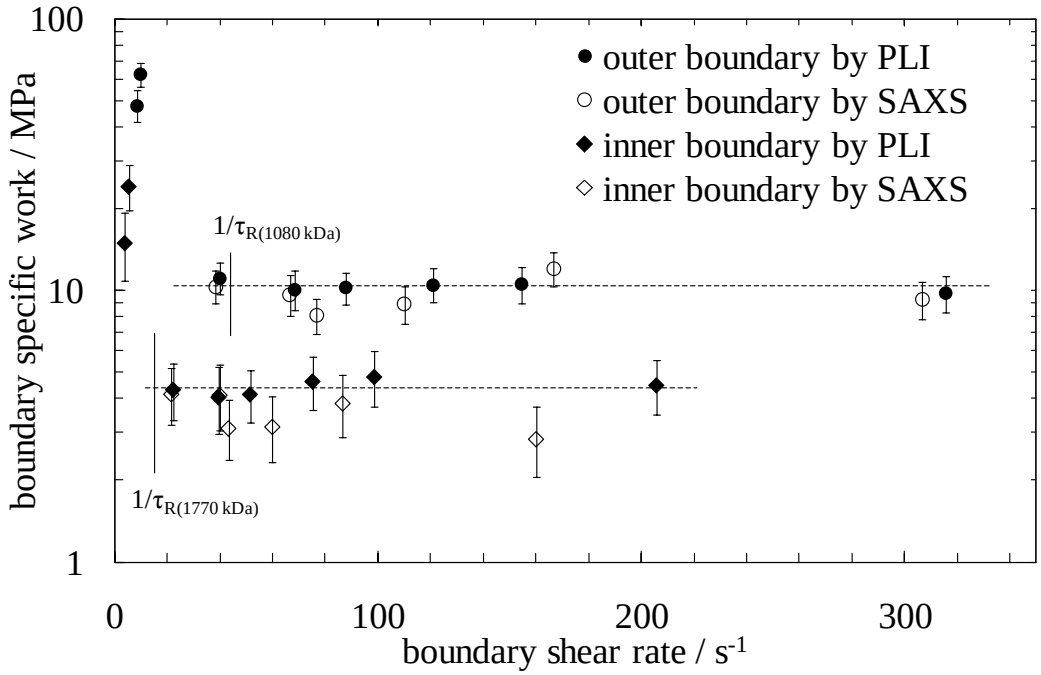

Figure 5.15. The plots of the boundary specific work w_b of hydrogenated polybutadiene trimodal blend (2 wt % 1770 kDa and 2 wt % 1080 kDa in 18 kDa) at different boundary shear rates $\dot{\gamma}_b$ at shearing temperature 388 K. The circles show the w_b of the outer boundary and the rhombuses are the w_b of the inner boundary. The w_b was calculated from both results by the PLI and degree of orientation by SAXS separately, and they are plotted as black (by PLI) and white markers (by SAXS), respectively. The critical specific work w_c (the average of the w_b by PLI at $\dot{\gamma}_b > \dot{\gamma}_{min}$) is shown by the dashed lines.

The boundary flow conditions of the trimodal blend were also measured at 383 and 391 K (**Figure 5.16 and 5.17**). Similarly to the result at 388 K, two pairs of the boundary flow conditions were detected. The w_b was proportional to the temperature, and this is consistent with previous research[13].

The w_b at higher boundary shear rate at 383 K showed higher w_b than the w_b at lower boundary shear rate. The reason for this could be a wall slip effect[17]. Since the viscosity of the sample is higher at 383 K than the viscosity at 388 and 391 K, a slip between the bulk and the surface region of the sample may occur and it would make the boundary specific work apparently higher.

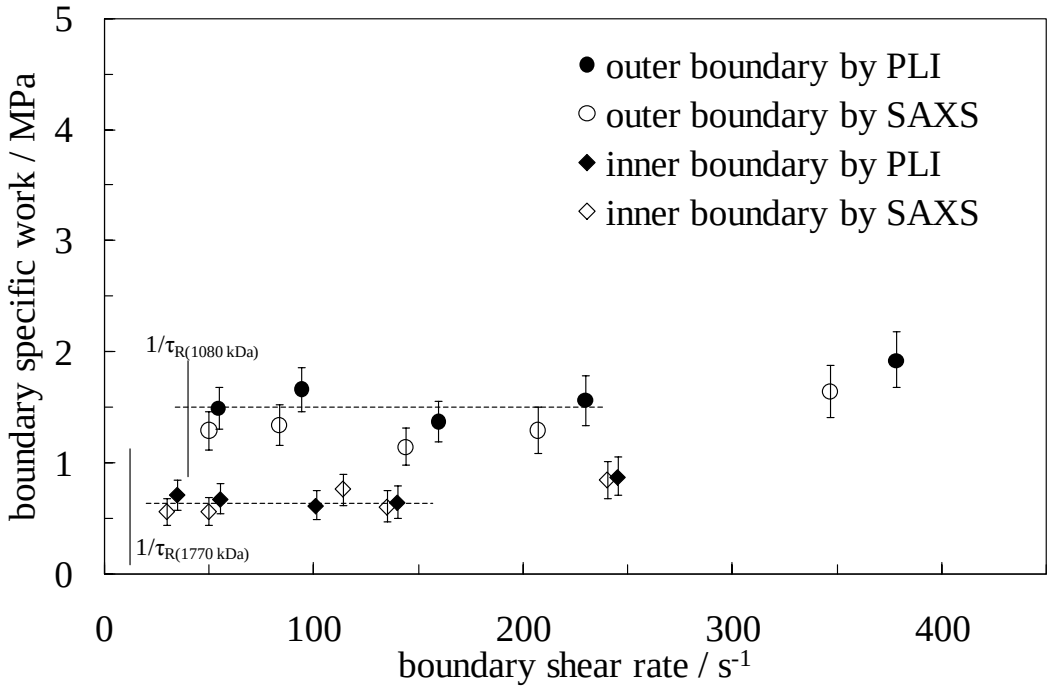

Figure 5.16. The plots of the boundary specific work w_b of hydrogenated polybutadiene trimodal blend (2 wt % 1770 kDa and 2 wt % 1080 kDa in 18 kDa) at different boundary shear rates $\dot{\gamma}_b$ at shearing temperature 383 K. The circles show the w_b of the outer boundary and the rhombuses are the w_b of the inner boundary. The w_b was calculated from both results by the PLI and degree of orientation by SAXS separately, and they are plotted as black (by PLI) and white markers (by SAXS), respectively. The critical specific work w_c (the average of the w_b by PLI at $\dot{\gamma}_b > \dot{\gamma}_{min}$) is shown by the dashed lines.

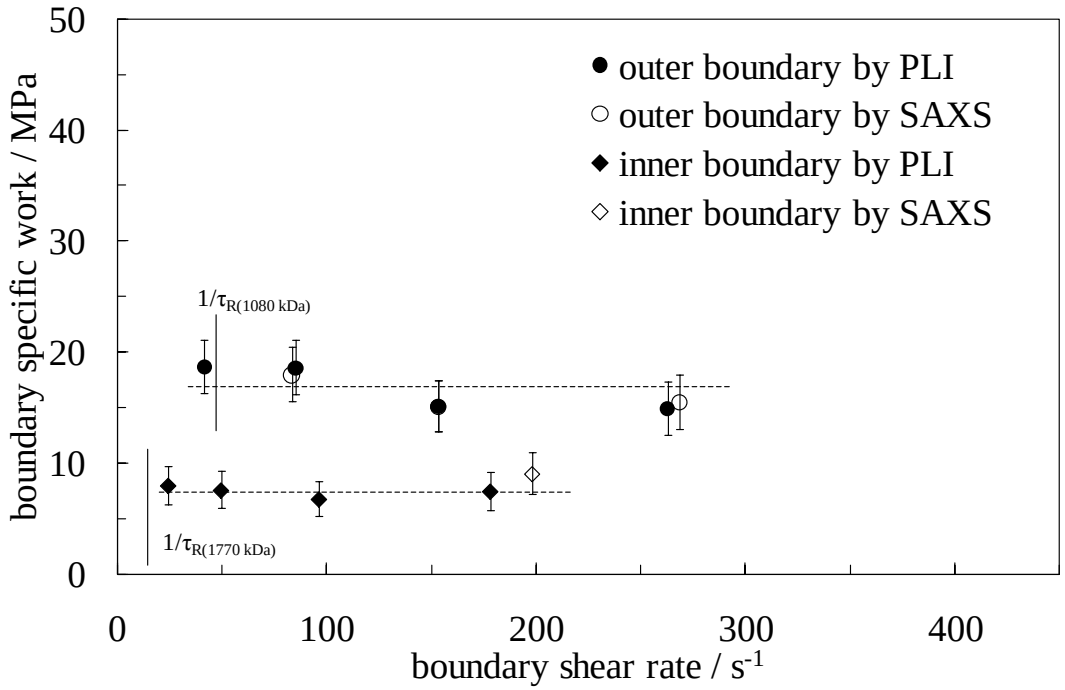

Figure 5.17. The plots of the boundary specific work w_b of hydrogenated polybutadiene trimodal blend (2 wt % 1770 kDa and 2 wt % 1080 kDa in 18 kDa) at different boundary shear rates $\dot{\gamma}_b$ at shearing temperature 391 K. The circles show the w_b of the outer boundary and the rhombuses are the w_b of the inner boundary. The w_b was calculated from both results by the PLI and degree of orientation by SAXS separately, and they are plotted as black (by PLI) and white markers (by SAXS), respectively. The critical specific work w_c (the average of the w_b by PLI at $\dot{\gamma}_b > \dot{\gamma}_{min}$) is shown by the dashed lines.

The results so far can be summarized by the following. The hydrogenated polybutadiene trimodal blend has two pairs of the boundary flow conditions corresponding to the two kinds of long chains with different molecular weight. The calculated w_b has a constant value (w_c) at $\dot{\gamma}_b > 1/\tau_R$ in qualitative agreement with the results of the bimodal blends and polydisperse polymers[13].

There is also quantitative correlations between the w_c of the trimodal blends compared with the w_c of their parent bimodal blends (**Figure 5.18**). The w_c of the outer boundary of the trimodal blend is much lower than the w_c of the bimodal blend comprised of the 2 wt % 1080 kDa chains in the matrix. This means that the amount of flow required to

form the oriented morphology in the 2 wt % 1080 kDa chains in the trimodal blend is much lower than 2 wt % 1080 kDa chains in the bimodal blend. On the other hand, the w_c of the inner boundary of the trimodal blend has a value of w_c quite close to that observed in the bimodal blend comprised of the 1770 kDa chains in the matrix. Therefore, it is suggested that (1) the boundary flow conditions corresponding to shorter chains are strongly affected by coexisting longer chains and (2) the coexisting shorter chains have a little effect on the boundary flow conditions corresponding to longer chains in multi-modal blends.

The important suggestion from the above results is that the longest chains dictate the flow-induced crystallisation of polydisperse polymers and this is in agreement with previous reports[9, 18-20]. When the polydisperse polymers are sheared, the longest chains are firstly stretched and form the shish-nuclei. Subsequently, other chains contribute to the formation of the shish nuclei by longer chains.

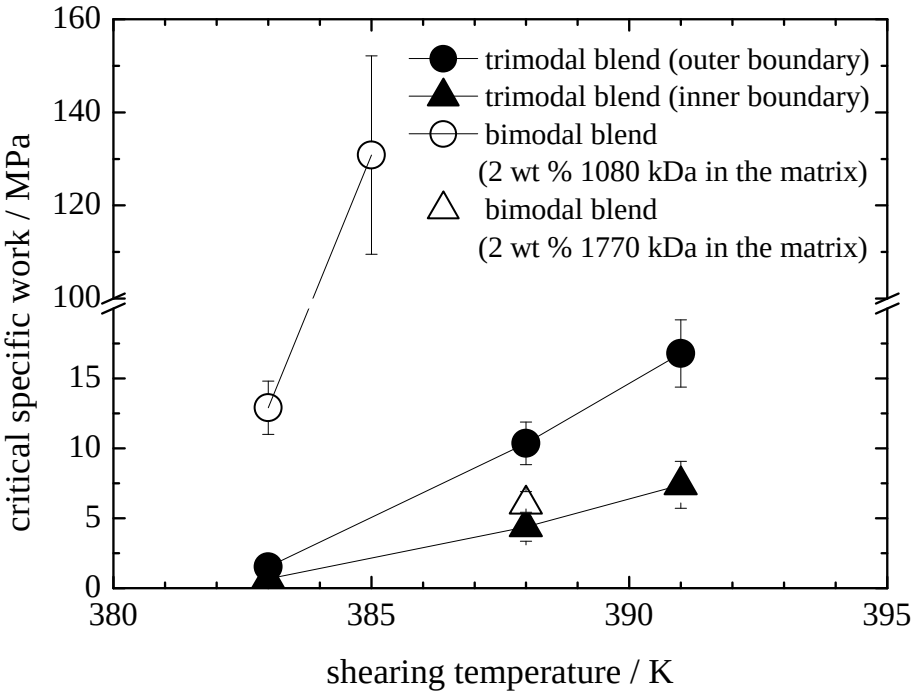

Figure 5.18. The critical specific work w_c of the trimodal (2 wt % 1770 kDa and 2 wt % 1080 kDa in 18 kDa) and bimodal blends (2 wt % 1770 kDa or 2 wt % 1080 kDa in 18 kDa) versus the shearing temperature.

It is noteworthy that an outer boundary can be observed for the trimodal blend at 388 and 392 K whereas such a boundary was not observed at these temperatures for the bimodal blend comprising of 2 wt % 1080 kDa chains in the matrix. At these temperatures, although the boundary flow conditions of the long chains is too extreme to create the stable shish nuclei by the 1080 kDa chains, the 1080 kDa can participate to the formation of the oriented morphology in the trimodal blend by the interaction with co-existing 1770 kDa chains.

It was previously reported that the relationship between the w_c and concentration of long chains is inversely proportional.[10] On this basis the w_c of a bimodal blend comprising of 4 wt % 1080 kDa chains in the matrix can be estimated to be 6.5 MPa at 383 K and this value is much higher than the w_c of the outer boundary of the trimodal blend. Although the trimodal blend contains a total of 4 wt % of long chains, the effect of the 1770 kDa chains on the boundary flow conditions of the 1080 kDa chains is not due to a simple matter of concentration.

The formation of shish nuclei can be interpreted by consideration of a mechanism involving a series of precursors.[21] In order to do this the formation of shish nuclei in the bimodal blend comprising of the 1770 kDa chains in the matrix has to be discussed first (**Figure 5.19, left**). The state of the long chains in the blend while shearing can be divided into three areas. Firstly, at $\dot{\gamma} < \dot{\gamma}_{\min}^{1770\ kDa}$, the long chains are not stretched and do not form any precursors and shish nuclei (**Figure 5.19, between centre and radius A**). Secondly, in the area which is sheared at $\dot{\gamma} > \dot{\gamma}_{\min}^{1770\ kDa}$ for an inadequate strain to surpass the boundary flow conditions, precursors can be formed in the direction of shear flow[11] but cannot form the shish nuclei because of the probability of the aggregation of the precursors is not sufficient (**Figure 5.19, between radii A and B**). Thirdly, in the outer area of the disk contains material sheared at $\dot{\gamma} > \dot{\gamma}_{\min}^{1770\ kDa}$ for enough strain to surpass the boundary flow conditions, the precursors aggregate and form the shish nuclei (**Figure 5.19, the outer zone of line B**).

The formation of the shish nuclei in the bimodal blend comprised of the 1080 kDa chains in the matrix can be interpreted in the same way excepting for the magnitude of $\dot{\gamma}_{\min}$ (**Figure 5.19, right**). Due to the shorter relaxation time of the 1080 kDa chains,

a greater shear rate is required to create the precursors (**Figure 5.19, radius C**). In addition, greater strain is needed to give enough probability of the aggregation of precursors to form the shish nuclei (**Figure 5.19, radius D**).

The scheme of the formation of the shish nuclei in the trimodal blend can be considered as follows (**Figure 5.19, centre**). In order to consider this simply, a hypothesis is applied to the mechanism that the concentration of precursors is very dilute; therefore the formation of the stable shish nuclei is dictated by the probability that two precursors meet. At first, at the area between the $\dot{\gamma}_{\min}^{1080\,kDa}$ and the boundary flow conditions of the inner boundary (**Figure 5.19, between radii C and E**), both 1770 and 1080 chains can be stretched and create precursors. However, any precursors cannot find a partner to aggregate with in this region.

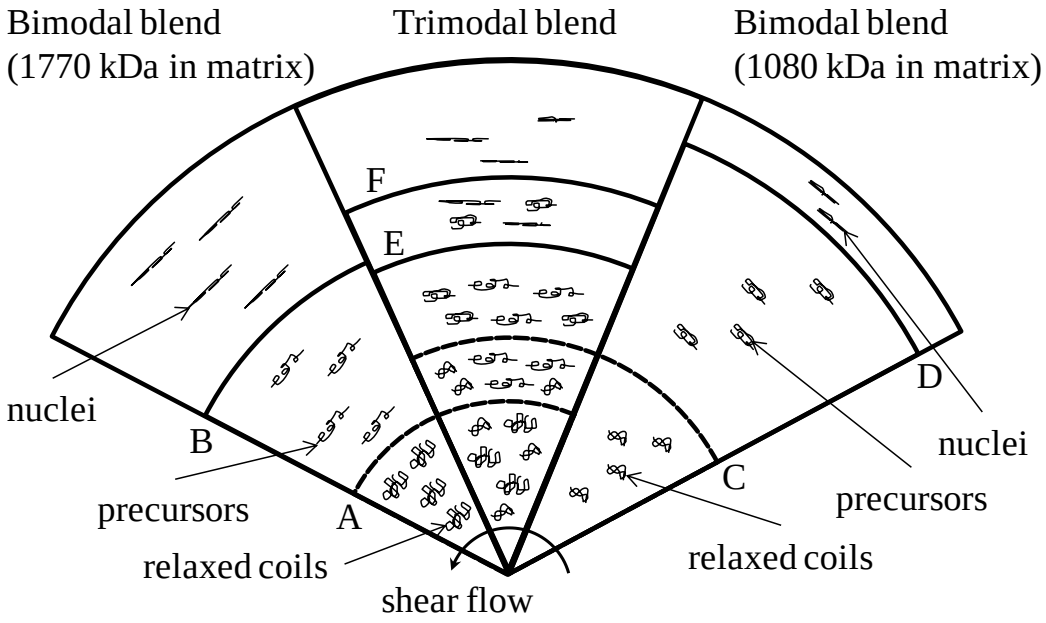

Figure 5.19. A schematic presentation of the shish nuclei formation in the trimodal and bimodal blends. The side and centre sectors indicate the shapes of the formation of the shish nuclei in the bimodal and trimodal blends, respectively. The circumferential lines show the minimum shear rate $\dot{\gamma}_{\min}^{1770kDa}$ required for stretching 1770 kDa chains (A), the boundary flow conditions of the bimodal blend (2 wt % 1770 kDa in 18 kDa) (B), the $\dot{\gamma}_{\min}^{1080kDa}$ for stretching the 1080 kDa chains (C), the boundary flow conditions of the bimodal blend (2 wt % 1080 kDa in 18 kDa) (D), the boundary flow conditions of the inner boundary of the trimodal blend (2 wt % 1770 and 1080 kDa in 18 kDa) (E) and the boundary flow conditions of the outer boundary of the trimodal blend (F).

At the boundary flow conditions of the inner boundary (**Figure 5.19, radius E**), there is sufficient probability of the aggregation to make the shish nuclei. We suggest that the precursors composed of the 1770 kDa chains aggregate with the precursors of both the 1770 and 1080 kDa chains. A long-lived 1770 kDa precursor being able to recruit some shorter-lived 1080 kDa precursors would account for the flow conditions at this boundary being slightly milder than the boundary flow conditions of the bimodal blend comprised of 2 wt % 1770 kDa chains in the matrix.

In order to discuss the difference of the boundary flow conditions between the bimodal blend and the inner boundary of the trimodal blend, a quantitative estimation of the number of long chains which participate to the formation of the shish nuclei is helpful. At the inner boundary, pair-wise aggregation can occur between two precursors composed of the 1770 kDa chains, and between two precursors composed of the 1770 and 1080 kDa chains but not between two precursors composed of the 1080 kDa chains. The effective concentration of the long chains which participate to the formation of the oriented morphology is therefore 3 %, that is 3/4 of 4 %. Since the relationship between the w_c and chain concentration is inversely proportional,[10] the difference in w_c between blends containing 2 % and 3 % long chains in the matrix can be estimated to be a factor of 1.5 and this compares very favourably with the ratio of 1.36 between the boundary work observed for the bimodal blend comprised of 2 wt % 1770 kDa chains in the matrix and the inner boundary of the trimodal blend. At the outer boundary of the trimodal blend, it is considered that the pair-wise aggregation between two precursors comprising 1080 kDa chains becomes effective in forming nuclei and, the slope of the degree of orientation (P2) versus strain changes at this position.

The boundary flow conditions of the outer boundary of the trimodal blend has even milder conditions than the boundary flow of the bimodal blend comprising of the 1080 kDa chains in the matrix. The reasons behind this can be that the boundary flow conditions of the outer boundary of the trimodal blend is where binary aggregation of two 1080 kDa precursors starts, whereas the boundary flow conditions of the bimodal blend is that the shish nuclei are created by sufficient aggregation between the precursors. The latter aggregation requires greater amount of flow than the former aggregation.

One issue that remains to be resolved is why there are two clearly defined boundaries at $\dot{\gamma}_b \gg \dot{\gamma}_{min}$, observed in the trimodal blend whereas only a single boundary can be detected in polydisperse polymers[13]. The pair of long chains in the trimodal blend used herein have well-separated relaxation times, therefore, each of their boundary flow conditions have significant differences and can be observed separately (**Figure 5.20 b**). Conversely, in continuously polydisperse polymers, boundary flow conditions corresponding to the individual chain lengths cannot be separated because of the relaxation times of the chains also present a continuous distribution (**Figure 5.20 c**). We propose, therefore, that only one boundary corresponding to the boundary flow conditions of the longest chain present at a sufficiently high concentration can be observed in the polydisperse polymers.

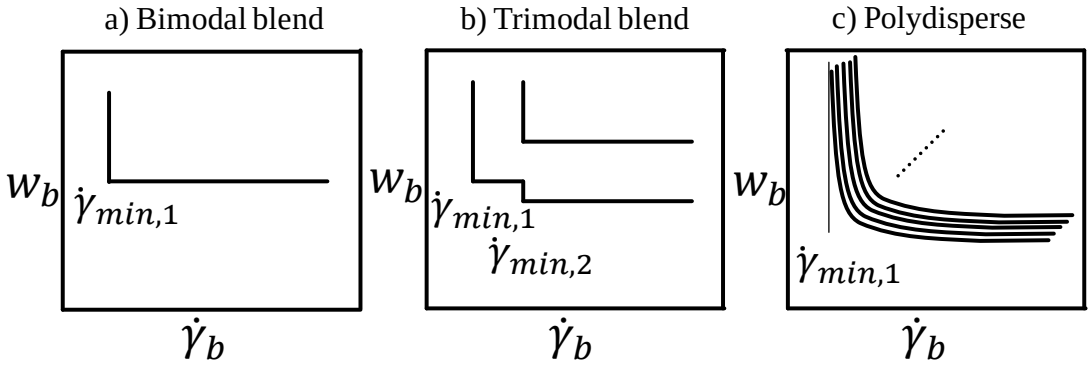

Figure 5.20. A schematic presentation of the boundary flow conditions of the bimodal blend comprised of monodisperse long chains in a matrix (a), trimodal blend (b) and polydisperse polymers (c). The $\dot{\gamma}_{min,1}$ is the $\dot{\gamma}_{min}$ of the longest chains. The $\dot{\gamma}_{min,2}$ is the $\dot{\gamma}_{min}$ of shorter long chains in the trimodal blend.

The boundary flow conditions of multi-modal blend polymers at $\dot{\gamma}_b \cong \dot{\gamma}_{min}$ can be considered as follows. In the case of the bimodal blend comprised of monodisperse long chains and a matrix (**Figure 5.20 a**), the w_c increases sharply (in fact diverges or goes to infinity) at $\dot{\gamma}_b \cong \dot{\gamma}_{min,1}$ ($\dot{\gamma}_{min,1}$ is the $\dot{\gamma}_{min}$ of the longest chains), because the longest chains in the bimodal blend are not stretched below $\dot{\gamma}_{min,1}$. The divergence is sharp and the graph of critical work versus shear rate is "L-shaped". In the trimodal blend (**Figure 5.20 b**) composed of the longest chains, shorter chains and the matrix, w_c has two plateaus against $\dot{\gamma}_b$. At $\dot{\gamma}_b > \dot{\gamma}_{min,2}$ ($\dot{\gamma}_{min,2}$ is the $\dot{\gamma}_{min}$ of the shorter chains in the

trimodal blend), the w_c corresponding to the longest chains includes a contribution from the aggregation of the longest chain precursors with precursors formed by the shorter chains. At $\dot{\gamma}_{\min,1} < \dot{\gamma}_b < \dot{\gamma}_{\min,2}$, the w_c of the longest chains should have greater value than the w_c at $\dot{\gamma}_b > \dot{\gamma}_{\min,2}$ because the precursors formed by the shorter chains no longer contribute. That is the L-shape for the longest chain has a step-down to a lower critical work because of the contribution of the shorter chains at a higher rate.

It has been shown that the w_c of polydisperse polymers increase gradually with decreasing $\dot{\gamma}_b$ at $\dot{\gamma}_b \cong \dot{\gamma}_{\min}$.[13] This gradual increase is a result of the ensemble of long chains in the polydisperse polymers (**Figure 5.20 c**). The w_c of the longest chains has an "L" shape, just like the long chain in **Figure 5.20 a**, and becomes infinite at $\dot{\gamma}_b = \dot{\gamma}_{\min,1}$. But there is a continuous distribution of small steps caused by the additional contribution to nucleation by the precursors to ever shorter chains being recruited by the aggregation process. This means that the observed w_c starts to increase from the $\dot{\gamma}_{\min}$ of the shortest chain that can form a precursor under the maximum prevailing shear rate: there is a minimum value of w_c that grows as $\dot{\gamma}_b$ decreases by removing the contributions of the shorter chains, and w_c finally diverges at $\dot{\gamma}_b = \dot{\gamma}_{\min,1}$ where rate of flow is too low to stretch any of the chains. What was a sharp L-shape in a binary blend becomes a smooth transition in a polydisperse polymer because of the accumulation of a large number of small steps.

5.4. Conclusions

The hydrogenated polybutadiene trimodal blend has a pair of boundary flow conditions to form the oriented morphology corresponding to the two kinds of long chains with different molecular weight. The boundary flow conditions measured by PLI and SAXS were consistent within the experimental errors associated with each technique. The calculated value of w_b was constant at $\dot{\gamma}_b > 1/\tau_R$ and this fact supports the hypothesis that the minimum shear rate to stretch long chains relates to $1/\tau_R$.

The difference of the boundary flow conditions of the trimodal and bimodal blends was interpreted by the shish nuclei formation mechanism involving binary aggregation of precursors. The minimum rate where flow can affect the formation of oriented

morphology is dominated by the behaviour of the longest chains and unaffected by the presence of shorter chains, whereas at higher flow rates shorter chains contribute to a reduction in the critical work because they can form precursors which interact with the longest chains. In trimodal blends this behaviour is manifest as having two distinct levels of nucleation of oriented crystallisation, and two thresholds of critical work. Applying this process to polydisperse polymers it is obvious that there will be a low-rate boundary where the critical work diverges followed by a smooth transition to a minimum value of critical work at high flow rate. We conclude that that the longest chains dictate the low-rate boundary flow conditions of polydisperse polymers and that the critical work has a region of rate-dependence due to the increasing contribution of shorter chains to the nucleation of oriented crystallites.

5.5. References

1. Stevenson, J. F., 10 Extrusion of Rubber and Plastics. In *COMPREHENSIVE POLYMER SCIENCE, 7, Speciality Polymers & Polymer Processing*, Aggarwal, S. L., Ed. Pergamon Press: Oxford, UK, 1989; pp 303-354.
2. Keller, A.; Kolnaar, H. W. H., Part II: Structure Development During Processing, 4 Flow-Induced Orienttion and Structure Formation In *Materials Science and Technology; A Comprehensive Treatment, Vol.18, Processing of Polymers*, Meijer, H. E. H., Ed. WILEY-VCH: Weinheim, Germany, 1997; pp 189-268.
3. Blackadder, D. A.; Schleinitz, H. M. *Nature* **1963,** 200, 778-779.
4. Pennings, A. J.; Kiel, A. M. *Kolloid Z. Z. Polym.* **1965,** 205, 160-162.
5. Keller, A.; Machin, M. J. *J. Macromolec. Sci. B* **1967,** 1, 41-91.
6. Keller, A., *Materials Science and Technology; A Comprehensive Treatment, Vol.18, Processing of Polymers*. WILEY-VCH: Weinheim, Germany, 1997; p 195-196.
7. Coppola, S.; Grizzuti, N. *Macromolecules* **2001,** 34, 5030-5036.
8. Elmoumni, A.; Winter, H. H.; Waddon, A. J. *Macromolecules* **2003,** 36, 6453-6461.
9. Meerveld, J. v.; Peters, G. W. M.; Hutter, M. *Rheol. Acta.* **2004,** 44, 119-134.
10. Mykhaylyk, O. O.; Chambon, P.; Graham, R. S.; Fairclough, J. P. A.; Olmsted, P. D.; Ryan, A. J. *Macromolecules* **2008,** 41, 1901-1904.
11. Eder, G.; Janeschitz-Kriegl, H.; Liedauer, S. *Progress in Polymer Science* **1990,** 15, (4), 629-714.
12. Janeschitz-Kriegl, H.; Ratajski, E.; Stadlbauer, M. *Rheol. Acta.* **2003,** 42, 355-364.
13. Mykhaylyk, O. O.; Chambon, P.; Impradice, C.; Fairclough, J. P. A.; Terrill, N. J.; Ryan, A. J. *Macromolecules* **2010,** 43, (5), 2389-2405.

14. Fernyhough, C. M.; Young, R. N.; Poche, D.; Degroot, A. W.; Bosscher, F. *Macromolecules* **2001,** 34, 7034-7041.

15. Nogales, A.; Hsiao, B. S.; Somani, R. H.; Srinivas, S.; Tsou, A. H.; Balta-Calleja, F. J.; Ezquerra, T. A. *Polymer* **2001,** 42, (12), 5247-5256.

16. Hermans, P. H., *Contribution to the Physics of Cellulose Fibres*. Elsevier: Amsterdam, Netherlands, 1946; p 221.

17. Morrison, F. A., *UNDERSTANDING Rheology*. Oxford University Press: Oxford, UK, 2001; p 382-392.

18. Seki, M.; Thurman, D. W.; Oberhauser, J. P.; Kornfield, J. A. *Macromolecules* **2002,** 35, (7), 2583-2594.

19. Somani, R. H.; Hsiao, B. S.; Nogales, A.; Srinivas, S.; Tsou, A. H.; Sics, I.; Balta-Calleja, F. J.; Ezquerra, T. A. *Macromolecules* **2000,** 33, (25), 9385-9394.

20. Jerschow, P.; Janeschitz-Kriegl, H. *Int. Polym. Process.* **1997,** 12, (1), 72-77.

21. Janeschitz-Kriegl, H.; Ratajski, E. *Polymer* **2005,** 46, (11), 3856-3870.

Chapter 6

Understanding of Essential Mechanical Work for Flow-induced Crystallisation in Polymers

6.1. Introduction

Processing conditions vary the properties of products formed from semi-crystalline polymers through their crystal morphologies. Revealing the relationship between processing conditions and the morphologies, therefore, is a significant contribution toimproving their properties. Shish-kebab structure is an oriented morphology observed in polyolefins which can be formed under flow and the formation of it affects the properties.[1] The formation mechanism of the shish-kebabs structure has been considered that longer chains in a polymer create shish structure first under flow, and then shorter chains attach to shish and form kebabs.[1] Boundary flow conditions which are required for the formation of the oriented morphology in polyolefins have been studied recently.[2-5] There are two important factors in order to form the oriented morphology, which are shear rate and total amount of flow. Firstly, a shear rate above the inverse of Rouse time of the longest chains is necessary to form the point nuclei in the polyolefin (minimum shear rate).[5] Secondly, a certain amount of flow is required to grow stable shish by the aggregation between the point nuclei.[6]

Using bimodal blends comprised of the small amount of low-polydispersity long chains in short chains (matrix) is an effective way to study the formation of the oriented morphology.[5] Only the long chains which have long relaxation time can create shish structure under flow. Although the shish structure is difficult to detect due to its low concentration, the short chains have a role enhancing the shish structure by making the kebabs and making it detectable. As the criterion for the amount of flow which is required for the formation of the oriented morphology, a specific work[5-8] can be used. The importance of this parameter is the fact that this parameter is independent of shear rate; therefore a direct application is possible for industrial processes. The relation between the specific work and the concentration of long chains in bimodal blends was already reported and it is inverse proportional.[5] The aim of this study is to elucidate the effect of the molecular weight of the matrix in model bimodal blends on the specific work in order to identify the effect on the specific work by the long chains on its own.

6.2. Experimental

6.2.1. Materials

Synthesised low-polydispersity hydrogenated polybutadiene (h-PBD) polymers[9] (M_w = 1770, 147, 52, 18 and 7 kDa) and polyethylene wax (PE wax, M_w = 5, 3 and 1 kDa) provided by Mitsui Chemicals were used in this study. The h-PBD polymer whose M_w is 1770 kDa was used as long chains and others were used as matrices.

6.2.2. Thermal properties

The shearing temperature used in this chapter was selected from the thermal properties of samples. The crystallization and melting temperature of PE wax and bimodal blends were measured by differential scanning calorimetry (DSC).

The crystallization of the bimodal blends (2 wt % 1770 kDa in 147, 52, 18, 7, 5, 3 and 1 kDa) was measured by using cooling step at -10 K / min (**Figure 6.1**). The crystallization starts from about 363-383 K in all samples. On the other hand, the melting points (the end of the melting peak) of the samples are about 388 K (**Figure 6.2**). The crystallization and melting temperature of PE wax (5, 3 and 1 kDa) were also measured and they were similar to the h-PBD samples (**Figure 6.3, 6.4**).

The lowest temperature used for rheology measurements in this chapter is 393 K. This temperature is higher than the melting point of the bimodal blends measured by DSC. Also, the temperature used for the shear experiments in this chapter is 388 K. Although this temperature is similar to the end of the melting peak of the bimodal blends, it is still higher than the temperature that the samples start to crystallize. It is considered, therefore, that the effect on the rheology and shear experiment resulting from the crystallization is negligible.

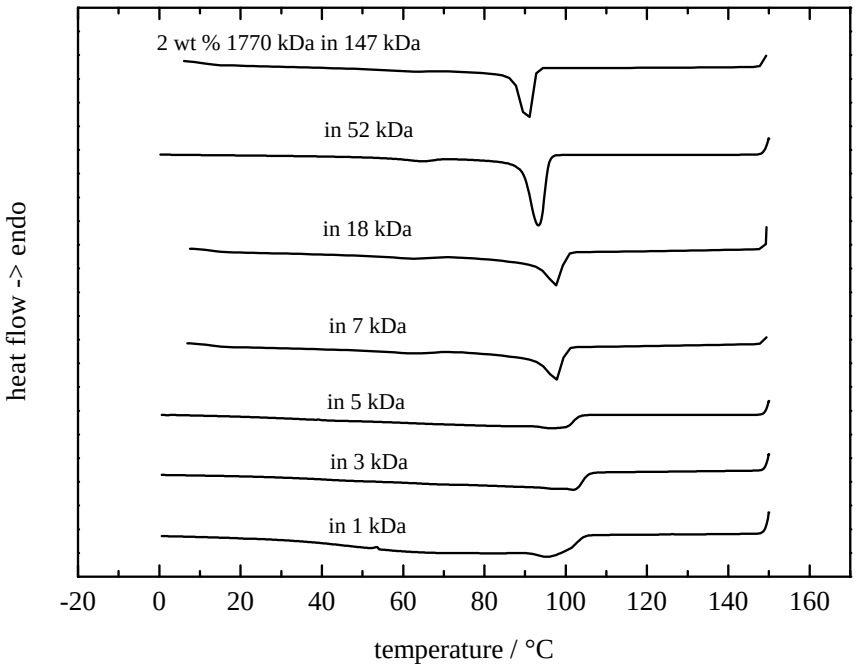

Figure 6.1. DSC diagram of the bimodal blends comprised of 2 wt % 1770 kDa h-PBD chains in 147, 52, 18, 7, 5, 3 and 1 kDa, cooling step. Cooling rate is 10 K / min.

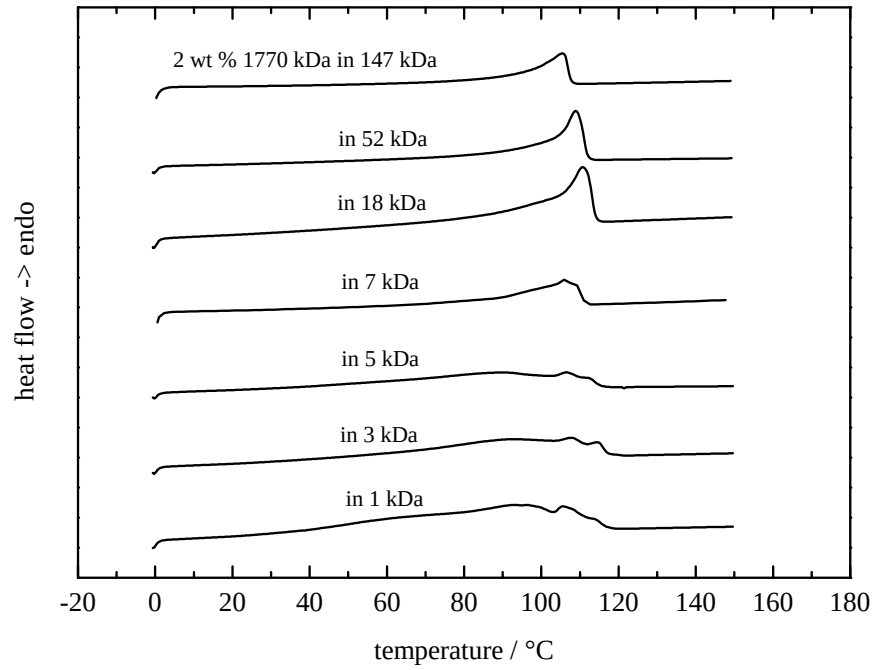

Figure 6.2. DSC diagram of the bimodal blends comprised of 2 wt % 1770 kDa h-PBD chains in 147, 52, 18, 7, 5, 3 and 1 kDa, heating step. Heating rate is 10 K / min.

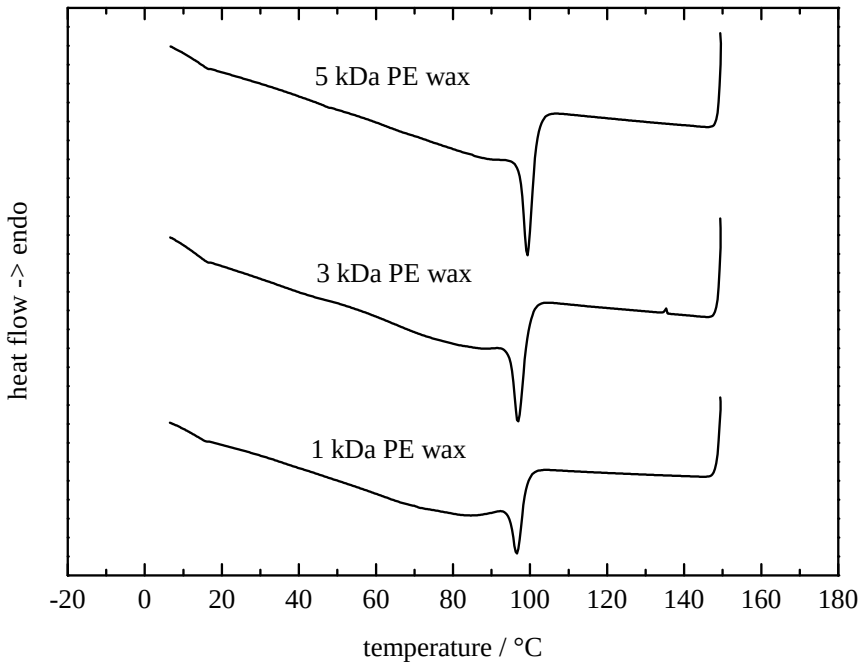

Figure 6.3. DSC diagram of PE wax (5, 3 or 1 kDa), cooling step. Cooling rate is 10 K / min.

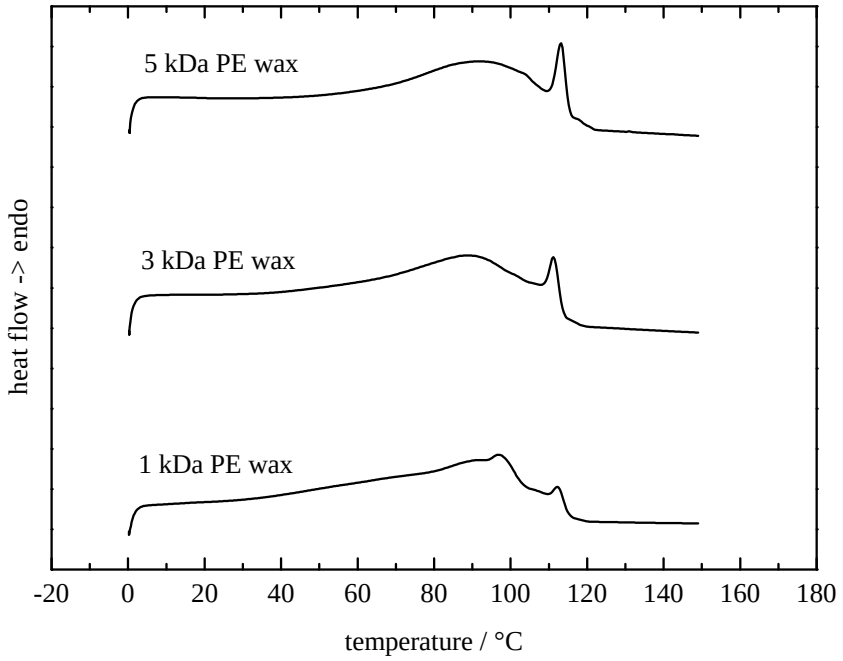

Figure 6.4. DSC diagram of PE wax (5, 3 or 1 kDa), heating step. Heating rate is 10 K / min.

6.2.3. Relaxation times of low-polydispersity polymers

The relaxation times of the low-polydispersity polymers were obtained from a storage modulus, *G*', and loss modulus, *G*'', measured by a rheometer (see chapter 3). The relaxation times of the materials used in this chapter were extracted from **Table 6.1** from the previous chapter.

Table 6.1. Molecular weight and relaxation times of low polydisperse hydrogenated polybutadiene used in this study at 388 K.

M_w, kDa	τ_R, s	τ_d, s	$\dot{\gamma}_{min} = 1/\tau_R$, s^{-1}
7	9.50×10^{-7}	3.08×10^{-6}	1052630
18	6.28×10^{-6}	9.78×10^{-5}	159240
52	5.24×10^{-5}	3.65×10^{-3}	19080
147	4.19×10^{-4}	1.05×10^{-1}	2390
1770	6.07×10^{-2}	231	16

6.2.4. Viscosity measurements and simulation

The viscosities of the matrices and bimodal blends were measured at different temperature (M_w = 147, 52, 7, 5, 3 and 1 kDa at 393, 403 and 413 K and M_w = 18 kDa at 388, 393 and 398 K), and then the master curves at the shearing temperature, 388 K, have been created from the viscosities by time-temperature superposition (**Figure 6.5**).

The viscosity of the h-PBD matrices and bimodal blends were simulated by using the linear theory and Rubinstein-Colby theory[10] (same parameters with the calculation of the relaxation times were used), respectively. Since the viscosity of high molecular weight chains, such as $M_w > 300\ M_e$, is overestimated by the Rubinstein-Colby theory (**Figure 6.6**),[11] a set of concentration and M_w parameters were selected in order to qualitatively match the simulated viscosity of the bimodal blends. Whilst the blend contains 2 % of 1770 kDa h-PBD chains, the simulation is based on 1.2 % of 700 kDa chains. The measured viscosities of the blends were then well reproduced by the

simulation and therefore it was confirmed that the prepared bimodal blends have reasonable viscosities.

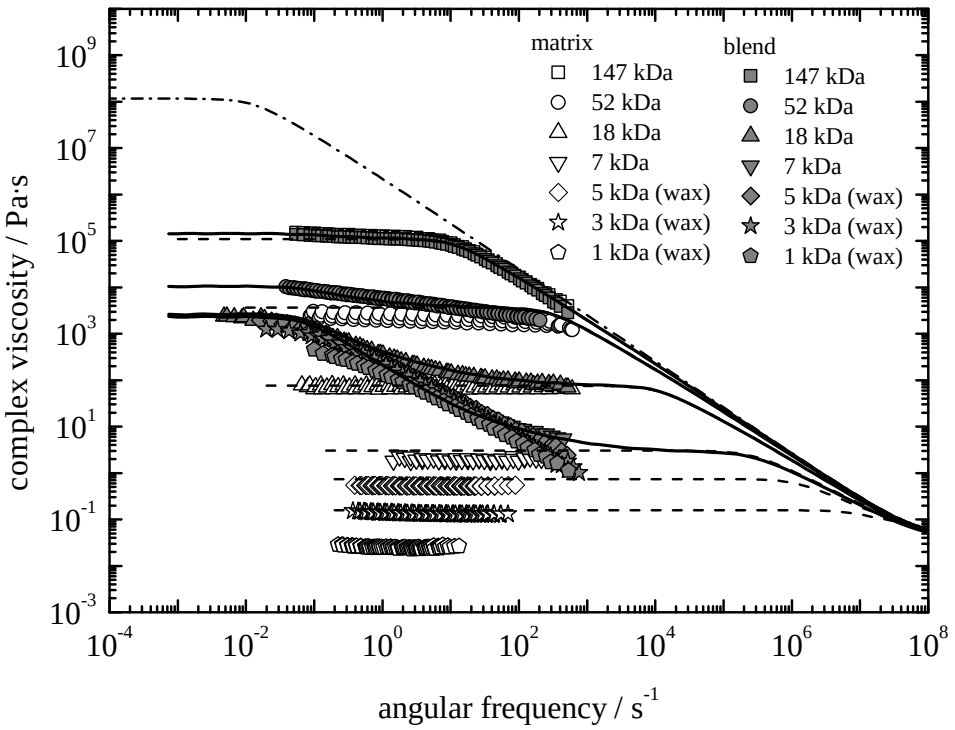

Figure 6.5. The complex viscosities of matrices (open symbols) and the bimodal blends comprised to 2 wt % long chains in hydrogenated polybutadiene matrix or PE wax (filled symbols) at 388 K plotted against angular frequency. The viscosities were measured by using rheometer at 413, 403 and 393 K, and then they were shifted to 388 K by using time-temperature superposition technique. The viscosities of the matrix with M_w = 147 kDa and the blend comprised of long chains in 147 kDa matrix are overlapping. Dashed lines indicate the viscosity simulation result of the matrices with M_w = 147, 52, 18, 7, 5 and 3 kDa by using the linear theory with common parameters. Dashed-dotted line indicates the viscosity simulation result of the long chains with M_w = 1770 kDa by using the linear theory. Solid lines indicate the viscosity simulation result of the blends comprised of 1.2 wt % 700 kDa in 147, 52, 18 or 7 kDa matrices by using the Rubinstein-Colby theory.

The bimodal blends with 5, 3 and 1 kDa matrices have viscosities of the same magnitude. This result means that the viscosities of the blends with 5, 3 and 1 kDa matrix are dictated by the viscosity of long chains due to the low viscosity of the matrix.

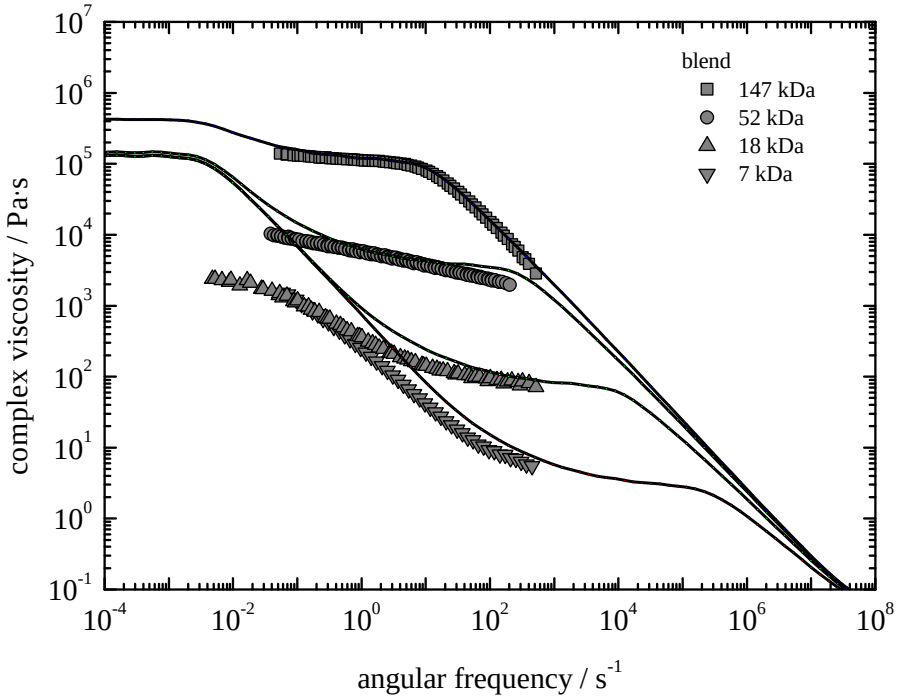

Figure 6.6. The complex viscosities of the bimodal blends (filled symbols) at 388 K. Solid lines indicate the viscosity simulation result of the blends comprised of 2 wt % 1770 kDa in 147, 52, 18 or 7 kDa matrices by using the Rubinstein-Colby theory.

The viscosity of the bimodal blend (2 wt % 1770 kDa in the matrices) estimated by the Rubinstein-Colby is greater than the measured viscosity. The reason of this can be explained as follows. When M_w of the long chains and matrix are different, the tube dilation[12] of the long chains happens. The number of the entanglements per a long chain decreases due to the dilation with the decrease of the concentration of the long chains. Since the Rubinstein-Colby theory is not including this effect and is considering that the number of entanglements is constant against concentration, the higher viscosity of the bimodal blend is estimated when the M_w of matrix is low. Therefore, adjusting M_w of the long chains to fit the simulated viscosity to the measured viscosity is therefore equivalent to adjust the number of the entanglements per a long chain decreased by the

tube dilation. The reason that the concentration needs to be adjusted could be that the concentration of the long chains dependence of G' used in the Rubinstein-Colby theory is lower than the real system.

The point that the long chains start to be affected by the matrix in bimodal blends can be predicted by using the Struglinski-Graessley parameter[13], G_r, which is defined by the following equation.

$$G_r = \frac{M_L M_e^2}{M_S^3} \quad \textbf{Eq. 6.1}$$

where M_L is the M_w of the long chains, M_S is the M_w of matrix and M_e is the M_w between two entanglements. When the parameter exceeds the critical value which has been reported around 0.5 [13], the matrix starts to affect the relaxation time of the long chains and acts as a solvent which can enlarge the diameter of the tube surrounding the long chains. In this study, the calculated G_r of the bimodal blends with 147 kDa, 52 kDa and 18 kDa are 0.0009, 0.02 and 0.49, respectively. Despite the G_r of the bimodal blend with the 52 kDa matrix, 0.02, which is below the critical value, the viscosity of the blend simulated by the Rubinstein-Colby theory is already apart from the measured viscosity. The reason of this can be also considered to the different concentration dependence of the G' between the value used in the theory and actual value.

6.2.5. Shear experiments

The shearing procedure used is the same as in previous chapters. The bimodal blends were sheared by using the same temperature protocol used in chapter 4 (sheared temperature = 388 K). A boundary position for each sheared sample disk was evaluated by using both a small angle X-ray scattering (SAXS, Bruker AXS Nanostar, Cu Kα radiation) and polarized light imaging (PLI). The boundary specific work, w_b, which is an essential mechanical work required for the formation of the oriented morphology, was calculated from the boundary position by using **Eq. 5.3** with a shear rate dependent viscosity of the sample which can be measured by a rheometer (**Figure 6.5, filled**

symbols). The critical specific work[5, 6], w_c, is defined by the average of the w_b sheared above the minimum shear rate, $\dot{\gamma}_{min}$, of the long chains.

6.2.6. Viscosity fitting of the blend

Firstly, in order to decide the strain used for viscosity measurements against frequency, the viscosity against strain was measured (**Figure 6.7 – 6.12**).

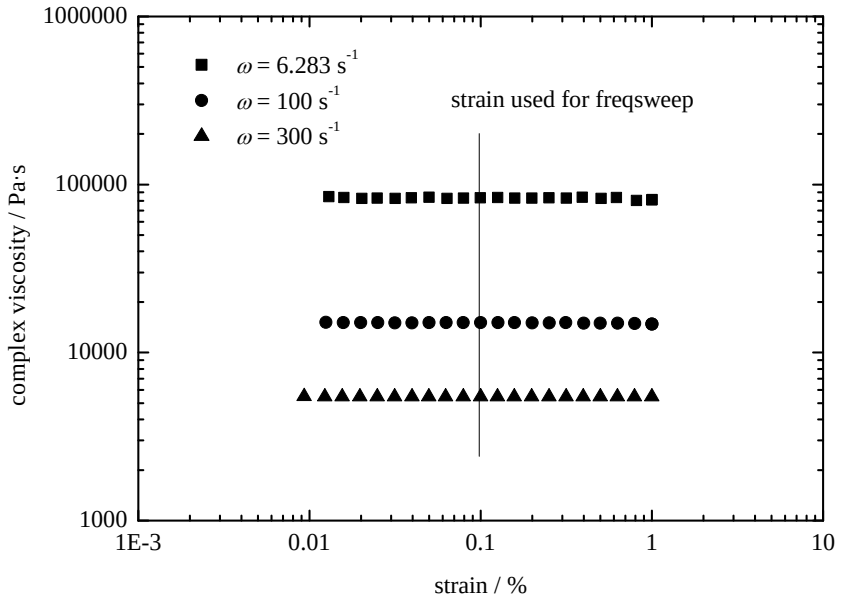

Figure 6.7. Strain sweep measurement for the h-PBD bimodal blend (2 wt % 1770 kDa in 147 kDa) at 393 K by 8 mm cone-plate geometry (cone angle = 6:36:00) at angular frequency = 6.3, 100 and 300 s^{-1}.

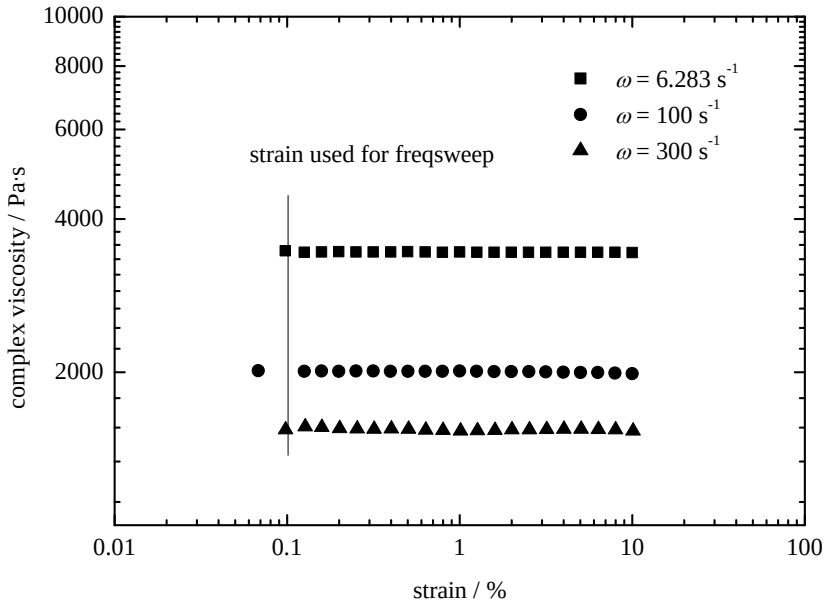

Figure 6.8. Strain sweep measurement for the h-PBD bimodal blend (2 wt % 1770 kDa in 52 kDa) at 393 K by 8 mm plate-plate geometry (gap = 0.5 mm) at angular frequency = 6.3, 100 and 300 s^{-1}.

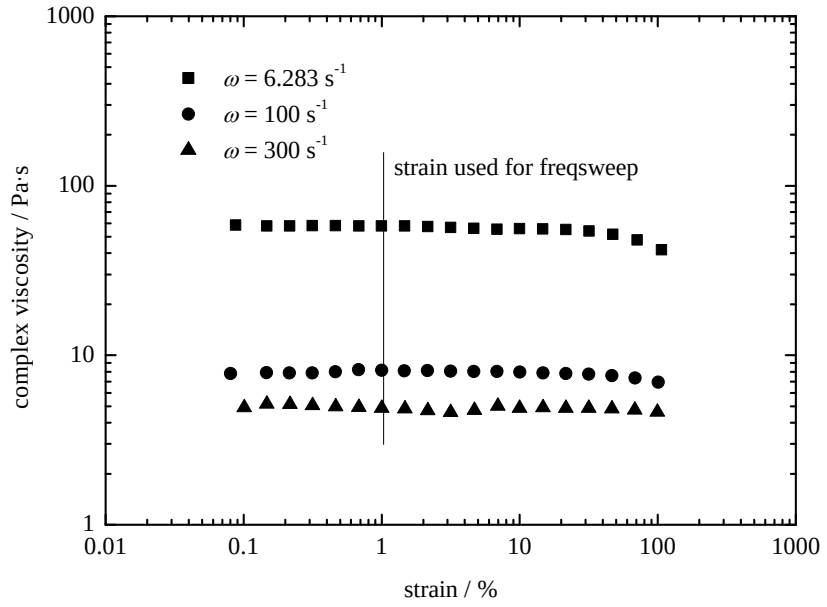

Figure 6.9. Strain sweep measurement for the h-PBD bimodal blend (2 wt % 1770 kDa in 7 kDa) at 393 K by 25 mm plate-plate geometry (cone angle = 6:36:00) at angular frequency = 6.3, 100 and 300 s^{-1}.

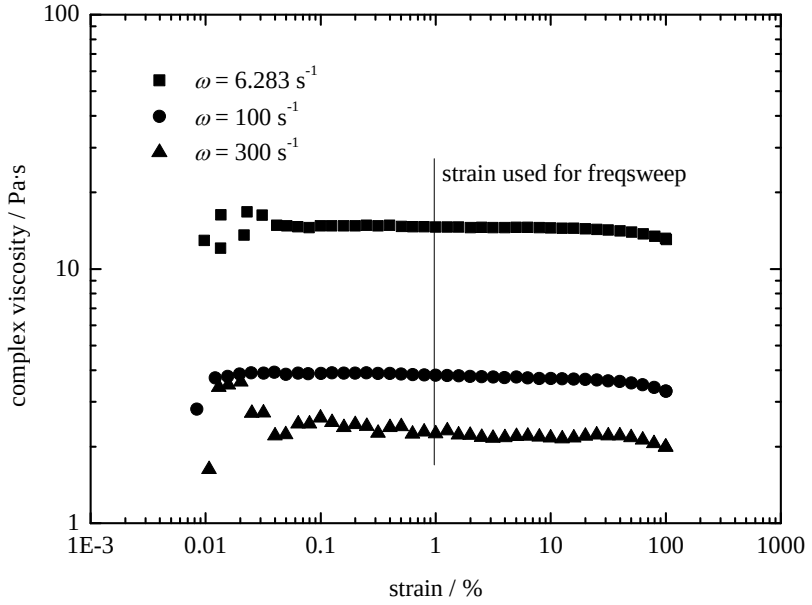

Figure 6.10. Strain sweep measurement for the bimodal blend (2 wt % 1770 kDa h-PBD in 5 kDa PE wax) at 393 K by 25 mm plate-plate geometry (cone angle = 6:36:00) at angular frequency = 6.3, 100 and 300 s^{-1}.

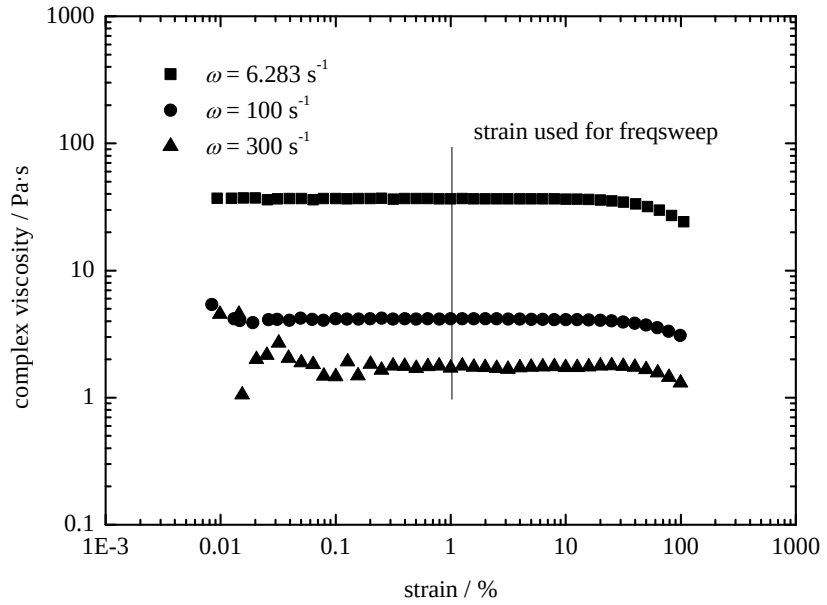

Figure 6.11. Strain sweep measurement for the bimodal blend (2 wt % 1770 kDa h-PBD in 3 kDa PE wax) at 393 K by 25 mm plate-plate geometry (cone angle = 6:36:00) at angular frequency = 6.3, 100 and 300 s^{-1}.

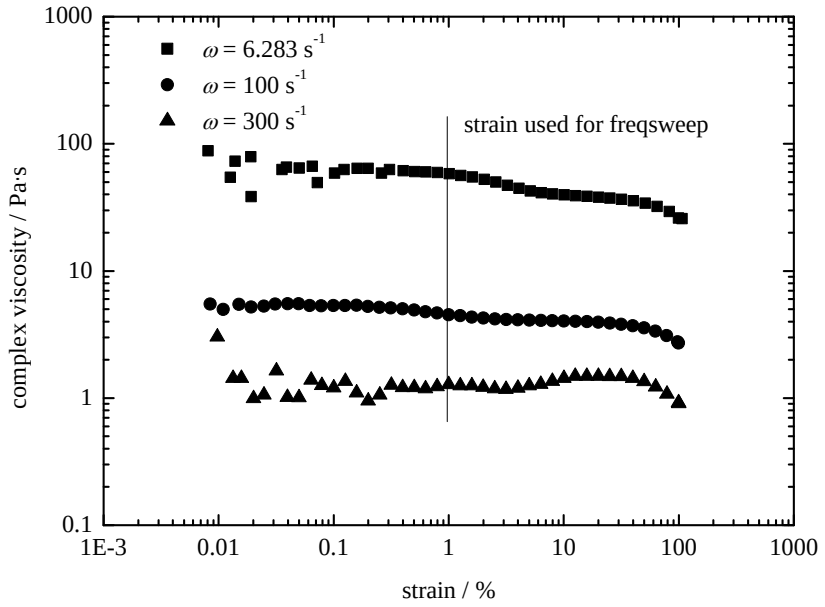

Figure 6.12. Strain sweep measurement for the bimodal blend (2 wt % 1770 kDa h-PBD in 1 kDa PE wax) at 393 K by 25 mm plate-plate geometry (cone angle = 6:36:00) at angular frequency = 6.3, 100 and 300 s^{-1}.

Secondly, the complex viscosities of the bimodal blends were measured by a rheometer by using the strain which has decided above and then the result was fitted by using a modified cross model in order to calculate the boundary specific work (**Figure 6.13 – 6.18**). The detail of this procedure was given in chapter 5. Obtained parameters are summarised in **Table 6.2**.

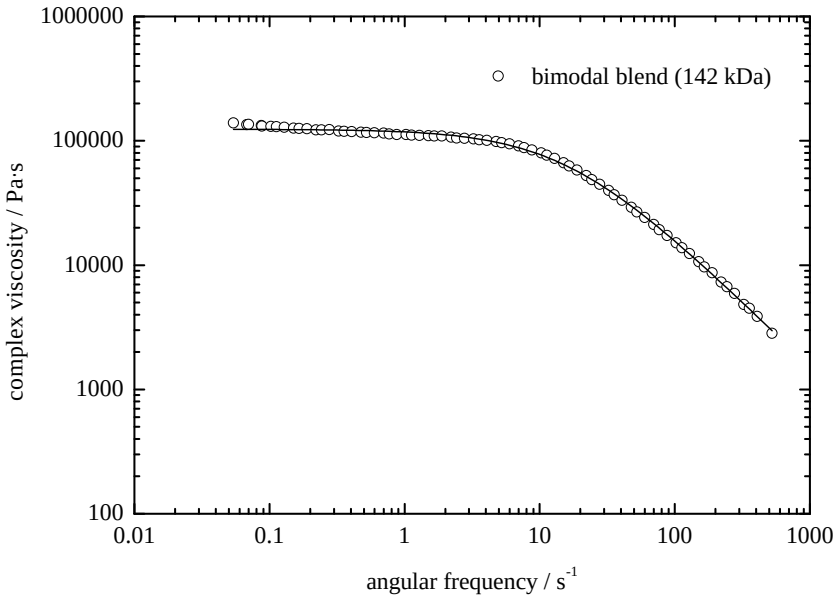

Figure 6.13. The complex viscosity (symbols) and fitting curve (line) of the hydrogenated polybutadiene bimodal blend (2 wt % 1770 kDa in 147 kDa). The viscosity was measured at 393, 403 and 413 K and then shifted to T = 383 K by using time-temperature superposition. The modified Cross model was used to fit the data.

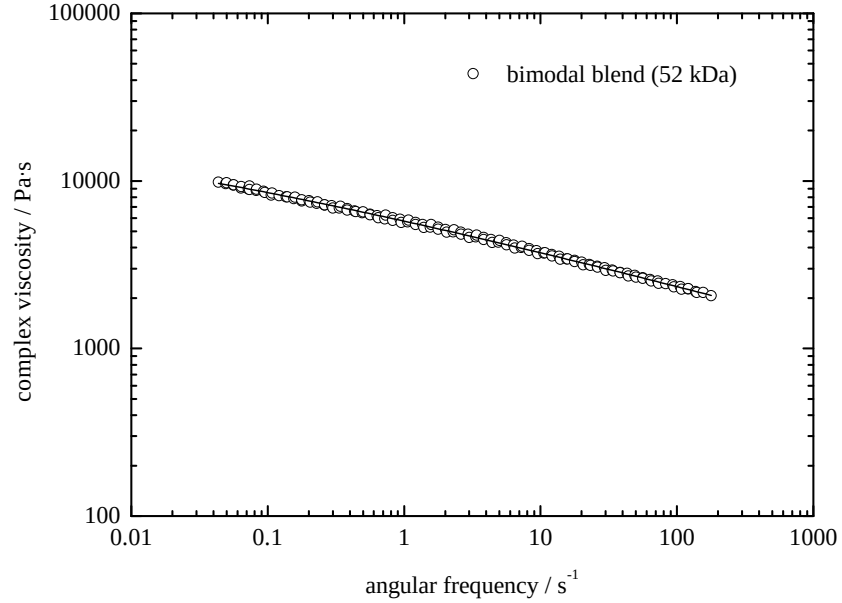

Figure 6.14. The complex viscosity (symbols) and fitting curve (line) of the hydrogenated polybutadiene bimodal blend (2 wt % 1770 kDa in 52 kDa).

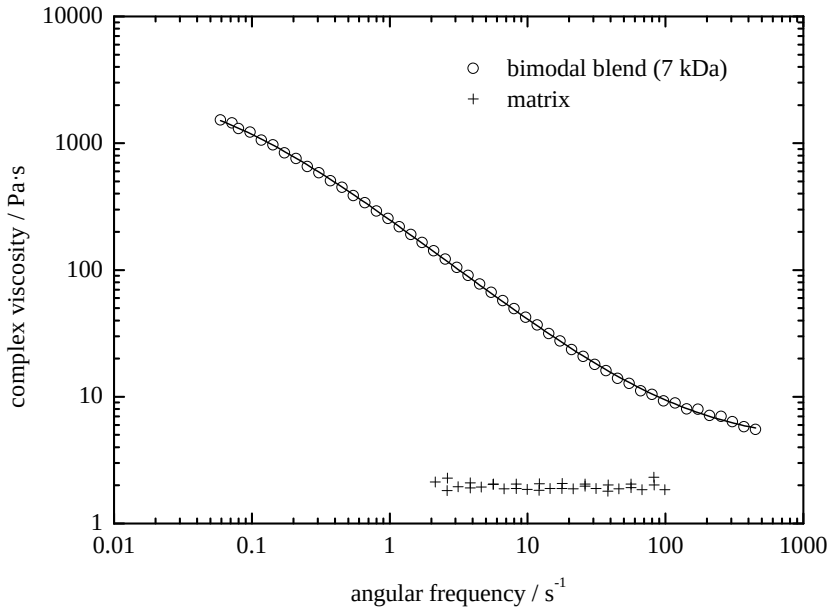

Figure 6.15. The complex viscosity (symbols) and fitting curves (lines) of the hydrogenated polybutadiene bimodal blend (2 wt % 1770 kDa in 7 kDa) and 7 kDa matrix.

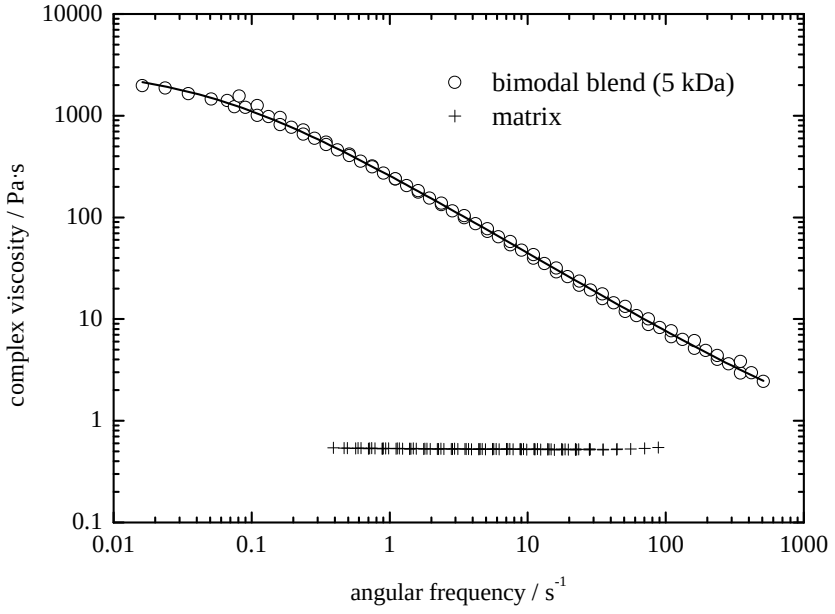

Figure 6.16. The complex viscosity (symbols) and fitting curves (lines) of the bimodal blend comprised of 2 wt % 1770 kDa hydrogenated polybutadiene in 5 kDa matrix (PE wax) and 5 kDa matrix.

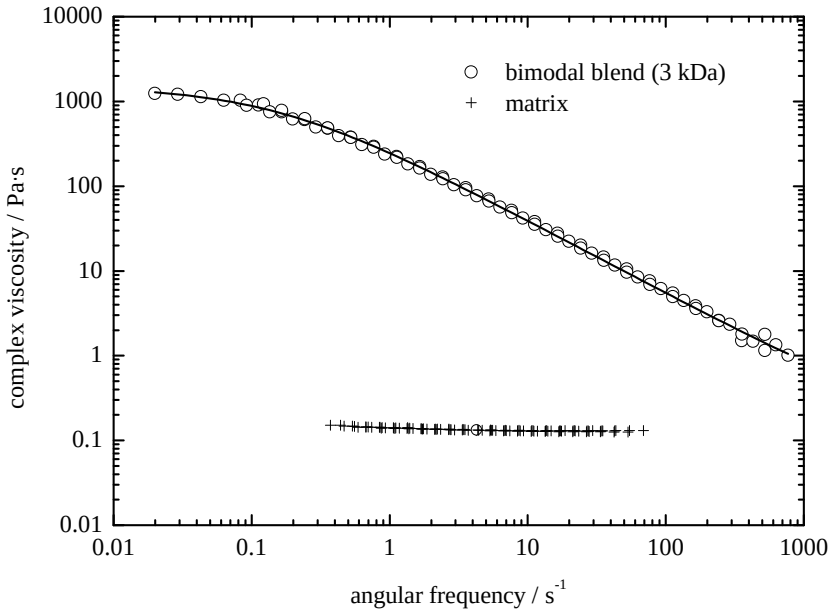

Figure 6.17. The complex viscosity (symbols) and fitting curves (lines) of the bimodal blend comprised of 2 wt % 1770 kDa hydrogenated polybutadiene in 3 kDa matrix (PE wax) and 3 kDa matrix.

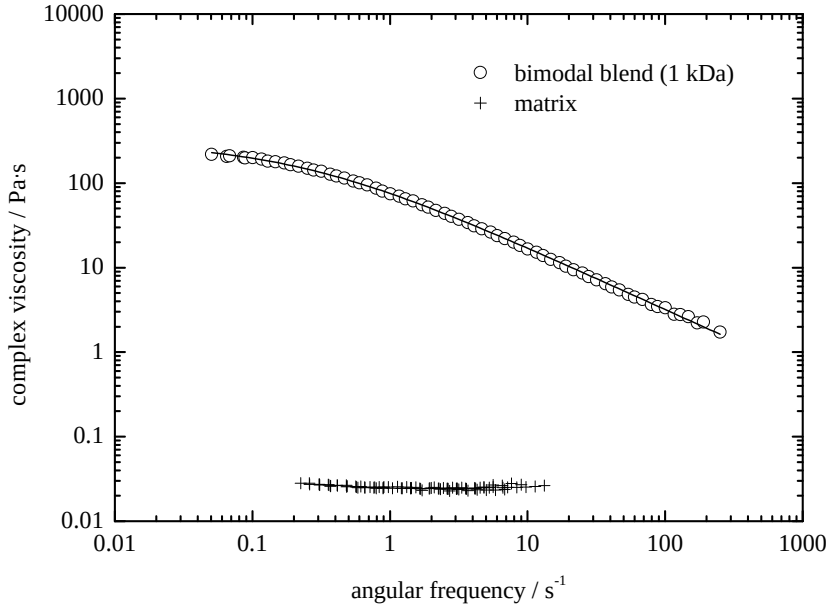

Figure 6.18. The complex viscosity (symbols) and fitting curves (lines) of the bimodal blend comprised of 2 wt % 1770 kDa hydrogenated polybutadiene in 1 kDa matrix (PE wax) and 1 kDa matrix.

Table 6.2. The summary of the fitting parameters (T = 388 K).

bimodal blends	η_1	η_2 [&]	ω_1	α_1
2 wt % 1770 kDa in 147 kDa	123880	0	16.2	1.07
2 wt % 1770 kDa in 52 kDa	28966	0	0.002	0.23
2 wt % 1770 kDa in 18 kDa*	2862	71	0.05	0.70
2 wt % 1770 kDa in 7 kDa[&]	3068	4.2	0.06	0.85
2 wt % 1770 kDa in 5 kDa[&]	2973	0.52	0.05	0.80
2 wt % 1770 kDa in 3 kDa[&]	1500	0.13	0.15	0.87
2 wt % 1770 kDa in 1 kDa[&]	304	0.02	0.23	0.75

*: the data was taken from chapter 5.

&: the viscosity curves were fitted with the matrix with a constraint that η_2 is a common parameters.

6.3. Results and discussion

The boundary positions of the sheared bimodal blends comprised of 2 wt % 1770 kDa in 147, 52, 18 and 7 KDa were checked by PLI and SAXS (**Figure 6.19**). A single boundary was identified in all bimodal blends as reported in the previous report[6]. The boundary positions of the bimodal blends (147, 18 kDa matrix) were calculated from both the results of PLI and P2 orientation function from SAXS. Since the boundaries of the blends (7 kDa matrix) are not clear because of high crystallinity of the matrix, the boundary positions were obtained from P2 function. The boundary positions of the blend (52 kDa matrix) were acquired from the PLI.

The bimodal blends comprised of the h-PBD long chains in PE wax do not indicate clear boundary on PLI image at room temperature because of high crystallinity. Also, the sheared samples were brittle and difficult to remove from the shear cell for SAXS measurements. Therefore, on-line measurements were used to check the boundary positions of the sheared discs before the sheared discs fully crystallize (**Figure 6.20**).

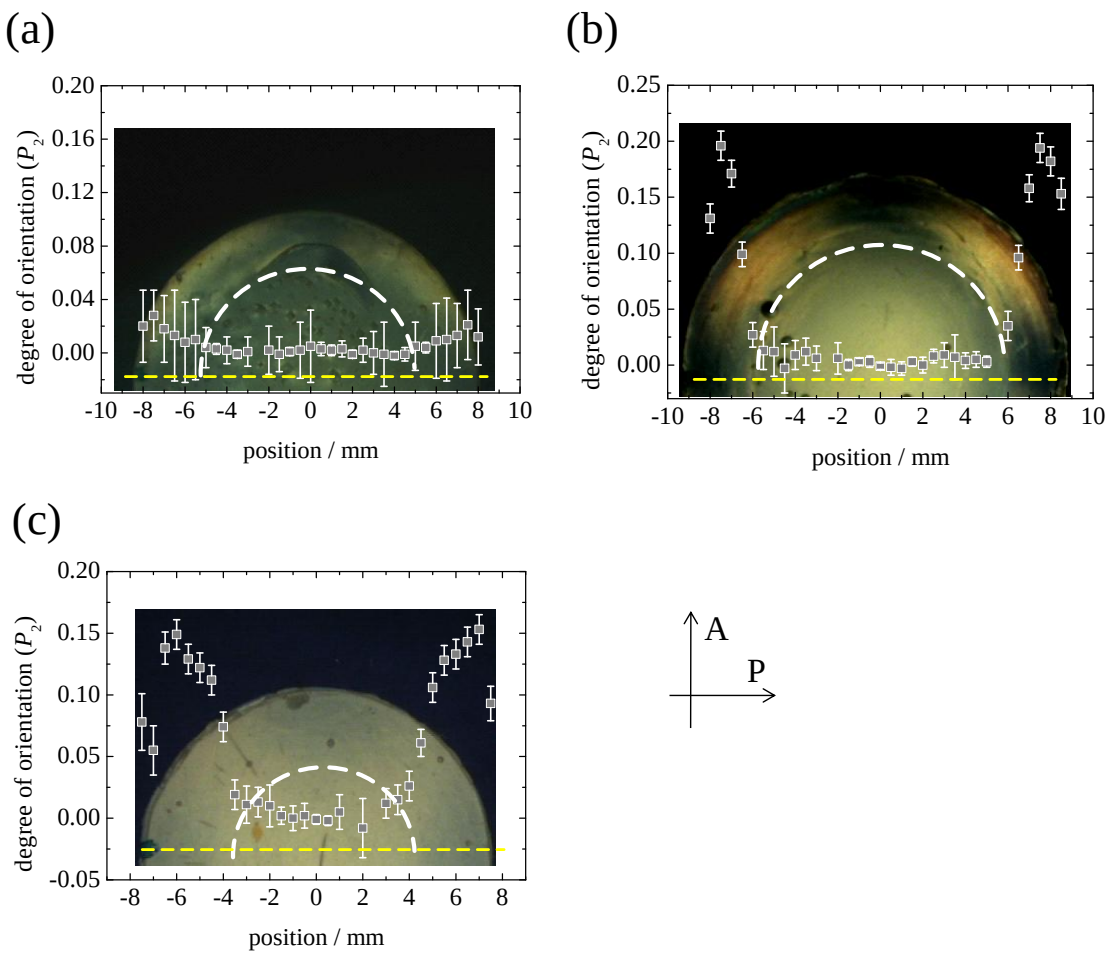

Figure 6.19. Polarised light images overlapped with SAXS- measured orientation function of the lamellae structure of hydrogenated polybutadiene blends: 2 wt % 1770 kDa in 147 kDa crystallized after shearing at 388 K, angular speed Ω = 6.7 rad / s for t_s = 2 s (a), 2 wt % 1770 kDa in 18 kDa at 388 K at Ω = 3.3 rad / s for t_s = 40 s (b) and 2 wt % 1770 kDa in 7 kDa at 388 K, Ω = 6.7 rad / s for t_s = 15 s (c). The directions of the polarizer (P) and analyser (A) are indicated by the arrows at lower right of the images. The diameter and the thickness of the sheared samples are 16 mm and 0.5 mm respectively. Dotted lines along the diameter of the PLIs indicate the direction of the SAXS scans. The dashed curve lines on the images indicate the position of a boundary.

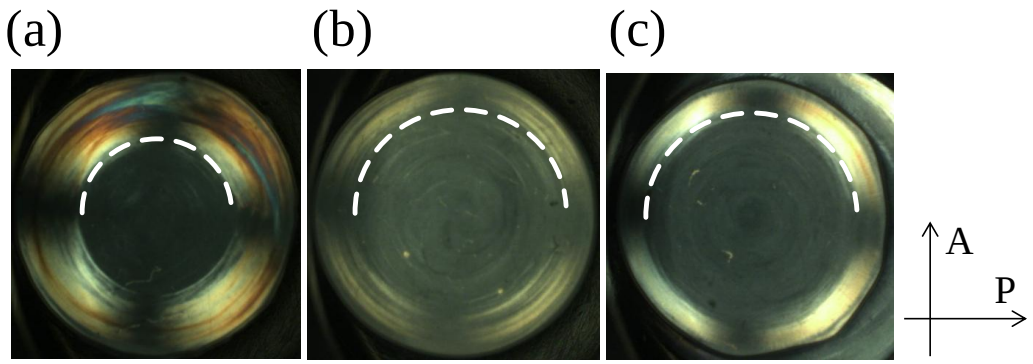

Figure 6.20. Polarised light images (online measurements) of hydrogenated polybutadiene blends: 2 wt % 1770 kDa in PE wax 5 kDa taken at 383 K after shearing at 388 K, angular speed Ω = 6.7 rad / s for t_s = 3 s (a), 2 wt % 1770 kDa in PE wax 3 kDa taken at 379 K after shearing at 388 K, angular speed Ω = 13.3 rad / s for t_s = 1.5 s (b) and 2 wt % 1770 kDa in PE wax 1 kDa taken at 377 K after shearing at 388 K, angular speed Ω = 6.7 rad / s for t_s = 10 s (c). The directions of the polarizer (P) and analyser (A) are indicated by the arrows at lower right of the images. The diameter and the thickness of the sheared samples are 16 mm and 0.5 mm respectively. The dashed curve lines on the PLIs indicate the position of a boundary.

The w_b of the bimodal blends were calculated from the boundary flow conditions obtained by using the *in-situ* method which was reported previously[5, 6] (**Figure 6.21**). The w_b was measured above the $\dot{\gamma}_{min}$ of 1770 kDa chains and was constant as already reported that the w_b is a constant at $\dot{\gamma}_b > \dot{\gamma}_{min}$ and defined as w_c which is independent of the shear rate and shearing duration.[5, 6]

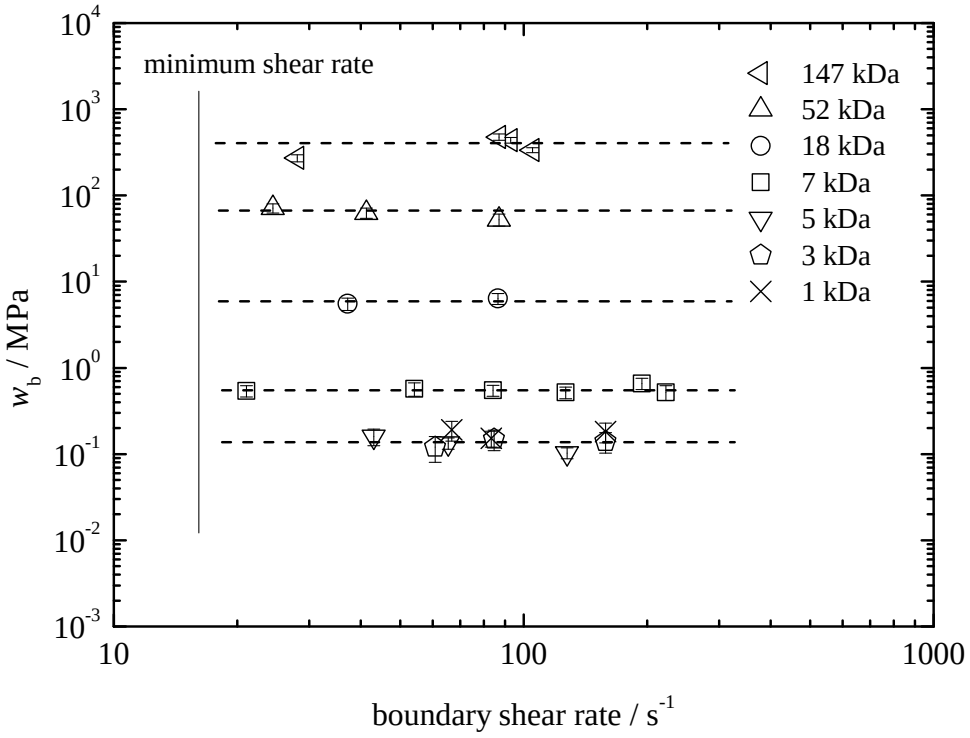

Figure 6.21. The boundary specific work, w_b, of the bimodal blends comprised of 2 wt % 1770 kDa in a matrix (147, 52, 18, 7, 5, 3 or 1 kDa) plotted against boundary shear rate. Dashed lines indicate the critical specific work, w_c, which is defined by the average of the w_b at above the minimum shear rate of 1770 kDa chains. The vertical solid line is the minimum shear rate of the 1770 kDa chains.

The w_c of the series of the bimodal blends measured at 388 K followed a power law against the M_w of the matrices (**Figure 6.22**). When the M_w of the matrix is below 5 kDa, the w_c is independent of the M_w of matrix. This constant w_c represents the minimum amount of flow, $w_{c,min}$, which is required for the formation of the oriented morphology by the 2 wt % of 1770 kDa long chains at 388 K without the contribution of a matrix. It is considered that the $w_{c,min}$ of a polymer is decided by the concentration and molecular weight of long chains and the magnitude of $w_{c,min}$. When the M_w of the matrix is above 5 kDa, the w_c rises with the increase of the M_w of the matrix. It can be interpreted that an additional amount of work, $w_{c,add}$, which is the inhibition given by the matrix, is required to be applied in addition to the $w_{c,min}$ in order to form the oriented morphology in the bimodal blends.

The reason that the w_c is dependent of the matrix M_w above 5 kDa can be considered as follows. When a certain mechanical work is applied to a polymer chain, the work is used to stretch and transport the chain. The work required to transport the chain is dependent on the viscosity of polymer chains which are surrounding the transported chain. In the bimodal blends, although the shorter chains in a matrix do not make stable shish nuclei due to their short relaxation times, it is supposed that a certain amount of work ($w_{c,add}$) is consumed to transport the long chains in a viscous matrix.

The relationship between w_c and M_w of matrix in **Figure 6.22** was fitted by a power law function, $w_c = M_w^a + w_{c,min} (= w_{c,add} + w_{c,min})$, where a is a fitting parameter and the $w_{c,min}$ is fixed at 1.5×10^5 which was calculated from the average w_c of the bimodal blend comprised of 5, 3 and 1 kDa matrix. The a was calculated to 2.5 and this value corresponds to the increment of the $w_{c,add}$ with increasing the M_w of the matrix. Since the zero shear viscosity of matrices should depend on $M_w^{3.4}$, it can be suggested that the w_c does not depend on the viscosity of the matrix.

The viscosity of the blend was plotted against the M_w of the matrix and the relationship was fitted by a power law function (**Figure 6.23**). The exponent of the function is 2.6 and this value is the result of two effects that the viscosity of the blend is higher than the zero shear viscosity of the matrix at low M_w region due to the contribution of the long chains and the viscosity of the blend is lower than the zero shear viscosity of the matrix because of shear thinning of the viscosity. The exponent, 2.6, is similar to the exponent of the fitted function of the w_c against M_w of the matrix; therefore it is supposed that the w_c and M_w relationship is dictated by the viscosity of the blend.

The critical M_w of matrix where the long chains start to be affected by the matrix (G_r = 0.5) is calculated to 52 kDa. The change of the slope of w_c cannot be observed above and below the critical M_w despite the change of the regime of the relaxation behaviour of the long chains. The zero shear viscosity of the 1 kDa matrix is apart from the fitted power law function. This can be considered that the 1 kDa matrix has less entanglement effect and the transition from the non-Newtonian fluid to the Newtonian fluid starts at this point.

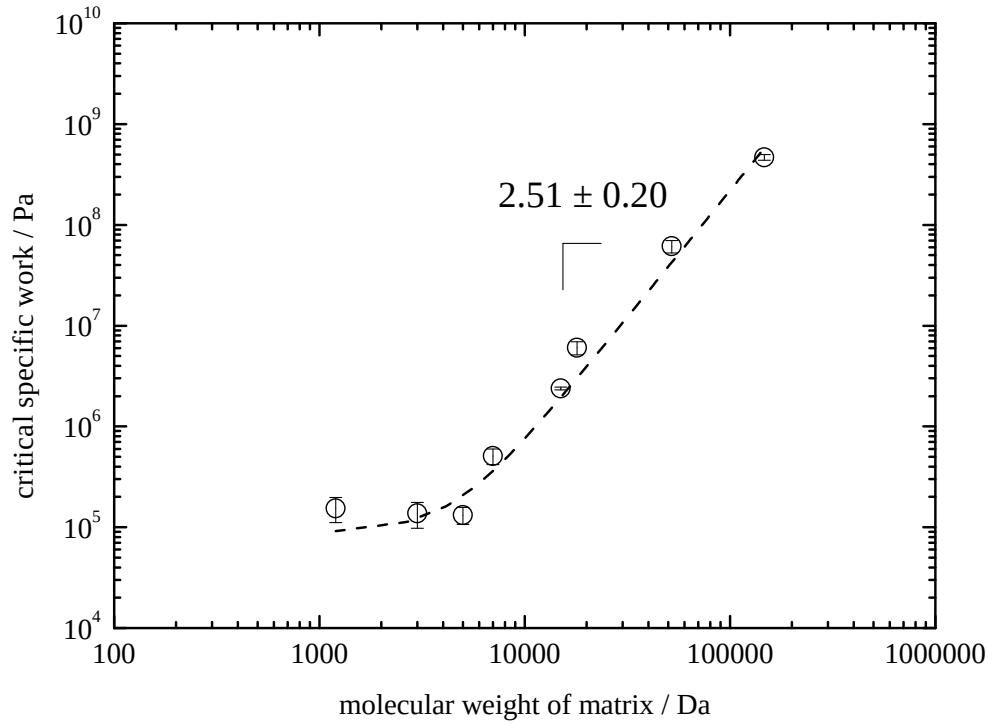

Figure 6.22. The critical specific work, w_c, of the bimodal blends measured at 388 K plotted against the M_w of matrices. A dotted line show the fitted curve by using exponential function $w_c = M_w^{\ a} + w_{c,min}$, where a is a fitting coefficient. The number above the fitted curve indicates the exponent of the fitted curve. The data point at M_w = 15 kDa was taken from the reference.[5]

In summary, it was found that there is a power law relationship between the M_w of matrix and the w_c which is amount of flow required to form an oriented morphology in polyethylene bimodal blends. The work was independent of the M_w of matrix when the M_w of matrix is below 5 kDa. This constant work represents the minimum amount of flow required for the formation of oriented morphology by only long chains in the bimodal blend. It was supposed that an additional amount of flow is required for the formation of oriented morphology in the bimodal blend comprised of the long chains in the matrix which has ordinary M_w. This additional amount of flow is almost zero when the M_w of matrix is below 5 kDa and increases with the rise of M_w of matrix in a power law.

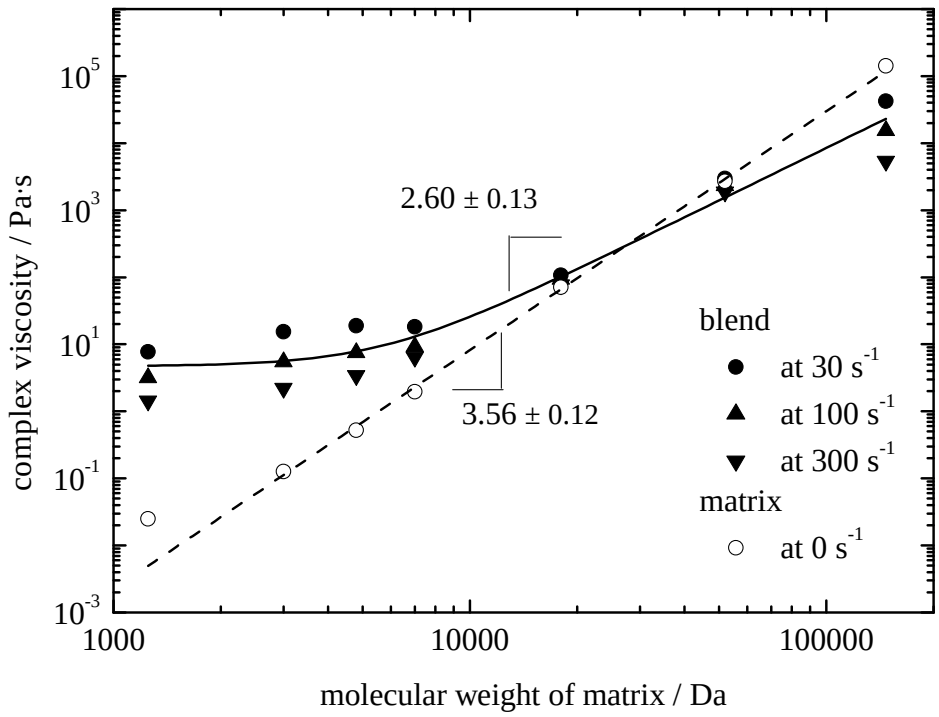

Figure 6.23. The complex viscosities of the bimodal blends at angular frequency = 30, 100 and 300 s^{-1} and the zero shear viscosity of the matrix at 388 K plotted against the M_w of matrix. The viscosity data was picked up from the data shown in **Figure 6.5**. The solid line shows the fitted curve of the averaged viscosities between 30 and 300 s^{-1} of the bimodal blends by using a power law function $\eta = M_w^a + c$, where η is the complex viscosity and, a and c are fitting coefficient. The dotted line indicates the fitted curve of the zero shear viscosity of the matrix by using a power law function $\eta_0 = M_w^a$, where η_0 is the zero shear viscosity and a is a fitting coefficient. The obtained exponents are noted next to the fitted curves.

The w_c was normalised by the complex viscosities of the bimodal blends at 30, 100 and 300 s^{-1} in order to indicate the relationship between the w_c and viscosity (**Figure 6.24**). The shear rate dependence of the normalised w_c is almost negligible when the M_w of the matrix is 15 kDa (the centre of the data points) and it becomes greater when lower or higher M_w of the matrix is used. Since the w_c is independent of the shear rate, it is considered that this shear rate dependence of normalised w_c is due to the shear rate dependence of the viscosity of the blends.

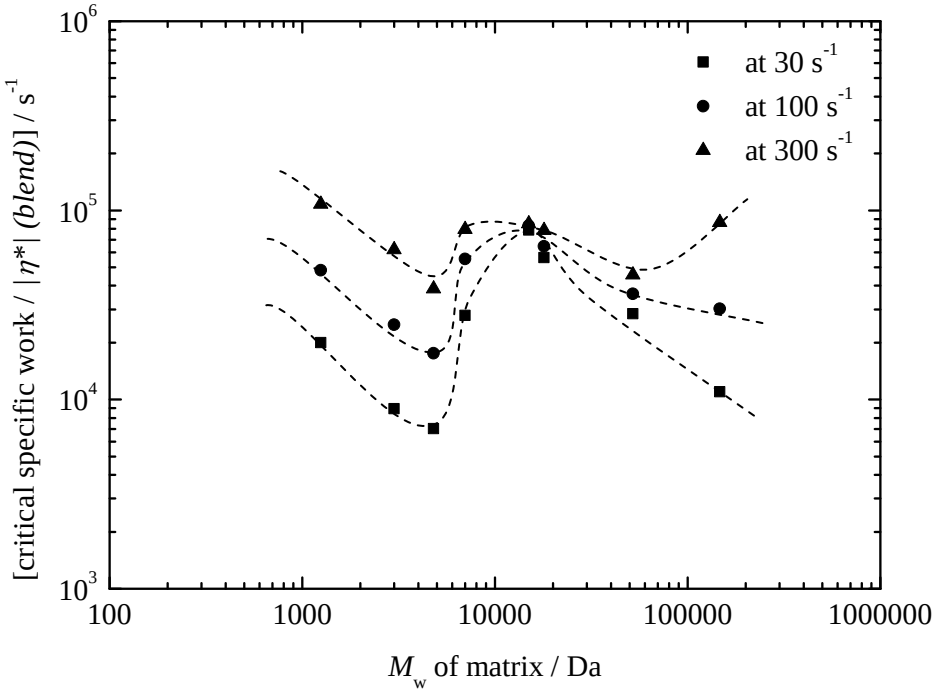

Figure 6.24. The critical specific work of the bimodal blends measured at 388 K divided by the complex viscosity of the blends at angular frequency = 30, 100 and 300 s^{-1}. Dashed lines are to guide the eye. The data points at M_w = 15 kDa were taken from the reference[5].

The viscosity of the bimodal blends can be simulated by using the Rubinstein-Colby theory. The viscosity of the blends (2 wt % 700 kDa long chains in a series of matrix) was predicted by the theory to check about the shear rate dependence of viscosity (**Figure 6.25**). Firstly, when the M_w of a matrix is 1 kDa, the viscosity shows strong ω dependence of viscosity at ω = 30 - 300, which is the range used for the shear experiments. This suggests that the blend viscosity has been affected by the shear thinning of the viscosity contribution of the long chains which dictates the viscosity of the blend. Secondly, the ω dependence is negligible when the M_w of the matrix is about 30 kDa. It is explained that the effect of the long chains is weaker than the low M_w matrix due to the high viscosity of the matrix. Thirdly, the ω dependence of viscosity is greater again when further high M_w matrix is used. It is considered that the shear thinning of the matrix is effective in this case.

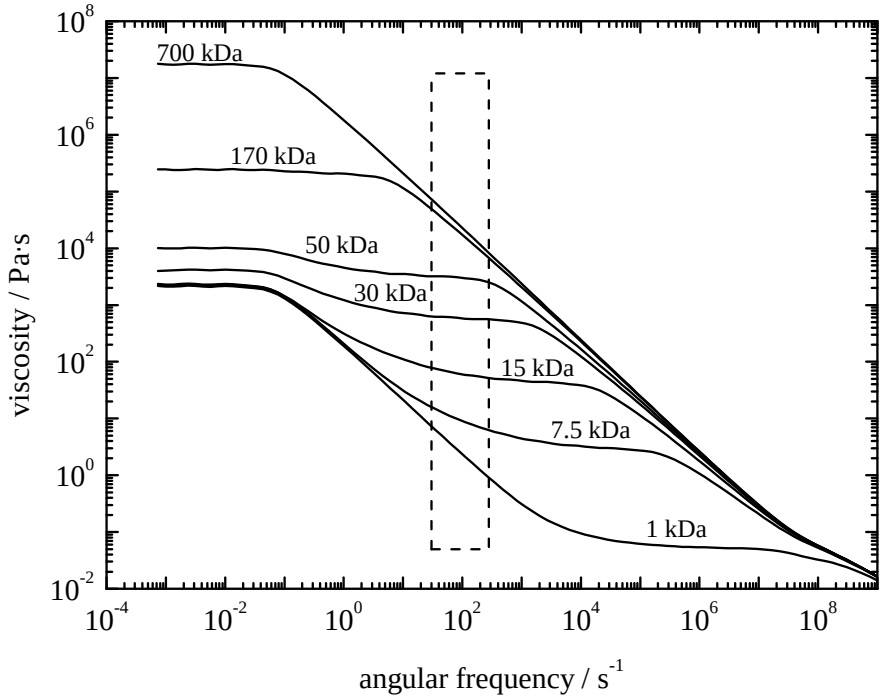

Figure 6.25. The viscosities of the blend (1.2 wt % 700 kDa chains in matrices with different molecular weight) at 388 K simulated by the Rubinstein-Colby theory. The molecular weights of matrices are indicated above the viscosity curves. The area enclosed by a dotted line shows the range of the angular frequency used for shear experiments ($30 \sim 300\ s^{-1}$).

The simulated viscosity was normalised by the viscosity at $\omega = 100\ s^{-1}$ and plotted against the M_w of matrix (**Figure 6.26**). This figure indicates that the shape of ω dependence of the viscosity of the bimodal blends predicted by the Rubinstein-Colby theory has the same form as the critical work normalised by the blend viscosity as a function of the matrix M_w. The ω dependence is weak at the centre and strong at the both edge of the spider shape as explained above.

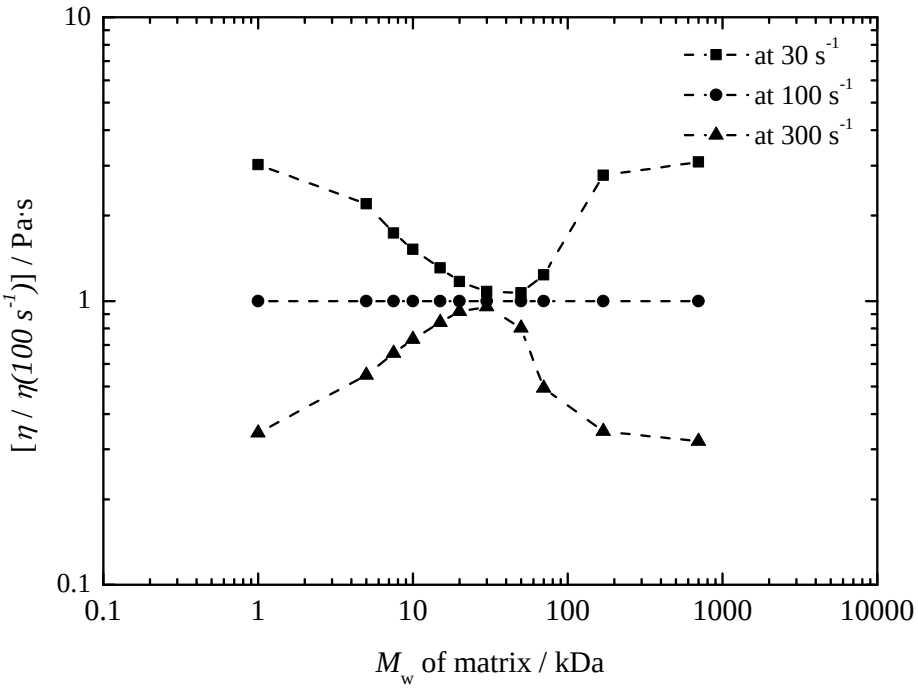

Figure 6.26. The viscosities at different angular frequency at 388 K simulated by the Rubinstein-Colby theory, normalized by the viscosity at angular frequency = 100 s^{-1}. The plots in this figure are corresponding to the cross section of the area enclosed by dotted line in **Figure 6.25**.

Although the critical specific work of the bimodal blends depends on the viscosity of the blend, the critical specific work normalised by the viscosity does not provide a constant value because of the ω dependence of the viscosity. The ω dependence of viscosity of the bimodal blends comprised of matrices with different M_w has a complicated "spider shape" due to shear thinning behaviour of both long chains and matrix. Conversely, the w_c provides a constant value against ω even though the w_c has included this complicated ω dependence of viscosity. The independence from ω is the advantage of the w_c for applications to industrial situation; however, the mechanism that by which w_c gives a constant value needs further consideration.

6.4. Conclusions

The boundary flow conditions were measured in the bimodal blends comprised of the long chains in a series of matrices with varying M_w. It was found that a power law

relationship exists between the M_w of the matrix and the w_c. When the M_w of the matrix is below 5 kDa, the w_c is independent of the M_w of the matrix and it has a constant value which represents the minimum amount of flow required for the formation of oriented morphology by only long chains without any contribution from the short chains. Above 5 kDa, the w_c increases with the rise of M_w of matrix in power law. It is considered that more mechanical work is required for stretching and transporting the short chains of the matrix when the matrix M_w is higher.

The w_c and the viscosity of the bimodal blends were compared and show high correlation. Therefore, it can be considered that when the Mw of the matrix is 5 kDa, the work which can overcome both a barrier based on the viscosity and the minimum amount of flow by only long chains is required for the formation of the oriented morphology. The w_c of the bimodal blends depends on the viscosity of the blend; however, the w_c normalised by the viscosity does not provide a constant value because of a complicated ω dependence of the viscosity of the blends due to shear thinning behaviour of both long chains and matrix. On the other hand, the w_c provides a constant value against ω in spite of the w_c incorporating this complicated ω dependence of viscosity.

6.5. References

1. Keller, A.; Kolnaar, H. W. H., Part II: Structure Development During Processing, 4 Flow-Induced Orienttion and Structure Formation In *Materials Science and Technology; A Comprehensive Treatment, Vol.18, Processing of Polymers*, Meijer, H. E. H., Ed. WILEY-VCH: Weinheim, Germany, 1997; pp 189-268.
2. Coppola, S.; Grizzuti, N. *Macromolecules* **2001,** 34, 5030-5036.
3. Elmoumni, A.; Winter, H. H.; Waddon, A. J. *Macromolecules* **2003,** 36, 6453-6461.
4. Meerveld, J. v.; Peters, G. W. M.; Hutter, M. *Rheol. Acta.* **2004,** 44, 119-134.
5. Mykhaylyk, O. O.; Chambon, P.; Graham, R. S.; Fairclough, J. P. A.; Olmsted, P. D.; Ryan, A. J. *Macromolecules* **2008,** 41, 1901-1904.
6. Mykhaylyk, O. O.; Chambon, P.; Impradice, C.; Fairclough, J. P. A.; Terrill, N. J.; Ryan, A. J. *Macromolecules* **2010,** 43, (5), 2389-2405.
7. Janeschitz-Kriegl, H.; Eder, G. *J. Macromol. Sci., Part B: Phys.* **2007,** 46, (3), 591-601.
8. Janeschitz-Kriegl, H.; Ratajski, E.; Stadlbauer, M. *Rheol. Acta.* **2003,** 42, 355-364.

9. Fernyhough, C. M.; Young, R. N.; Poche, D.; Degroot, A. W.; Bosscher, F. *Macromolecules* **2001,** 34, 7034-7041.

10. Rubinstein, M.; Colby, R. H. *J. Chem. Phys.* **1988,** 8, 5291-5306.

11. Rubinstein, M.; Colby, R. H., *Polymer Physics*. Oxford university Press: Oxford, 2003.

12. Wang, S. F.; Wang, S. Q.; Halasa, A.; Hsu, W. L. *Macromolecules* **2003,** 36, (14), 5355-5371.

13. Struglinski, M. J.; Graessley, W. W. *Macromolecules* **1985,** 18, (12), 2630-2643.

Chapter 7

Conclusions and Future Work

7.1. Conclusions

In the chapter 3, the characterization of hydrogenated polybutadiene (h-PBD) samples was carried out. The relaxation times of synthesized low-polydispersity h-PBD samples were obtained from the G' and G'' by using the Linear theory. The viscosity simulated by the linear theory reproduced the measured viscosity the h-PBD samples having the wide range of M_w. The Rolie-Poly model was used to calculate the relaxation times of h-PBD. The magnitude of the relaxation time estimated by the model was consistent with the results by the linear theory.

In the chapter 4, the oriented and un-oriented morphology of the sheared h-PBD bimodal blend was observed by the optical microscopy and compared with the polarised light imaging, small angle X-ray scattering and wide angle X-ray diffraction.

In the chapter 5, we clarified the role for long chains with different lengths in the mechanism of flow induced crystallisation of polymers. It was found that the h-PBD trimodal blend comprised of two different kinds of long chains with chain length in a matrix has two pairs of the boundary flow conditions required for the formation of oriented morphology. The difference between the boundary flow conditions of the trimodal and bimodal blends was interpreted by the shish nuclei formation mechanism involving binary aggregation of precursors. The minimum rate where flow can affect the formation of oriented morphology is dominated by the behaviour of the longest chains and unaffected by the presence of shorter chains, whereas at higher flow rates shorter chains contribute to a reduction in the critical specific work because they can form precursors which interact with the longest chains. The boundary flow conditions of polydisperse polymers were explained by applying this process. The magnitude of the boundary specific work is dictated by the concentration and the molecular weight of the longest chains in the polydisperse polymers. Other long chains contribute to the boundary flow conditions of the longest chains and make the shear-rate dependence of the boundary flow conditions a smooth divergence (**Figure 5.20**).

In the chapter 6, the role for short chains (whose inverse Rouse time is greater than applied shear rate) in flow induced crystallisation of polymers was investigated. The boundary flow conditions of bimodal blends comprised of long chains in a series of

matrices with different length were measured and it was found that there is a power law relationship between the M_w of the matrix and the critical work which is required amount of flow for the formation of the oriented morphology (**Figure 6.21**). It is considered that more mechanical work is required for stretching and transporting the short chains of the matrix when the matrix M_w is higher. The work was independent of the M_w of matrix when the M_w of matrix is below 5 kDa. This constant work represents the minimum amount of flow required for the formation of oriented morphology by only long chains in the blend without any contribution from the matrix. The viscosity of the blends and the matrix M_w relationship is also power law function having a similar exponent with the w_c and the matrix M_w relationship, however, the w_c normalised by the viscosity does not provide a constant value because of the angular frequency dependence of the viscosity. The angular frequency dependence is a complicated spider-shape against M_w of matrix due to the contribution of the long chains, short chains and their shear thinning effect. This result means that the simple estimation of w_c of the bimodal blends from their viscosity does not work and suggests that a specific mechanism exists for the independence of shear rate of the w_c, and further consideration is needed to clarify the mechanism.

In summary, the mechanism of flow induced crystallisation of polymers which has polydispersity was clarified in this study. The roles of the polymer chains with different molecular weight can be described as follows. The concentration and the molecular weight of the longest chains (**Figure 7.1, A**) in polydisperse polymers dictate the magnitude of the boundary flow conditions. The boundary specific work of the longest chains is constant against flow rate and diverges at the minimum shear rate of the longest chains rapidly. Other long chains (**Figure 7.1, B**), which can be stretched under the applied flow, can contribute to the boundary flow conditions of the longest chains through the increase of the concentration of the precursors of shish nuclei. The boundary specific work of the polydisperse polymers is not constant above the minimum shear rate of the longest chains and indicates a smooth divergence against the flow rate due to the contribution of the other long chains and their minimum shear rate. Shorter chains (**Figure 7.1, C**), which cannot be stretched under the flow, have the role to shift the magnitude of the boundary flow conditions. The required energy (critical work) to form the oriented morphology is dependent on the molecular weight of the shorter chains. The mechanism of this dependence closely relates to the contribution to the viscosity of the polymers by the shorter chains.

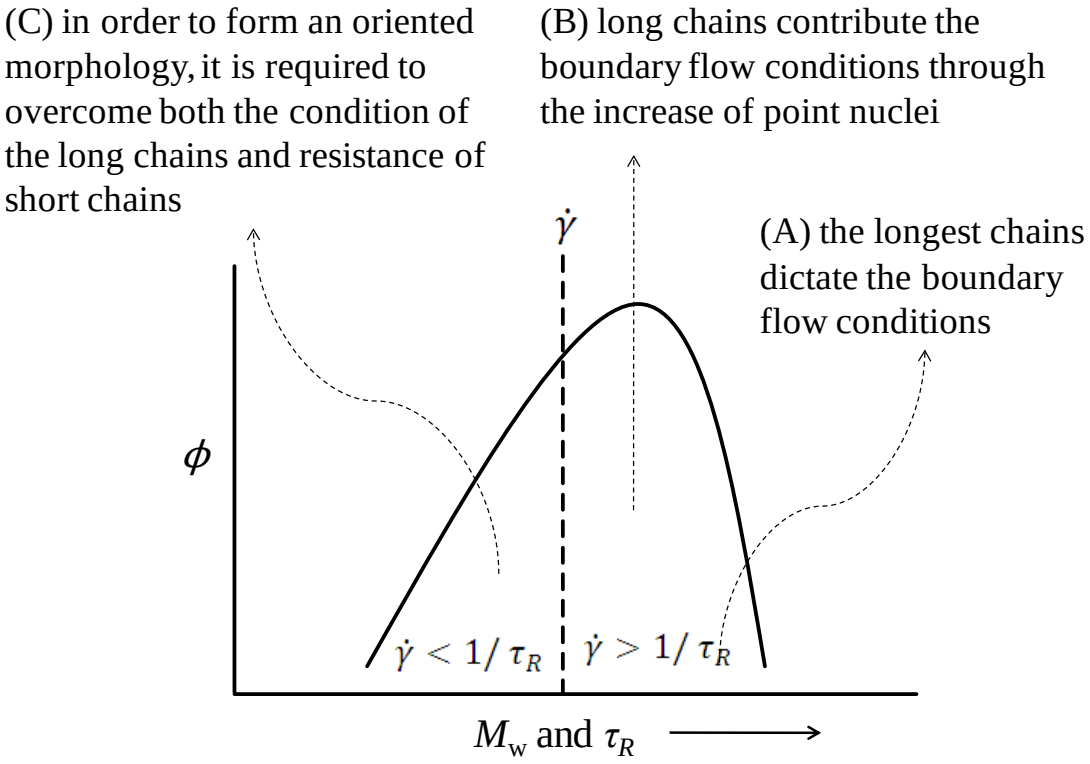

Figure 7.1. Explanation drawings of the conclusions of this research. A smooth curve indicates the molecular weight distribution of polydisperse polymers. A dashed line shows the magnitude of shear rate applying to a polydisperse polymer. The right area from the dashed line indicates long chains which can be stretched by the shear due to the relatively long relaxation times. The left area from the dashed line indicates short chains which cannot be stretched by the shear. The texts above the figure describe the roles of the polymer chains in each part of molecular weight distribution.

7.2. Future work

The modelling of the relationship between structures and processing conditions can be interesting as a further work. In this work, the interaction between the longest and longer chains, and the contribution by short chains, which affect the boundary flow conditions required to form the oriented morphology were clarified. Also, the relationship between the concentration of the long chains and the critical specific work, the relaxation times of the long chains and the critical specific work were already reported[1, 2]. From those information, the prediction of the boundary flow conditions of polydisperse polymers could be established.

The study about the relationship between the critical specific work and major properties, such as mechanical, thermal and optical properties of polyolefins is significant subject. If the certain relationship between the critical specific work and the property was found, it can be a simple and powerful method to control the property for industrial applications since the critical specific work is independent of the shear rate in processes.

7.3. References

1. Mykhaylyk, O. O.; Chambon, P.; Graham, R. S.; Fairclough, J. P. A.; Olmsted, P. D.; Ryan, A. J. *Macromolecules* **2008,** 41, 1901-1904.

2. Mykhaylyk, O. O.; Chambon, P.; Impradice, C.; Fairclough, J. P. A.; Terrill, N. J.; Ryan, A. J. *Macromolecules* **2010,** 43, (5), 2389-2405.